

# **The Genesis of Magnetic Fields in White Dwarfs**

**Gordon P. Briggs**

**May 2018**

**Mathematical Sciences Institute  
Australian National University**



**Australian  
National  
University**

**A thesis submitted for the degree of  
Doctor of Philosophy  
of the Australian National University**

© Gordon P. Briggs  
May 2018  
All rights reserved

*For my Mother*



*“ ... the day of the Lord will come as a thief in the night; in which the heavens shall pass away with a great noise, and the elements shall melt with fervent heat, the earth also and the works that are therein shall be burned up.”*

2 Peter 3:10



## Declaration

I hereby declare that the work in this thesis is my own except where indicated below. The work was carried out between March 2010 and May 2018 at the Australian National University (ANU), Canberra. It has not been submitted in whole or in part for any other degree at this or any other university.

This thesis is submitted as a Thesis by Compilation in accordance with the relevant ANU policies. The chapters refer to material submitted to, accepted or published by a peer-reviewed astrophysics journal. The extent of the contribution of this candidate to the research and authorship is detailed below.

My collaborators have been Lilia Ferrario (LF, chair of supervisory pane), Christopher A. Tout (CAT, member of the supervisory panel), Dayal T. Wickramasinghe (DTW, member of the supervisory panel), Jarrod Hurley, Adela Kawka, Stephane Vennes and Ernst Paunzen.

- The BSE code was originally developed by Jarrod Hurley. I made extensive modifications to the code over the years to allow the modelling of the properties of merging white dwarfs and magnetic cataclysmic variables.
- **Chapter 2: Merging Binaries and Magnetic White Dwarfs.** This chapter is a reproduction of the paper published in Monthly Notices of the Royal Astronomical Society, viz: *Briggs, Ferrario, Tout, Wickramasinghe & Hurley, MNRAS (2015), 447(2): 1713–1723. Merging binary stars and the magnetic white dwarfs*. GPB developed all the codes, wrote the paper and made the plots. LF made suggestions, corrected mistakes and added some relevant material. CAT and DTW reviewed the paper and made further suggestions.

- **Chapter 3: Genesis of the Magnetic Field.** This chapter is a reproduction of a paper in publication in Monthly Notices of the Royal Astronomical Society, viz: *Briggs, Ferrario, Tout & Wickramasinghe, MNRAS (2018), (In press). Genesis of magnetic fields in isolated white dwarfs*. I developed all the codes, wrote the paper and made the plots. LF made suggestions, corrected mistakes and added some relevant material. CAT and DTW reviewed the paper and made further suggestions.
- **Chapter 4: Origin of Magnetic Fields in Cataclysmic Variables.** This chapter is a reproduction of the paper submitted for publication in Monthly Notices of the Royal Astronomical Society, viz: *Briggs, Ferrario, Tout & Wickramasinghe, MNRAS (2018), Origin of Magnetic Fields in Cataclysmic Variables*. I developed all the codes, wrote the paper and made the plots. LF made suggestions, corrected mistakes and added some relevant material. CAT and DTW reviewed the paper and made further suggestions.
- **Chapter 5: A Double Degenerate White Dwarf System.** This chapter is a reproduction of the paper published in Monthly Notices of the Royal Astronomical Society, viz: *Kawka, Briggs, Vennes, Ferrario, Paunzen & Wickramasinghe, MNRAS (2017), 466(1): 1127–1139. A fast spinning magnetic white dwarf in the double-degenerate, super-Chandrasekhar system NLTT 12758*. The main body of the work was carried out by the co-authors. I calculated the evolution of the system and wrote the section *5.4.4 Evolution of NLTT 12758*.

I also carried out the work on the following conference paper while LF presented it.

- *Briggs, Ferrario, Tout & Wickramasinghe, Contributions of the Astronomical Observatory Skalnaté Pleso, vol. 48, no. 1, p. 271-272.*

This conference paper is not included here.

Gordon P. Briggs  
May 2018



## **Acknowledgements**

I wish to acknowledge the help and encouragement of my supervisors Chris Tout, Dayal Wickramasinghe and especially Lilia Ferrario who coached me along the way about the science of white dwarfs and common envelope evolution. I thank Jarrod Hurley for providing the SSE and BSE computer codes and Adela Kawka for inviting me to collaborate and contribute to the paper on NLTT-12758. A special thank you goes to my little four legged friend Rufus, who kept me company and took me out for doggochinnos when I was stressed.

I also gratefully acknowledge the receipt of an Australian Postgraduate Award.



## Abstract

Magnetic fields generated by a dynamo mechanism due to differential rotation during stellar mergers are often proposed as an explanation for the presence of strong fields in certain classes of magnetic stars, including high field magnetic white dwarfs (HFMWDs). In the case of the HFMWDs, the site of the differential rotation has been variously proposed to be the common envelope itself, the massive hot outer regions of a merged degenerate core or an accretion disc formed by a tidally disrupted companion that is subsequently incorporated into a degenerate core.

In the present study I explore the possibility that the origin of HFMWDs is consistent with stellar interactions during the common envelope evolution (CEE). In this picture the observed fields are caused by an  $\alpha - \Omega$  dynamo driven by differential rotation. The strongest fields would arise when the differential rotation equals the critical break up velocity and would occur from the merging of two stars during CEE or double degenerate (DD) mergers in a post common envelope (CE) stage. Those systems that do not coalesce but emerge from the CE on a close orbit and about to initiate mass transfer will evolve into magnetic cataclysmic variables (MCVs),

The population synthesis calculations carried out in this work have shown that the origin of high fields in isolated white dwarfs (WDs) and in WDs in MCVs is consistent with stellar interaction during common envelope evolution. I compare the calculated field strengths to those observed and test the correlation between theory and observation by means of the Kolmogorov–Smirnov (K–S) test and show that the resulting correlation is good for values of the CE energy efficiency parameter,  $\alpha_{\text{CE}}$ , in the range 0.1–0.3.



## Acronyms

AGB	Asymptotic Giant Branch;
CE	Common envelope;
CEE	Common Envelope Evolution;
CS	Fully or deeply Convective MS Star ( $\text{Mass} < 0.7M_{\odot}$ );
CV	Cataclysmic Variable star system;
DD	Double Degenerate binary star system;
HFMWD	High Field Magnetic White Dwarf;
HRD	Hertzsprung–Russell diagram of stellar evolution;
ISM	Inter-Stellar Medium;
IMF	Initial Mass Function;
MCV	Magnetic Cataclysmic Variable star system;
MS	Main Sequence of the Hertzsprung-Russell diagram;
$M_{\odot}$	One Solar mass;
RGB	Red Giant Branch
$R_{\odot}$	One Solar Radius;
SDSS	Sloan Digital Sky Survey;
WD	White Dwarf star;



# Contents

<b>Declaration</b>	<b>vii</b>
<b>Acknowledgements</b>	<b>ix</b>
<b>Abstract</b>	<b>xi</b>
<b>Acronyms</b>	<b>xiii</b>
<b>1 Introduction</b>	<b>1</b>
<b>2 Merging Binaries and Magnetic White Dwarfs</b>	<b>7</b>
2.1 Abstract . . . . .	7
2.2 Introduction . . . . .	7
2.3 Common Envelope Evolution and Formulism . . . . .	10
2.4 Population synthesis calculations . . . . .	12
2.5 Population Synthesis Results . . . . .	16
2.5.1 Example Evolutionary Histories . . . . .	18
2.5.2 Mass distribution of the synthetic population . . . . .	22
2.6 Comparison with observations . . . . .	24
2.7 Discussion and Conclusions . . . . .	34
<b>3 Genesis of the Magnetic Field</b>	<b>37</b>
3.1 Abstract . . . . .	37
3.2 Introduction . . . . .	38
3.3 Population synthesis calculations . . . . .	39
3.3.1 Theoretical magnetic field strength . . . . .	40
3.3.2 Parameters calibration . . . . .	42
3.4 Discussion of results . . . . .	45
3.5 Comparison to observations . . . . .	47
3.6 Incidence of magnetism among cool white dwarfs . . . . .	48

3.7	Conclusions . . . . .	51
<b>4</b>	<b>Origin of magnetic fields in cataclysmic variables</b>	<b>53</b>
4.1	Abstract . . . . .	53
4.2	Introduction . . . . .	53
4.3	Evolution and space density of MCVs . . . . .	55
4.3.1	Where are the progenitors of the MCVs? . . . . .	58
4.4	Population synthesis calculations . . . . .	59
4.5	Synthetic population statistics . . . . .	62
4.5.1	Magnetic CV evolution examples . . . . .	66
4.5.2	Property distributions of the synthetic population . . . . .	67
4.6	Comparison to observations . . . . .	75
4.7	Discussion and Conclusions . . . . .	82
<b>5</b>	<b>A Double Degenerate White Dwarf System</b>	<b>85</b>
5.1	Abstract . . . . .	85
5.2	Introduction . . . . .	85
5.3	Observations . . . . .	88
5.3.1	Spectroscopy and Spectropolarimetry . . . . .	88
5.3.2	Photometry . . . . .	90
5.4	Analysis . . . . .	94
5.4.1	Binary parameters . . . . .	94
5.4.2	Rotation . . . . .	95
5.4.3	Stellar and atmospheric parameters . . . . .	101
5.4.4	Evolution of NLTT 12758 . . . . .	110
5.5	Discussion . . . . .	113
5.6	Conclusions . . . . .	115
<b>6</b>	<b>Conclusions</b>	<b>119</b>
6.1	The Study Method in Review . . . . .	120
6.2	The Isolated Magnetic WDs . . . . .	121
6.3	The Magnetic Cataclysmic Variables . . . . .	122
6.4	Evolution of a Double Degenerate System: NLTT 12578 . . . . .	123
6.5	A Final Word . . . . .	124
	<b>References</b>	<b>125</b>



## List of Figures

2.1	Theoretical mass distribution of remnant WDs formed by merging for a range of values $\alpha$ and a Galactic disc age of 9.5 Gyr. "DD WDs" are WDs resulting from DD mergers, "ONe WDs" are Oxygen–Neon WDs, "CO WDs" are Carbon–Oxygen WDs and "He WDs" are Helium WD remnants after merging. . . . .	17
2.2	Mass distribution of theoretical HFMWDs for $\alpha = 0.10$ separated according to their pre-CE progenitors. Other paths also contribute but are less than 1 per cent of the total. The Galactic disc age is chosen to be 9.5 Gyr. The stellar types are identified in Table 2.1. . . . .	23
2.3	CDFs of masses of observed SDSS DR7 (Kleinman et al., 2013) non-magnetic, magnitude-limited and converted-volume-limited field WDs and the theoretical (BSE) volume-limited population of non-magnetic WDs from single star evolution for a Galactic disc age of 9.5 Gyr. . . . .	30
2.4	Mass distribution of 27 observed HFMWDs (objects taken from Table 2.9) compared with the computed sample. . . . .	31
2.5	CDFs of volume-limited-converted masses of observed SDSS DR7 (Kleinman et al., 2013) non-magnetic, field WDs and the observed MWDs. The population of observed MWDs is not strictly a volume limited sample since it comes from various surveys as discussed in the text. A formal application of the K–S test has $D = 0.4417$ and $P = 3 \times 10^{-5}$ . . . . .	32
2.6	CDF of observed and BSE theoretical HFMWD masses for a Galactic disc age of 9.5 Gyr and $\alpha = 0.10$ . The K–S test has $D = 0.1512$ and $P = 0.7095$ . . . . .	33

3.1	Density plot of the probability given by the K–S test that the CDFs of the theoretical and observed magnetic field distributions are drawn from the same population. This was generated for a range of $\alpha$ and $B_0$ (see text). The probability is colour-coded according to the palette shown on the right hand side of the figure. The sub-structures in this plot are caused by the discretisation of $\alpha$ and $B_0$ . . . . .	41
3.2	CDFs of observed (red) and BSE theoretical magnetic field distributions for a Galactic disc age of 9.5 Gyr and various $\alpha$ . . . . .	43
3.3	Theoretical magnetic field strength for a Galactic disc age of 9.5 Gyr and various $\alpha$ . The histograms are superimposed, not stacked, to highlight the contribution made by each type of WD to the overall distribution. The blue, red and yellow histograms represent, respectively, CO, ONe, He WDs. The green histograms depict the merged DD systems. . . . .	44
3.4	Theoretical magnetic field distribution of HFMWDs showing the PRE progenitors for various $\alpha$ . The light blue, yellow and purple histograms represent, respectively, the AGB/MS, AGB/CS and RGB/CS merging pairs. The red histograms depict the merged DD systems. . . . .	46
3.5	Theoretical field distribution for $\alpha = 0.2$ of the total of the four types of HFMWDs (pink histogram) compared to the field distribution of the observed HFMWDs (blue histogram). . . . .	50
4.1	The orbital period distribution of MCVs (top) and of the CVs (bottom). The MCVs are subdivided into Polars (solid black line histogram) and IPs (shaded histogram). We have used the latest version (v7.20) of the Ritter & Kolb (2003) CV catalogue to create this figure. . . . .	57
4.2	The orbital period distribution of PCEBs (solid black line histogram, Nebot Gómez-Morán et al., 2011) and PREPs (shaded histogram, Ferrario et al., 2015a). . . . .	59
4.3	Theoretical period distribution of magnetic systems just before they start RLOF for various $\alpha$ 's. The period distribution of the primary WD types is shown as the superimposed coloured categories. The total of the distribution is shown as the pink background histogram peaking around 2.8 to 3.0 hrs. This is to be compared with the observed distribution for PREPs in Fig. 4.2 . . . . .	68
4.4	Same as Fig.4.3 but with the secondary star types shown as the superimposed coloured categories. Both secondary star types are MS stars. The CS type is a deeply or fully convective MS star with $M < 0.7 M_\odot$ . . . . .	69

4.5	Theoretical mass distribution of the WD primary star of magnetic systems just before they start RLOF for various $\alpha$ . The distributions of the three WD types are shown as three superimposed coloured categories.	73
4.6	As in Fig 4.5 but for the secondary star types shown as the coloured categories. Both secondary star types are MS stars. The CS type is a deeply or fully convective MS star with $M < 0.7 M_{\odot}$ .	74
4.7	Pink shaded histogram: Total theoretical magnetic field distribution of the WD primary stars in magnetic systems just before they start RLOF for the indicated $\alpha$ . The histograms of the three types of WDs making up the total theoretical magnetic field distribution are shown as the foreground coloured histograms. These three are made partially transparent so that details of the other histograms can be seen through them.	77
4.8	Theoretical cumulative distribution functions for the magnetic fields of MCV WDs at RLOF for $\alpha = 0.10, 0.15, 0.20, 0.30$ and $0.40$ and the CDF of the observed magnetic field of 81 systems taken from Ferrario et al. (2015a)	78
4.9	Comparison of the theoretical magnetic field strength for $\alpha = 0.1$ and the observed magnetic field strength of the 81 MCVs taken from Ferrario et al. (2015a)	79
4.10	Comparison of the mass distributions for the observed pre-CV white dwarf masses taken from Zorotovic et al. (2011) and the theoretical mass distribution of the WDs as the systems start RLOF for $\alpha = 0.10$ .	80
4.11	Cumulative Distribution Functions of the mass distributions for the observed pre-CV WD masses taken from Zorotovic et al. (2011) and the theoretical distribution of the WDs as the systems start RLOF for $\alpha = 0.10, 0.15, 0.20, 0.30$ and $0.40$ . The K-S statistics for this plot are shown in the fourth and fifth columns of table 4.7	81
5.1	Low dispersion CTIO/R.-C. and NTT/EFOSC2 spectra of NLTT 12758 revealing Zeeman splitted Balmer lines.	91
5.2	EFOSC2, FORS2 and X-shooter spectra of NLTT 12758 showing variations in the $H\alpha$ core. The mid-exposure UT time is listed for each spectrum.	93

5.3	(Top panel) period analysis of the FORS2, EFOSC2 and X-shooter data with 66 and 90% confidence level (dashed lines). (Middle panel) radial velocity measurements (Table 5.3) of the DA (open squares) and DAP stars (full squares) phased on the orbital period and the best-fitting sine curves (Table 5.4) and (bottom panel) velocity residuals for the DAP star. The longest period is marked at $90^\circ$ on the top horizontal axis along with the actual period at $45^\circ$ . . . . .	96
5.4	Integrated polarization measurements of the two individual $\sigma$ components phased on the rotation period of 22.6 minutes revealing a complete reversal of the field vector. The top panel shows the measurements for the blue-shifted $\sigma_-$ component and the bottom panel shows the measurements of the red-shifted $\sigma_+$ component. . . . .	98
5.5	Co-added FORS2 circular polarization spectra (top panel) and flux spectra (bottom panel) at three phase ranges showing the flip in the sign of the $\sigma$ components of $H\alpha$ . The spectrum with zero polarization corresponds to a nearly orthogonal viewing angle to the magnetic axis. . . . .	99
5.6	Schematic view of the geometry of the double degenerate system NLTT 12758. The rotation plane of the magnetic white dwarf is assumed to coincide with the orbital plane, and the spin axis is marked $\omega$ . The spin axis is at an angle $i$ with respect to the observer and the magnetic field axis $B$ is at an angle $\alpha$ with respect to the observer. . . . .	100
5.7	(Top panel) period analysis of the measured $R$ photometric measurements. (Middle panel) photometric $R$ magnitudes phased on the best rotation period and (bottom panel) residuals. . . . .	102
5.8	(Top panel) Observed Balmer line profiles of NLTT 12758 compared to the best-fitting models. The best-fit shows that the components of NLTT 12758 are a non-magnetic DA white dwarf (dashed lines) paired with a magnetic DA white dwarf (dotted lines). Confidence contours at 66, 90, and 99% are shown in the $T_{\text{eff,DAP}}$ vs $T_{\text{eff,DA}}$ plane (bottom right) and $\log g$ vs $T_{\text{eff}}$ for both stars (bottom left). . . . .	107
5.9	The left panel compares the best-fitting photometry (open circle) to the observed photometry (solid black circles). The contribution of individual stars are plotted in different grey shades as hexagonals. The right panel plots the confidence contours (66, 90, and 99%) of the spectroscopic fit (in black) and the contours of the SED fit (grey full lines). Note that $\log g = 8.4$ for star 1 (DA) and $\log g = 8.2$ for star 2 (DAP). . . . .	108

## List of Tables

2.1	Stellar types distinguished within the BSE algorithms. . . . .	12
2.2	Fraction of binary systems that merge during CE for various values of $\alpha$ . The fraction of WDs born from merged stars in a single generation of binary systems of age 9.5 Gyr (the age of the Galactic disc) is $N$ . The remaining six columns give the smallest and the largest parameters on the search grid for systems that are found to have merged. The parameters are the progenitors' ZAMS masses and orbital period. . . .	14
2.3	Fraction of merging DD systems, WDs formed by merging of two degenerate objects outside a CE in a single generation of binary systems of age 9.5 Gyr. Other columns are as in Table 4.1 . . . . .	15
2.4	Types and fractions per cent of WDs formed from CE and DD by merging binary systems in a population aged 9.5 Gyr. All DD WDs are of CO type. . . . .	18
2.5	Evolutionary history of an example binary system that merges during CE. Here $\alpha = 0.2$ , $P_0 = 219.6$ d, S1 is the primary star and S2 is the secondary star. . . . .	20
2.6	Evolutionary history of an example of WD that formed in a DD coalescence. Here $\alpha = 0.1$ , $P_0 = 3144$ days, S1 is the primary star and S2 the secondary star. . . . .	21
2.7	The contributions per cent of pre-CE progenitor pairs to theoretical HFMWDs when $\alpha = 0.1$ . The stellar type 'CS' is a deeply or fully convective low-mass main sequence star (see Table 2.1). . . . .	22
2.8	The theoretical incidence of HFMWDs as a fraction of magnetic to non-magnetic field WDs as a function of the CE efficiency parameter $\alpha$ . . . . .	24
2.9	Known HFMWDs with poloidal field strength $B_{\text{pol}} \geq 10^5$ G. In comparison with our models we exclude five of these WDs with $B_{\text{pol}} < 1$ MG (1, 3, 18, 20 & 32) and two of extremely low mass (19 & 29) that cannot be formed within the BSE formalism. . . . .	27

2.10	Kolmogorov-Smirnov $D$ statistic and $P$ of the mass distributions of the theoretical (BSE) and observed MWD populations being drawn from the same distribution for various values of $\alpha$ . The theoretical population is for a Galactic disc age of 9.5 Gyr. . . . .	33
4.1	We have indicated with $N$ (second column) the fraction of PREPs that emerge from CE for different efficiency parameters $\alpha$ (first column) in a single generation of binaries. The other columns give the smallest and the largest progenitor masses and initial orbital periods. . . . .	60
4.2	The number of PCEBs born, the fraction of PREPs from PCEBs and of MCVs (magnetic systems already exchanging mass) from PREP as a function of the CE efficiency parameter $\alpha$ over the age of the Galactic Disc. The number of PREPs is maximum close to $\alpha = 0.15$ while the number of MCVs is maximum at $\alpha = 0.10$ . . . . .	62
4.3	Evolutionary history of an example binary system that becomes a MCV after CEE with $\alpha = 0.1$ . Here RLO = Roche Lobe Overflow. . . . .	64
4.4	Evolutionary history of a second example binary system that becomes a MCV after CE with $\alpha = 0.4$ . . . . .	65
4.5	The fraction of the combinations of types of WD primaries and secondary types just before RLOF commences for various $\alpha$ . The stellar type CS is a deeply or fully convective low-mass MS star with $M < 0.7 M_{\odot}$ . . . . .	71
4.6	Kolmogorov-Smirnov $D$ statistic and probability $P$ of the magnetic field distributions of the observed and synthetic populations of MCVs for a range of $\alpha$ . . . . .	76
4.7	K-S $D$ statistic and probability $P$ of the WD mass distributions of the observed MCVs listed by Ferrario et al. (2015a, second and third columns) and our synthetic populations for $\alpha$ given in the first column. We show the K-S results of the observed Pre-CV masses of Zorotovic et al. (2011) and our synthetic populations at the start of RLOF (fourth and fifth columns). . . . .	81
5.1	Spectroscopic observation log. . . . .	89
5.1	Spectroscopic observation log - continued . . . . .	90
5.2	Photometric measurements of NLTT 12758 . . . . .	92
5.3	Radial velocity measurements . . . . .	95
5.4	Summary of NLTT 12758 parameters . . . . .	109

5.5	Evolution of a binary star system of approximately the size of NLTT 12758 starting from ZAMS through to the end of their interaction and the production of a double degenerate WD pair. $M1$ and $M2$ are the masses of the primary and secondary stars respectively (in solar masses), $S1$ and $S2$ are the stellar types varying throughout their evolution as shown in Table 1 in Briggs et al. (2015, and chapter 2). $Sepn$ is the stellar separation in solar radii, $Period$ is the orbital period in days and the $Event - Type$ is the event happening to the system at the time given in column 2. . . . .	112
5.6	Known double degenerates containing a magnetic white dwarf . . . .	116





# Chapter 1

## Introduction

For decades astrophysicists have been working to develop computer codes that can model the nuclear and hydrodynamic evolution of stars for ranges of masses and metallicities. This led to computer codes such as those described by Schwarzschild (1958) and Iben (1965) through to codes such as the Kippenhahn code (Kippenhahn et al., 1967; Kippenhahn & Weigert, 1990) which in turn led to GARSTEC (Garching Stellar Evolution Code) utilised at the Max-Planck Institute in Garching Germany (Weiss & Schattl, 2008). The TYCHO stellar evolution code derives from previous work on supernovae by David Arnett (1996). At Cambridge University (UK), the STARS code was originally written by Eggleton (1971) and was developed through to the versions described by Han et al. (1994) and Pols et al. (1995).

### **Non-Hydrodynamic Methods:**

These detailed evolution codes can take many hours to run for a single stellar formulation so that for population studies where it is necessary to evolve a large sample of stars a more rapid method of generating the population must be found. One method is to compute detailed stellar models from a number of computer runs of differing input parameters such as stellar masses and metallicities and to present the results in a tabular form that is easy to interpolate as required (e.g. Schaller et al., 1992; Charbonnel et al., 1993; Mowlavi et al., 1998; Pols et al., 1998).

A second method is to construct a set of formulae that represent the results of the stellar evolution codes analytically. Tout et al. (1996) initially fitted analytical functions of mass and metallicity to stars at all stages of evolution and achieved a fit with an error of generally less than 7.5 per cent in mass and 3 per cent in radius over the range of metallicities from  $Z = 0.0001$  to 0.03. Thus these analytic formulae are designed to represent the motion of a star in the Hertzsprung-Russell diagram as a function of time. Follow-up work was carried out by Hurley, Pols & Tout (2000) achieving fits within 5 per cent of the detailed computer codes. They present stellar luminosity, radius and core mass as a function of age from the ZAMS to the remnant stages and describe a mass-loss scheme that can be integrated into the formulae.

## **Binary Star Evolution**

Rappaport, Verbunt & Joss (1983) used a composite polytrope model for the core and envelope of the stars in a binary system while carrying out detailed stellar evolution of the binary for all other relevant aspects. This technique, faster than detailed models, was used to study the effects of magnetic braking using a range of braking laws.

The method using analytical formulae to represent the time evolution allows a much faster computation of stellar interactions in binary stars and N-body situations such as cluster environments (e.g. Hurley & Shara, 2002; Hurley, 2008). In a binary star system Roche-lobe overflow, Common Envelope Evolution (CEE) and magnetic braking with tidal friction are facilitated by the compact nature of the formulae over the tabular interpolation. Tout et al. (1997) provide an algorithm for rapid evolution of binary stars applied to the evolution of Algol variables. They explain how their algorithm can be incorporated into N-body simulations of colliding stars.

Hurley, Tout & Pols (2002) present a rapid binary star evolution algorithm, BSE, that allows modelling mass transfer, mass accretion, CEE, collision, supernovae kicks as well as spin and orbital momentum losses owing to tidal interactions. By comparing systems with and without tidal evolution they show that tides are required to draw correct conclusions from population synthesis studies. Orbit circularisation occurs on a dynamical timescale that is short compared to the nuclear evolution timescale so orbit eccentricity is of minor importance in the evolution of binary systems. A comprehensive review of the theory of binary star evolution outlining the various factors that contribute to their interactions can be found in Tout (2006). He sets out the mathematical basis of the factors, viz: orbit, tides, mass transfer, its stability and period evolution. He also discusses the binary evolution of Algol binaries and their critical mass ratio, cataclysmic variables, CEE and type Ia supernovae.

In this work I modify the Binary Star Evolution (BSE) code to model the origin of isolated and binary High Field Magnetic White Dwarfs (HFMWDs).

## **White Dwarfs and Magnetic Fields**

This work concentrates on the origin of HFMWDs some of which are observed to have fields as high as  $10^9$ G.

A number of recent reviews give a good overview of the physics of white dwarfs (WD)s. Isern et al. (2002, and references therein) discuss their evolution and summarise the four stages of neutrino, fluid, crystallisation and Debye cooling. They also discuss the use of WDs in the determination of the age of the Galaxy.

Wickramasinghe & Ferrario (2000, WF) deal extensively with magnetism in isolated and binary WDs. WF give an extensive review of the methods of measuring magnetic fields in WDs followed by the observations, physical properties and theoretical

considerations of isolated HFMWDs. They finish this extensive review by examining HFMWDs in interacting binary systems in particular the AM Herculis systems.

The most relevant previous work on which this project is based is that of Regós & Tout (1995) and Tout & Regós (1995b). In these papers they present a model that could be applied to Cataclysmic Variables (CVs) to explain the presence of strong fields. In particular, they show that the differential velocity between the increasing orbital rate of the shrinking orbit of the binary combined with the decreasing rotation rate of the envelope sets up an  $\alpha - \Omega$  dynamo that creates strong magnetic fields. They also show that the interaction between stellar winds driven by the magnetic fields and the envelope provides a simple explanation for the range of remnant fields observed in WDs. This work was then used by Zangrilli et al. (1997) to show how dynamo generated fields can interact with a CE to create the orbital period gap of CVs.

Webbink & Wickramasinghe (2002) continue the discussion about the period gap in AM Her binaries. They find that magnetic braking causes the angular momentum loss in CVs, and that it is its reduction due to trapping of the secondary's wind by the magnetosphere of the primary that causes Magnetic CVs (MCVs) to fill the period gap.

### **Competing hypotheses for the origin of magnetic fields in white dwarfs**

The first model of the formation of magnetic fields in WDs was the fossil field theory, first proposed by Woltjer (1964) and Landstreet (1967). They predicted the existence of highly magnetic WDs by proposing that the fields are of a fossil origin from before the main sequence (MS) with magnetic flux frozen in from the ISM and conserved in some way during evolution to the WD phase (Mestel & Landstreet, 2005).

Tout et al. (2004) discuss the possibility of magnetic fields in WDs being fossil remnants of the fields in Ap and Bp stars and that their magnetic fields are fossil remnants from fields in the pre-MS stars. Wickramasinghe & Ferrario (2005) propose several scenarios for the origin of HFMWDs. Their first scenario is that only the chemically peculiar Ap and Bp stars on the main sequence evolve into HFMWDs. In the second scenario they assume that all intermediate-mass MS stars have large scale fields that are below the detectability limit. Once these stars evolve to WD stage their magnetic flux is conserved and become HFMWDs. The second scenario gives a better match to the observed mass and field distribution of HFMWDs. They also speculate on the possibility of very low-field magnetic white dwarf having progenitors among the F type stars. This would suggest a bi-modal distribution of magnetic fields with the HFMWDs having fossil fields originating from upper MS stars and low-field magnetic WDs having dynamo generated fields in lower MS stars.

Many papers have been written on the fossil field model. However none of them

solve the duplicity problem. That is that HFMWDs should occur as often in detached binaries as in single stars whereas no WD in a binary system has been found to be magnetic. Liebert et al. (2005) discuss the results of the Sloan Digital Sky Survey (SDSS) and the discovery that there are no HFMWDs found in the subset of WDs with main sequence companions. They give possible solutions for these observations but conclude that the sample size of stars may be too small to resolve the issue. However a much larger and statistically significant sample of binaries studied by Liebert et al. (2015a) led to the same conclusion.

As an alternative to the fossil field model, Tout et al. (2008) examine the possibility of magnetic fields being generated during CEE. They propose that the closer the binary pair at the end of the CE phase the stronger the magnetic field. They then go on to propose that the binaries that merge while in the CE are the progenitors of the isolated HFMWDs. See also Wickramasinghe, Tout & Ferrario (2014).

### **Goals of the present work**

The goal of my research is to test the viability of the formation of magnetic fields during CEE. A CE arises when the radius of the more massive, more evolved, primary star of a binary star system expands during a normal phase of stellar evolution and the orbital radius of the binary is such that the primary overfills its Roche lobe. Mass transfer from the primary star on to the secondary star then occurs. As the primary expands further the envelope grows in size until it eventually engulfs both stars.

This CE mechanism, first proposed by Paczyński (1976) and Ostriker (1976), describes mass transfer becoming unstable if the normal evolutionary process of the primary donor star is affected by loss of mass to the secondary. If the time scale for mass transfer is short compared with the time scale on which the accretor can adjust thermally to the on-flowing material the accreted layer heats up, expands and fills the Roche lobe of the accretor. Any further mass loss from the donor star is deposited into the CE that now engulfs both stars.

The transfer of orbital energy into the heating of the envelope causes a spiral-in of the binary orbit that accelerates the mass transfer and leads to a run-away process causing the orbit to spiral-in even faster. If the primary star is ascending the red Red Giant Branch (RGB) or the Asymptotic Giant Branch (AGB) and has developed a deep convective envelope, its radius increases in response to mass loss. This combined with the shrinking Roche lobe as the orbit spirals in, causes a dynamically unstable mass transfer to occur (Hjellming & Webbink, 1987; de Kool, 1992; Iben & Livio, 1993).

The resultant drag on the secondary and the transfer of orbital angular momentum from the secondary to the on-flowing material causes the orbit to shrink. As the orbit

shrinks, the kinetic energy of the orbit increases but the potential energy decreases more. This loss of energy heats and further expands the envelope, which is then ejected into space.

An important quantitative model of CEE is the energy formulism. In this model the change in orbital energy  $E_{\text{orb}}$  of the in-spiralling cores is equated to the energy required to heat and eject the envelope to infinity, the binding energy  $E_{\text{bind}}$ . This ratio is represented by the parameter

$$\alpha = \frac{\Delta E_{\text{orb}}}{\Delta E_{\text{bind}}}, \quad 0.0 \leq \alpha \leq 1.0$$

Ricker & Taam (2012) carried out a hydrodynamic evolution of the CE phase of a low-mass binary composed of a  $1.05 M_{\odot}$  red giant and a  $0.6 M_{\odot}$  companion. They followed the evolution for five orbits and found that only about 25 per cent of the orbital energy loss goes into ejecting the envelope inferring a value for  $\alpha$  of 0.25. In general, the process ends when the envelope has been ejected and the stars are either on a much tighter orbit or have merged. Circularization and spiral-in begin rapidly after the beginning of CE and the phase is probably short-lived, of the order  $10^3$ yr. In considering the progenitors of HFMWDs, the interest is in the situation where the two stars have merged while considering the progenitors of MCVs, the interest is in the situation when the two stars emerge from CE on a very tight orbit and are about to exchange mass.

This work is organised as follows. In chapter 2, I show that population synthesis studies of stars merging during CEE can explain the incidence of magnetism among WDs and the mass distribution of HFMWDs. In chapter 3, I show that these calculations can also reproduce very well the observed magnetic field distribution. In chapter 4, I synthesize a population of binary systems to explore the hypothesis that the magnetic fields in the MCVs also originate during stellar interactions in the CEE phase and find that the observed characteristics of the MCVs are consistent with those of a population of binaries that is born already in contact or close to contact, as first proposed by Tout et al. (2008). This finding is also in agreement with the hypothesis advanced by Schwöpe et al. (2009) that the binaries known as PREPs (pre-polars), where a HFMWD accretes matter from the wind of a low-mass companion, are the progenitors of the MCVs. Finally, in chapter 5, I show that the evolutionary path of the double degenerate super Chandrasekhar system NLTT 12758 is consistent with that of a binary that underwent two phases of CEE. The thesis ends in chapter 6 with a summing up and conclusions derived from the research.



# Chapter 2

## Merging Binaries and Magnetic White Dwarfs

This chapter is a reproduction of the paper published in Monthly Notices of the Royal Astronomical Society, viz:

*Briggs, Ferrario, Tout, Wickramasinghe & Hurley, MNRAS (2015), 447(2): 1713–1723. Merging binary stars and the magnetic white dwarfs*

### 2.1 Abstract

A magnetic dynamo driven by differential rotation generated when stars merge can explain strong fields in certain classes of magnetic stars, including the HFMWDs. In their case the site of the differential rotation has been variously proposed to be within a CE, the massive hot outer regions of a merged degenerate core or an accretion disc formed by a tidally disrupted companion that is subsequently incorporated into a degenerate core. We synthesize a population of binary systems to investigate the stellar merging hypothesis for observed single HFMWDs. Our calculations provide mass distribution and the fractions of WDs that merge during a CE phase or as DD systems in a post CE phase. We vary the CE efficiency parameter  $\alpha$  and compare with observations. We find that this hypothesis can explain both the observed incidence of magnetism and the mass distribution of HFMWDs for a wide range of  $\alpha$ . In this model, the majority of the HFMWDs are of the Carbon–Oxygen type and merge within a CE. Less than about a quarter of a per cent of HFMWDs originate from DD stars that merge after CE evolution and these populate the high-mass tail of the HFMWD mass distribution.

Keywords: white dwarfs – magnetic fields – binaries: general – stars: evolution

### 2.2 Introduction

Magnetic fields are seen in main-sequence stars of most spectral types. They are usually considered to be either of fossil origin, arising from a conserved primordial field, or generated in a contemporary dynamo (Mestel & Landstreet, 2005). The latter

is the accepted explanation for magnetic stars with convective envelopes such as the low-mass ( $M < 1.5 M_{\odot}$ ) main-sequence stars. The origin of the fields in the higher-mass magnetic Ap and Bp main-sequence stars with radiative envelopes is less certain. While a fossil origin remains possible, it has been proposed that magnetic fields may be generated by a dynamo mechanism driven by various instabilities, including the magnetorotational instability, in differentially rotating radiative regions of single stars (see e.g. Potter, Chitre & Tout, 2012).

The origin of the HFMWDs has been the topic of much discussion in recent years. The incidence of magnetism in WDs in the high field group ( $B > 10^6$  G) is estimated to be about 8-16 per cent (Liebert, Bergeron & Holberg, 2003; Kawka et al., 2007). A traditional explanation has been that the fields are of a fossil origin from the main sequence with magnetic flux conserved in some way during evolution to the WD phase (Mestel & Landstreet, 2005). Kawka et al. (2007) pointed out that the strongly magnetic Ap and Bp stars could not be their sole progenitors because the birth rate of these main-sequence stars is insufficient to explain the observed birth rate of the HFMWDs. However this turned out not to be a strong argument against the fossil hypothesis. In an earlier paper Wickramasinghe & Ferrario (2005) noted that it could be reconciled if about 40 per cent of late B stars had fields below the observed threshold for Ap and Bp stars. This would be consistent with the observations of Power et al. (2008) who conducted a volume-limited study of the magnetic Ap and Bp stars within 100 pc of the Sun. Their study has shown that the incidence of magnetism in intermediate mass stars increases with the mass of the stars. At  $1.7 M_{\odot}$  the fraction of magnetic among non-magnetic stars is only 0.1 per cent, while at  $3.5 M_{\odot}$  it is 37.5 per cent.

Some 50 per cent of stars are in binary systems. As these evolve some can interact and merge. So one may expect that some stars that appear single today are the result of the merging of two stars. The possibility of generating strong magnetic fields during such merging events has often been discussed in the literature as an alternative explanation for magnetic fields in certain classes of stellar object. Indeed, as an alternative to the fossil field model, Ferrario et al. (2009) proposed that the strong fields in the magnetic A, B and O stars are generated as stars merge.

Here we focus on the hypothesis that the entire class of HFMWDs with fields  $10^6 < B/G < 10^9$  owe their magnetic fields to merging (Tout et al., 2008). This model was first devised to explain the observation that there are no examples of HFMWDs in wide binary systems with late-type companions while a high fraction of non-magnetic WDs are found in such systems (Liebert et al., 2005).

In the CE scenario, when a giant star fills its Roche lobe, unstable mass transfer can lead to a state in which the giant's envelope engulfs both cores. As the two cores



spiral together, energy and angular momentum are transferred from their orbit to the differentially rotating CE until it is ejected, leaving behind a close binary system, or a merged single object. In the original model for formation of HFMWDs Tout et al. (2008) envisaged that the fields are generated by a dynamo in the CE and diffuse into the partially degenerate outer layers of the proto-WD before the CE is ejected. If the end product is a single star it can have a highly magnetic core and if it is a very close binary, it can become a MCV. Potter & Tout (2010) attempted to model this phenomenon and found a potential problem in that the time-scale for the diffusion of the field into the WD is generally significantly longer than the expected CE lifetime.

Wickramasinghe, Tout & Ferrario (2014) suggested that strong magnetic fields in WDs are generated by a dynamo process that feeds on the differential rotation in the merged object as it forms. A weak poloidal seed field that is already present in the pre-WD core is amplified by the dynamo to a strong field that is independent of its initial strength but depends on the amount of the initial differential rotation. We note in this context that weak fields of  $B \leq 1$  kG may be present in most WDs (Landstreet et al., 2012). Presumably these can be generated in a core–envelope dynamo in the normal course of stellar evolution.

Nordhaus et al. (2011) proposed an alternative but similar model (hereinafter the disc field model). They noted that if the companion were of sufficiently low mass it would be disrupted while merging and form a massive accretion disc around the proto-WD. Fields generated in the disc via the magnetorotational instability or other hydrodynamical instabilities could then be advected on to the surface of the proto-WD and so form a HFMWD. Such a model could apply to some merging cores within the CE, depending on component masses, and to post-CE merging DDs. It depends on the time-scale for the diffusion of the field into the WD envelope.

García-Berro et al. (2012) used the results of a three-dimensional hydrodynamic simulation of merging DDs to argue that a massive hot and differentially rotating convective corona forms around the more massive component and used equipartition arguments to estimate that fields of about  $3 \times 10^{10}$  G could be generated. They also presented a population synthesis study of WDs that formed specifically as merging DDs, assuming a CE energy efficiency parameter  $\alpha = 0.25$ , and showed that there is general agreement with the observed properties of high-mass WDs ( $M_{\text{WD}} > 0.8 M_{\odot}$ ) and HFMWDs. However they did not consider merging when the companion is a non-degenerate star.

We hypothesize that single WDs that demonstrate a strong magnetic field are the result of merging events, so we carry out a comprehensive population synthesis study of merging binary systems for different CE efficiencies  $\alpha$ . We consider all possible

routes that could lead to a single WD. We isolate the WDs formed by the merging of two degenerate cores, either as WDs, a red giant plus a WD or two red giants, from those formed by a giant merging with a main-sequence star and show that the observed properties of the HFMWDs are generally consistent with the CE hypothesis for  $0.1 \leq \alpha \leq 0.3$ . Both groups contribute to the observed distribution but main-sequence companions merging with degenerate cores of giants form most of the HFMWDs.

### 2.3 Common Envelope Evolution and Formulism

When one of the stars in a binary system becomes a giant, it expands and overfills its Roche lobe. Mass transfer soon proceeds typically, but not always, on a dynamical time-scale (Han et al., 2002). The giant envelope rapidly engulfs both the companion star and the core of the donor to form a CE. The two dense cores, that of the giant and the accreting star itself, interact with the envelope, transferring to it orbital energy and angular momentum. The envelope can be partly or wholly ejected and the orbit of the engulfed star shrinks. It is not known how long this process takes but it is generally thought to last for more of a dynamical stellar time-scale than a thermal or nuclear time-scale. It probably has never been observed. If the companion succeeds in fully ejecting the envelope the two cores survive in a binary system with a much smaller separation. If the envelope is not fully ejected the orbit may completely decay and the two stars coalesce. When the envelope of a giant engulfs a degenerate companion the two cores can merge but if the companion is non-degenerate it either merges with the envelope or accretes on to the giant core. When the initial masses of the two stars are within a few percent both can expand to giants at the same time and Roche lobe overflow (RLOF) leads to a double CE.

The CE process was first proposed to explain binary star systems, such as CVs, whose orbital separations are smaller than the original radius of the progenitor primary star. A mechanism was needed to explain how this could occur. The possible existence of CEs was first proposed by Bisnovatyi-Kogan & Sunyaev (1971). Its qualitative description is based on evolutionary necessity rather than mathematical physics. While it is sufficient to explain a variety of exotic stars and binaries that could not otherwise be explained, a full mathematical model has yet to be developed to describe the interaction in detail and to test the various theories.

A simple quantitative model of CEE is the energy or  $\alpha$  formulism (van den Heuvel, 1976). For this the change in orbital energy  $\Delta E_{\text{orb}}$  of the in-spiralling cores is equated to the energy required to eject the envelope to infinity, the binding energy  $E_{\text{bind}}$ . The total orbital energy, kinetic plus potential, of a binary star with masses  $m_1$  and  $m_2$

and separation  $a$  is  $E_{\text{orb}} = -Gm_1m_2/2a$ . However the envelope ejection cannot be completely efficient so Livio & Soker (1988) introduced an efficiency parameter  $\alpha$  to allow for the fraction of the orbital energy actually used to eject the envelope.

$$\Delta E_{\text{orb}} = \alpha E_{\text{bind}}. \quad (2.1)$$

Following Tauris & Dewi (2001) we use a form of the binding energy that depends on the detailed structure of the giant envelope and adopt

$$E_{\text{bind}} = -\frac{Gm_1m_{1,\text{env}}}{\lambda R_1}, \quad (2.2)$$

where  $R_1$  is the radius of the primary envelope. The constant  $\lambda$  was introduced by de Kool (1990) to characterize the envelope structure. Our  $\lambda$  depends on the structure of the particular star under consideration. It is sensitive to how the inner boundary between the envelope and the remnant core is identified (Tauris & Dewi, 2001) and includes the contributions from the thermal energy of the envelope on the assumption that it remains in equilibrium as it is ejected.

The initial orbital energy is that of the secondary star  $m_2$  and the primary core  $m_{1,c}$  at the orbital separation  $a_i$  at the beginning of CEE and is given by

$$E_{\text{orb},i} = -\frac{1}{2} \frac{Gm_{1,c}m_2}{a_i} \quad (2.3)$$

and the final orbital energy is

$$E_{\text{orb},f} = -\frac{1}{2} \frac{Gm_{1,c}m_2}{a_f}, \quad (2.4)$$

where  $a_f$  is the final orbital separation. Thus we have

$$\Delta E_{\text{orb}} = E_{\text{orb},f} - E_{\text{orb},i}. \quad (2.5)$$

From this we can calculate  $a_f$  which is the separation of the new binary if the cores do not merge. If  $a_f$  is so small that either core would overfill its new Roche lobe, then the cores are considered to merge when  $a_f$  is such that the core just fills its Roche lobe. Setting  $a_f$  to this separation we calculate  $E_{\text{orb},f}$  and  $\Delta E_{\text{orb}}$  with equations 2.4 and 2.5.

Then we calculate a final binding energy for the envelope around the merged core

$$E_{\text{bind,f}} = E_{\text{bind,i}} + \frac{\Delta E_{\text{orb}}}{\alpha}. \quad (2.6)$$

Assuming this envelope has a normal giant structure  $R(m, m_c)$  we calculate how much mass must be lost. In the case of a double CE, the initial orbital energy is that of both cores and the binding energies of the two envelopes added.

Some difficulties with the energy formulation arise because  $\alpha$  can depend on the duration of the CE phase. If it lasts longer than a nuclear or thermal time-scale then alterations in the envelope, owing to adjustments in its thermal equilibrium, can change its structure and hence  $\lambda$ . Changes to the energy output from the core, owing to the decreasing weight of the diminishing envelope, can also affect the thermal equilibrium and thence  $\lambda$ . We do not consider these complications in this work. Nor do we include ionization and dissociation energy, as proposed by Han et al. (1994) in the envelope binding energy.

## 2.4 Population synthesis calculations

**Table 2.1:** Stellar types distinguished within the BSE algorithms.

Type	Description
0.	Deep or fully convective low-mass MS star (CS)
1.	Main-sequence star (MS)
2.	Hertzsprung gap star (HG)
3.	First giant branch (RGB)
4.	Core helium Burning
5.	First asymptotic giant branch (early AGB)
6.	Second asymptotic giant branch (late AGB)
7.	Main-sequence naked helium star
8.	Hertzsprung gap naked helium star
9.	Giant branch naked helium star
10.	Helium WD (He CE)
11.	Carbon/oxygen WD (CO WD)
12.	Oxygen/neon WD (ONe WD)
13.	Neutron star
14.	Black hole
15.	Massless supernova/remnant

We evolve synthetic populations of binary star systems from the zero-age main se-

quence (ZAMS). Each system requires three initial parameters, the primary star mass, the secondary star mass and the orbital period. The primary masses  $M_1$  are allocated between 0.8 and  $12.0 M_{\odot}$  and the secondary star masses  $M_2$  between 0.1 and  $12.0 M_{\odot}$ . The binary orbits are specified by a period  $P_0$  at ZAMS between 0.1 and 10 000 d and zero eccentricity. Each parameter was uniformly sampled on a logarithmic scale for 200 divisions. This scheme gives a synthetic population of some 6 million binary systems. We calculate the effective number of actual binary systems by assuming that the primary stars are distributed according to Salpeter’s mass function (Salpeter, 1955)  $N(M) dM \propto M^{-2.35} dM$ , where  $N(M) dM$  is the number of stars with masses between  $M$  and  $M + dM$ , and that the secondary stars follow a flat mass ratio distribution for  $q \leq 1$  (e.g. Ferrario, 2012). The initial period distribution was taken to be logarithmically uniform in the range  $-1 \leq \log_{10} P_0/d \leq 4$ .

Each binary system was evolved from the ZAMS to an age of 9.5 Gyr, taken to be the age of the Galactic disc (e.g. Oswalt et al., 1996; Liu & Chaboyer, 2000), with the rapid binary star evolution (BSE) algorithm developed by Hurley, Tout & Pols (2002). This is an extension of their single star evolution algorithm (Hurley, Pols & Tout, 2000) in which they use analytical formulae to approximate the full numerical hydrodynamic and nuclear evolution of stars. This includes mass-loss episodes during various stages of evolution. The BSE code adds interactions between stars, such as mass transfer, RLOF, CEE, supernova kicks and angular momentum loss by gravitational radiation and magnetic braking as well as tidal interaction. I summarize the type of stars that play a role in the BSE code in Table 2.1.

In the BSE model we use the  $\alpha$  (energy) formalism for CE phases and have taken a fixed  $\lambda = 0.5$  as representative of the range expected for our stars. We take  $\alpha$  to be a free parameter between 0.1 and 0.9. Efficiencies of  $\alpha > 1$  are only possible if additional energy sources are involved in the process. We do not consider this here. We use the full suite of mass-loss rates described by Hurley, Pols & Tout (2000). We found that, in order to generate sufficient low-mass WDs,  $\eta = 1.0$  for Reimers’ mass-loss parameter is necessary so we have used this throughout.

**Table 2.2:** Fraction of binary systems that merge during CE for various values of  $\alpha$ . The fraction of WDs born from merged stars in a single generation of binary systems of age 9.5 Gyr (the age of the Galactic disc) is  $N$ . The remaining six columns give the smallest and the largest parameters on the search grid for systems that are found to have merged. The parameters are the progenitors' ZAMS masses and orbital period.

$\alpha$	$N$ per cent	$M_{1\min}/M_{\odot}$	$M_{2\min}/M_{\odot}$	$P_{0\min}/\text{d}$	$M_{1\max}/M_{\odot}$	$M_{2\max}/M_{\odot}$	$P_{0\max}/\text{d}$
0.05	11.58	1.08	0.10	348.9	11.06	2.77	16.3
0.10	10.35	1.08	0.10	195.6	11.06	2.90	20.5
0.20	8.86	1.08	0.10	97.7	11.21	2.77	20.5
0.25	8.17	1.08	0.10	82.1	11.21	4.06	932.9
0.30	7.55	1.08	0.10	65.2	11.21	4.06	784.3
0.40	6.51	1.08	0.10	48.8	11.21	4.06	587.3
0.50	5.70	1.08	0.10	38.7	11.21	4.06	493.7
0.60	5.06	1.08	0.10	30.7	11.21	4.06	391.7
0.70	4.60	1.08	0.10	25.8	11.21	3.87	195.6
0.80	4.18	1.08	0.10	23.7	11.21	3.12	82.1
0.90	3.75	1.08	0.10	19.3	11.06	4.06	415.0

**Table 2.3:** Fraction of merging DD systems, WDs formed by merging of two degenerate objects outside a CE in a single generation of binary systems of age 9.5 Gyr. Other columns are as in Table 4.1

$\alpha$	$N$ per cent	$M_{1\min}/M_{\odot}$	$M_{2\min}/M_{\odot}$	$P_{0\min}/\text{d}$	$M_{1\max}/M_{\odot}$	$M_{2\max}/M_{\odot}$	$P_{0\max}/\text{d}$
0.05	$4.49 \times 10^{-5}$	2.41	1.79	1867.9	4.21	2.17	3331.3
0.10	$4.89 \times 10^{-4}$	2.02	1.79	1245.9	4.21	2.28	2097.0
0.20	$1.01 \times 10^{-4}$	1.99	1.98	932.9	4.21	2.28	1867.9
0.25	$1.29 \times 10^{-4}$	1.99	1.98	784.3	4.21	2.28	1867.9
0.30	$1.69 \times 10^{-4}$	1.52	1.52	587.3	4.27	2.23	1867.9
0.40	$2.62 \times 10^{-4}$	1.52	1.52	587.3	4.21	2.34	1663.8
0.50	$3.42 \times 10^{-4}$	1.52	1.52	587.3	4.27	2.28	1570.3
0.60	$4.07 \times 10^{-4}$	1.52	1.52	587.3	6.24	1.59	12.2
0.70	$4.36 \times 10^{-4}$	1.52	1.52	587.3	6.33	1.59	11.5
0.80	$4.11 \times 10^{-4}$	1.54	1.52	587.3	6.59	1.71	10.2
0.90	$3.74 \times 10^{-4}$	1.54	1.52	587.3	6.42	1.71	9.7

Alternatively sufficient low-mass WDs could be formed with smaller  $\eta$  if the Galactic disc were somewhat older. Meng et al. (2008) produce them with  $\eta = 0.25$  in populations of 12 Gyr in age. The metallicity is taken to be solar ( $Z = 0.02$ ) in all our calculations.

From all evolved systems we select those that could generate single HFMWDs. To this end we select all pairs of WDs that merge outside any CE and leave a single WD remnant. These are our WD–WD (DD) mergers. Added to these are WD remnants of systems that underwent at least one CE phase and merged during the last CE phase and satisfy two further criteria. Firstly, either one or both of the stars must have a degenerate core before merging and secondly, there must be no further core burning before the remnant WD is exposed. We assume that such a core burning would be convective and destroy any frozen-in high magnetic field.

## 2.5 Population Synthesis Results

Assuming a constant star formation rate, each synthetic population was integrated to the Galactic disc age over the entire parameter space with  $0.05 \leq \alpha \leq 0.9$ . Table 4.1 lists the fraction by type of all binary systems that merge in a CE and Table 2.3 those that merge as DDs in a single generation of stars of age 9.5 Gyr. The tables also show the limits of the parameter space within which the cores merge. The minimum ZAMS masses of the systems that merged and ended their lives as single WDs are listed in the columns  $M_{1_{\min}}$  and  $M_{2_{\min}}$  and the minimum initial period in the column  $P_{0_{\min}}$ . The maximum ZAMS masses and period are shown in the columns  $M_{1_{\max}}$ ,  $M_{2_{\max}}$  and  $P_{0_{\max}}$ . For systems that merge during a CE phase the minimum ZAMS primary mass is determined by the age of the Galactic disc and thus by the time taken by this star to evolve off the main sequence. For the DD route both stars must evolve to WDs. After the last CE episode, the two stars continue their evolution to the WD final stage. The stars are then brought together by gravitational radiation and eventually coalesce. This process takes longer than the CE route. As a consequence, the main-sequence evolution lifetime of the primary star must be shorter and thus the minimum ZAMS mass must be larger than that required to merge during CEE. Otherwise such systems would not be able to coalesce within the age of the Galactic disc.

For low values of  $\alpha$  the envelope clearance efficiency is low and the time for the envelope to exert a drag force on the orbit is largest. Correspondingly, Table 4.1 shows that, for low  $\alpha$ , the number of coalescing stars in the CE is maximal.

As  $\alpha$  increases, the time for ejection of the envelope decreases and the number of systems that merge while still in the CE also decreases. WDs formed from merged stars



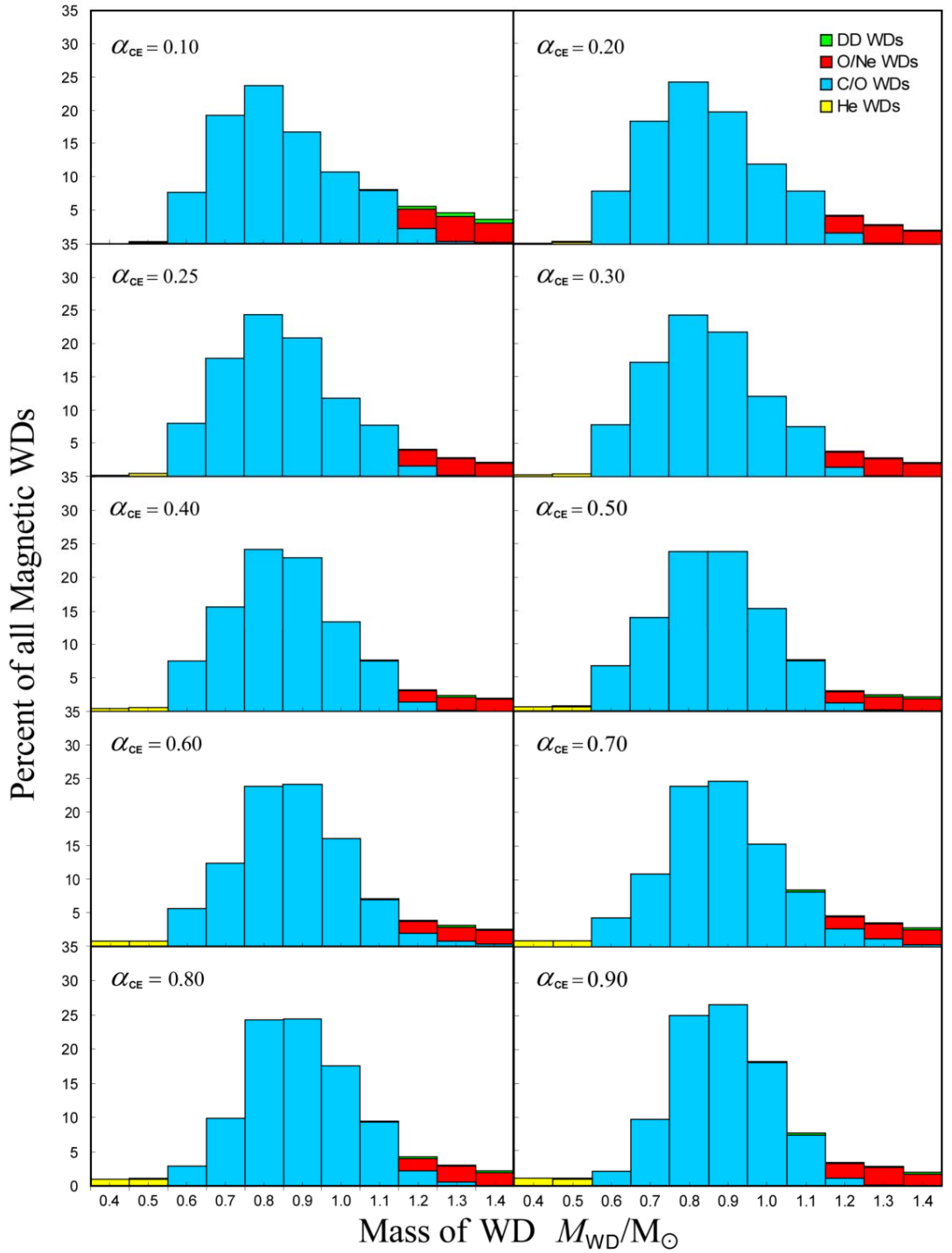


**Figure 2.1:** Theoretical mass distribution of remnant WDs formed by merging for a range of values  $\alpha$  and a Galactic disc age of 9.5 Gyr. "DD WDs" are WDs resulting from DD mergers, "ONe WDs" are Oxygen–Neon WDs, "CO WDs" are Carbon–Oxygen WDs and "He WDs" are Helium WD remnants after merging.

**Table 2.4:** Types and fractions per cent of WDs formed from CE and DD by merging binary systems in a population aged 9.5 Gyr. All DD WDs are of CO type.

$\alpha$	Common envelope			Double degenerate
	He	CO	ONe	CO
0.05	0.04	88.77	11.04	0.15
0.10	0.16	88.73	9.79	1.32
0.20	0.43	92.14	7.08	0.36
0.25	0.55	92.24	6.74	0.47
0.30	0.68	92.10	6.63	0.58
0.40	0.94	92.89	5.42	0.75
0.50	1.20	92.55	5.41	0.84
0.60	1.45	91.70	5.95	0.89
0.70	1.68	91.20	6.27	0.85
0.80	1.92	91.12	6.12	0.84
0.90	2.20	90.42	6.47	0.91

are of the three types He, CO and ONe. The small fraction of He WDs increases with  $\alpha$  while that of the ONe WDs falls. The He WDs originate when RGB stars coalesce with very low-mass main-sequence stars. At low  $\alpha$  these stars merge when there is very little envelope left and the resulting giant can lose the rest of its envelope before helium ignition. As  $\alpha$  is increased, more of the envelope remains after coalescence and the stars pass through core helium burning before being exposed as CO WDs. The ONe WDs form when the most evolved AGB stars coalesce with their companions. These stars have only rather weakly bound envelopes so that as  $\alpha$  is increased more of them emerge from the CE phase detached. For the DD case we find that only CO WDs are formed in the models. Table 2.4 sets out the types and fractions of all WDs that form from CE and DD merging systems as a function of  $\alpha$ . The lack of merged He WDs seems to indicate that, while it is true that very low-mass WDs ( $M \lesssim 0.4 M_{\odot}$ ) must arise from binary interaction, they do not arise from DD mergers within a Galactic disc age of 9.5 Gyr.

### 2.5.1 Example Evolutionary Histories

The precise evolutionary history of a binary system depends on its particular parameters. For example the number of CE events that can occur can vary from one to several

(Hurley, Tout & Pols, 2002). Here we give a few examples to illustrate the difference between CE and DD merging events.

### **Common Envelope Coalescence**

Table 2.5 sets out the evolutionary history of an example system that merges during a CE with  $\alpha = 0.2$ . The progenitors are a primary star S1 of  $4.44 M_{\odot}$  and a secondary S2 of sub-solar mass  $0.72 M_{\odot}$ . At ZAMS the initial period is 219.6 d and the orbit is circular with a separation of  $264.7 R_{\odot}$ . S1 evolves first and reaches the early AGB at 161.77 Myr having lost  $0.02 M_{\odot}$  on the way. Roche lobe overflow starts 0.2 Myr later with mass flowing from S1 to S2. At this point the orbital separation has decreased to  $141.4 R_{\odot}$  because orbital angular momentum has been lost through tidal spin up of S1. A CE develops and the two cores coalesce when their separation reaches  $0.53 R_{\odot}$ . A further  $0.6 M_{\odot}$  of the envelope has been lost. At 162.78 Myr, approximately 0.9 Myr after coalescing, S1 becomes a late stage AGB star. After a further 0.7 Myr it becomes a CO WD.

### **DD coalescence**

In the DD pathway both stars survive the CE without merging and both continue to evolve to WDs approaching each other through gravitational radiation to eventually coalesce. Table 2.6 illustrates this for  $\alpha = 0.1$ . At ZAMS the progenitors are a  $3.7 M_{\odot}$  primary and a  $1.9 M_{\odot}$  secondary with an initial period of 3444 d and a separation of  $1603 R_{\odot}$ , again in a circular orbit. The primary evolves through to a late stage AGB star after 270.5 Myr losing  $0.6 M_{\odot}$  on the way. The separation falls to  $1509 R_{\odot}$ . As a late AGB star S1 loses  $0.9 M_{\odot}$  of which  $0.02 M_{\odot}$  is accreted by S2 from the wind. Approximately 0.5 Myr later, at 271 Myr with S1 of mass  $2.68 M_{\odot}$  and S2  $1.95 M_{\odot}$ , RLOF commences and a CE develops. The orbital separation falls to  $374 R_{\odot}$  when the envelope is ejected. S2 continues to evolve, first as a blue straggler then through the Hertzsprung gap, red giant and core helium burning stages until it becomes an early AGB star at 1513.4 Myr. At 1517.3 Myr RLOF begins again and a second CE forms. At an orbital separation of only  $2.43 R_{\odot}$  the envelope is ejected and S2 emerges as a CO WD of mass  $0.54 M_{\odot}$ . A long period of orbital contraction by gravitational radiation follows until at 9120.8 Myr the two WDs are separated by  $0.04 R_{\odot}$  and RLOF from S2 to S1 begins followed rapidly by coalescence of the DDs. The remnant star is still a CO WD but now of mass  $1.36 M_{\odot}$ .

**Table 2.5:** Evolutionary history of an example binary system that merges during CE.  
 Here  $\alpha = 0.2$ ,  $P_0 = 219.6$  d, S1 is the primary star and S2 is the secondary star.

Stage	Time/Myr	$M_1/M_\odot$	$M_2/M_\odot$	$a/R_\odot$	Remarks
1	0.0000	4.444	0.719	264.679	ZAMS
2	138.1295	4.444	0.719	264.679	S1 becomes a Hertzsprung gap star
3	138.7479	4.444	0.719	264.739	S1 becomes a red giant
4	139.1676	4.443	0.719	179.877	S1 starts core helium burning. Some mass loss occurs
5	161.7637	4.402	0.719	181.495	S1 first AGB
6	161.9691	4.402	0.719	141.380	S1 begins RLOF
7	161.9691	4.524	-	0.529	CE: S1, S2 coalesce; RLOF ends
8	162.8725	4.494	-	-	S1 becomes late AGB
9	163.5543	0.924	-	-	S1 becomes a CO WD

**Table 2.6:** Evolutionary history of an example of WD that formed in a DD coalescence.  
Here  $\alpha = 0.1$ ,  $P_0 = 3144$  days, S1 is the primary star and S2 the secondary star.

Stage	Time/Myr	$M_1/M_\odot$	$M_2/M_\odot$	$a/R_\odot$	Remarks
1	0.0000	3.673	1.928	1603.362	ZAMS
2	222.4734	3.673	1.928	1603.362	S1 becomes a Hertzsprung gap star
3	223.6164	3.673	1.928	1603.416	S1 becomes a Red Giant
4	224.6021	3.672	1.928	1603.678	S1 starts core helium burning
5	268.5530	3.645	1.928	1611.505	S1 becomes early AGB
6	270.4541	3.614	1.928	1583.219	S1 becomes late AGB
7	270.9681	2.682	1.947	1509.115	S1 begins RLOF, mass transfers on to S2, mass loss occurs
8	270.9681	0.821	1.947	374.233	CEE begins, S1 emerges as a CO WD, RLOF ends
9	1260.0681	0.821	1.947	374.233	Begin Blue Straggler phase
10	1267.0548	0.821	1.947	374.233	S2 becomes a Hertzsprung gap star
11	1277.4509	0.821	1.946	374.245	S2 becomes a Red Giant
12	1306.9423	0.821	1.943	375.353	S2 starts core helium burning
13	1513.3615	0.821	1.926	377.768	S2 becomes early AGB
14	1517.2953	0.821	1.913	324.600	S2 begins Roche lobe overflow
15	1517.2953	0.821	0.536	2.433	CEE begins. S2 evolves to a CO WD, RLOF ends
16	9120.8467	0.821	0.536	0.040	S2 begins RLOF
17	9120.8467	1.357	-	0.000	S1, S2 coalesce

**Table 2.7:** The contributions per cent of pre-CE progenitor pairs to theoretical HFMWDs when  $\alpha = 0.1$ . The stellar type ‘CS’ is a deeply or fully convective low-mass main sequence star (see Table 2.1).

Progenitor pairs	Fraction per cent
AGB/MS	60.96
AGB/CS	17.00
RGB/CO WD	14.00
AGB/HG	2.72
AGB/CO WD	2.21
CO WD/CO WD	1.32
RGB/RGB	0.97
RGB/AGB	0.46
RGB/CS	0.16
AGB/AGB	0.20

### 2.5.2 *Mass distribution of the synthetic population*

With the selected CE and DD merged systems we generate a population of putative MWDs by integration over time from  $t = 0$  to 9.5 Gyr, our chosen age for the Galactic disc. The star formation rate is taken to be constant over the lifetime of the Galactic disc. Whereas Tables 4.1 and 2.3 show the relative numbers of merged WDs from a single generation of binary stars, continuous star formation over the lifetime of the Galaxy builds up a population of WDs that favours higher-mass systems because at lower-mass, especially in later generations, they do not have enough time to evolve. Similarly, the slow orbital contraction by gravitational radiation means that potential DD coalescence in later generations is not complete and the fraction of those WDs is further reduced in the present day population. Fig. 2.1 shows the mass distribution for CO, ONe and DD WDs in a present day population formed over the age of the Galactic disc, 9.5 Gyr. Fig. 2.2 shows the contributions from the various pre-CE progenitor pairs that formed the post-CE WDs either through the CE or DD path when  $\alpha = 0.1$ . Other paths also contribute but to less than 3 per cent of the total each. Table 4.5 lists their contributions summed over all WD masses.

In order to calculate the incidence of HFMWDs we used the same BSE code to model single star evolution through to the WD stage also for a Galactic disc age of 9.5 Gyr under the assumption that all WDs originating from single star evolution are non-magnetic.. Table 2.8 sets out the incidence of HFMWDs as a percentage of the incidence of field WDs for a range of  $\alpha$ .

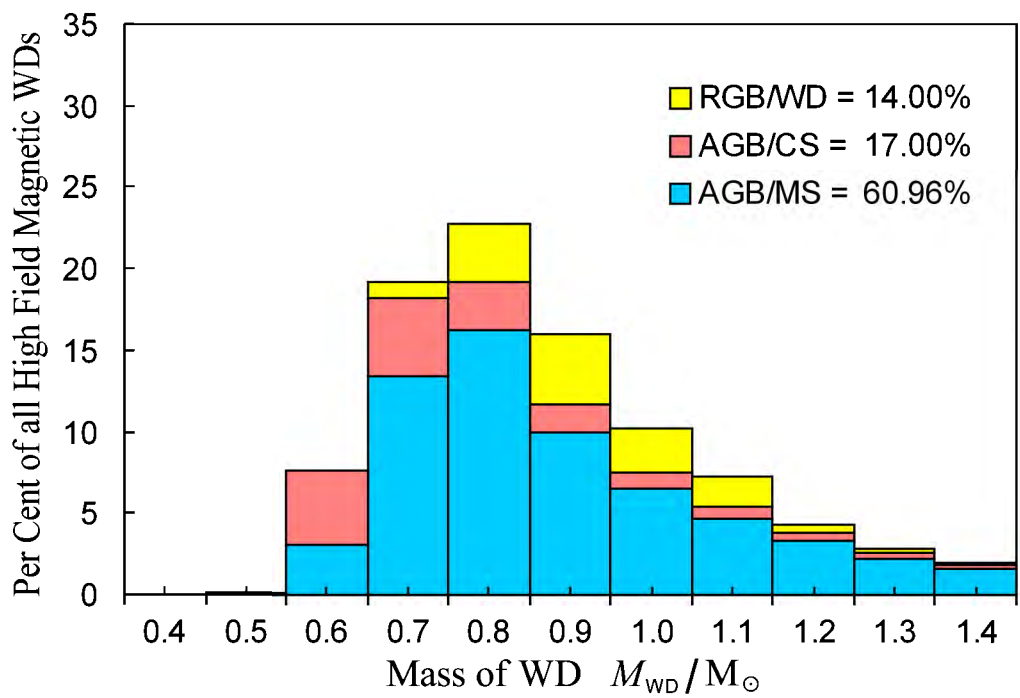


**Figure 2.2:** Mass distribution of theoretical HFMWDs for  $\alpha = 0.10$  separated according to their pre-CE progenitors. Other paths also contribute but are less than 1 per cent of the total. The Galactic disc age is chosen to be 9.5 Gyr. The stellar types are identified in Table 2.1.

**Table 2.8:** The theoretical incidence of HFMWDs as a fraction of magnetic to non-magnetic field WDs as a function of the CE efficiency parameter  $\alpha$ .

$\alpha$	HFMWDs per cent		
	CE	DD	Total
0.05	21.63	$3.16 \times 10^{-2}$	21.67
0.10	18.99	$2.58 \times 10^{-1}$	19.25
0.20	16.12	$5.80 \times 10^{-1}$	16.18
0.25	14.78	$7.02 \times 10^{-2}$	14.85
0.30	13.50	$8.03 \times 10^{-2}$	13.58
0.40	11.85	$8.80 \times 10^{-2}$	11.67
0.50	10.10	$8.64 \times 10^{-2}$	10.18
0.60	8.94	$8.11 \times 10^{-2}$	9.02
0.70	8.15	$7.01 \times 10^{-2}$	8.22
0.80	18.99	$6.33 \times 10^{-2}$	7.50
0.90	18.99	$6.24 \times 10^{-2}$	6.78

## 2.6 Comparison with observations

We compare our theoretical predictions with observations of HFMWDs. Our comparison includes (i) the incidence of magnetism among single WDs and (ii) the mass distribution of single HFMWDs. This is not a simple task because the observational data base of HFMWDs is a mixed bag of objects from many different ground and spaceborne surveys. It is plagued by observational biases. In magnitude-limited surveys, such as the Palomar-Green (PG) or the Hamburg-Schmidt surveys, one of the biases against the detection of magnetic WDs has been that since these are generally more massive than their non-magnetic counterparts (Liebert, 1988), their radii are smaller and therefore they are less luminous. Similar biases would also apply to UV and X-ray surveys. However Liebert, Bergeron & Holberg (2003) have argued that, in any *explicitly magnitude-limited survey*, it may be possible to correct for the difference in search volume for the MWDs. Thus a re-analysis of the data of the PG survey, that took into account the different volumes that are sampled by different mass WDs, gave an estimate for the fraction of HFMWDs of at least  $7.9 \pm 3$  per cent (Liebert, Bergeron & Holberg, 2003). Volume-limited samples are expected to be less affected by the ra-



dius bias but contain very few MWDs with known masses or temperatures. A nearly complete volume-limited sample of nearby WDs by Kawka et al. (2007) shows that up to  $21 \pm 8$  per cent of all WDs within 13 pc have magnetic fields greater than about 3 kG and  $11 \pm 5$  per cent are HFMWDs with  $B \geq 1$  MG.

The synthetic population generated by `bse` is a volume-limited sample and so is not directly comparable with a magnitude limited sample such as the Sloan Digital Sky Survey Data Release 7 (SDSS DR7) WD catalogue (Kleinman et al., 2013) which has 12 803 members. Liebert, Bergeron & Holberg (2003) estimated that the limiting distance to which a WD can be found in a magnitude-limited survey is proportional to its radius  $R_{\text{WD}}$ . Thus the survey volume for a given mass scales as  $R_{\text{WD}}^3$ . We correct this bias by weighting each WD found by the SDSS in proportion to  $1.0/R_{\text{WD}}^3$  relative to the radius of a  $0.8 M_{\odot}$  WD. The cumulative distribution function (CDF) for the corrected mass distribution along with the CDF for the uncorrected mass distribution of the SDSS WDs is shown in Fig. 2.3. The theoretical CDF obtained with `bse` for the mass distribution of single WDs is shown for comparison.

We note that the `bse` code we use does not produce low-mass WDs because of the limited age of the Galactic disc. However Han et al. (1994) and Meng et al. (2008) have constructed single star models using different assumptions utilizing a superwind that produces low-mass WDs in older populations. This is also reflected in the inability of the `bse` results to demonstrate the existence of a significant fraction of low-mass He WDs.

From a theoretical point of view the problem of the determination of surface gravities and masses from line spectra of HFMWDs has also proved to be insoluble, except for low-field objects ( $B \lesssim 3$  MG) for which one can assume that the magnetic field does not affect the atmospheric structure. In these objects the field broadening is negligible and standard zero-field Stark broadening theories can be used to calculate the line wings (e.g. Ferrario et al., 1998) and thus to determine the mass of the MWD. In principle it should also be possible to use stationary field components that are insensitive to field structure to estimate gravities from line profiles for HFMWDs. Regrettably this is not yet possible because a full theory of Stark broadening in the presence of crossed electric and magnetic fields (Main et al., 1998) has not yet been developed. For now, reliable mass determinations are only available for a few low-field MWDs, for MWDs which have good trigonometric parallaxes and MWDs with WD companions whose atmospheric parameters can be established (e.g. RE J0317-853, Barstow et al., 1995; Ferrario et al., 1997b). Currently there are 34 known MWDs with reasonably accurately determined masses with magnetic fields stronger than  $10^5$  G. These are listed in Table 2.9 with their poloidal magnetic field strengths, effective temperatures,

masses and references in the literature. If we restrict ourselves to the HFMWDs with  $B > 1$  MG we end up with 29 objects. When comparing with our models we exclude a further two extremely low-mass WDs because it is not possible to form these within the BSE formalism. The most recent additions to this list are the two common proper motion pairs from the SDSS reported by Dobbie et al. (2013). We shall test our hypothesis on this restricted mass sample with the caveat that we may well be still neglecting observational biases. We also note that the observational sample is neither volume nor magnitude limited.

**Table 2.9:** Known HFMWDs with poloidal field strength  $B_{\text{pol}} \geq 10^5$  G. In comparison with our models we exclude five of these WDs with  $B_{\text{pol}} < 1$  MG (1, 3, 18, 20 & 32) and two of extremely low mass (19 & 29) that cannot be formed within the BSE formalism.

No.	White Dwarf	Aliases	$B_{\text{pol}}/\text{MG}$	$T_{\text{eff}}/\text{K}$	Mass/ $M_{\odot}$	References
1	0009+501	LHS 1038, G217-037, GR381	$\lesssim 0.2$	$6540 \pm 150$	$0.74 \pm 0.04$	1,23
2	0011-134	LHS 1044, G158-45	$16.7 \pm 0.6$	$3010 \pm 120$	$0.71 \pm 0.07$	2,3
3	0257+080	LHS 5064, GR 476	$\approx 0.3$	$6680 \pm 150$	$0.57 \pm 0.09$	2
4	0325-857	EUVE J0317-855	185 – 450	33000	$1.34 \pm 0.03$	4
5	0503-174	LHS 1734, LP 777-001	$7.3 \pm 0.2$	$5300 \pm 120$	$0.37 \pm 0.07$	2,3
6	0584-001	G99-37	$\approx 10$	$6070 \pm 100$	$0.69 \pm 0.02$	5,6,7
7	0553+053	G99-47	$20 \pm 3$	$5790 \pm 110$	$0.71 \pm 0.03$	2,7,8
8	0637+477	GD 77	$1.2 \pm 0.2$	$14870 \pm 120$	0.69	9,10
9	0745+304	SDSS J074853.07+302543.5	11.4	$21000 \pm 2000$	$0.81 \pm 0.09$	44
10	0821-252	EUVE J0823-254	2.8 – 3.5	$43200 \pm 1000$	$1.20 \pm 0.04$	11
11	0837+199	EG 061 <sup>b</sup> , LB 393	$\approx 3$	$17100 \pm 350$	$0.817 \pm 0.032$	12
12	0912+536	G195-19	100	$7160 \pm 190$	$0.75 \pm 0.02$	2,13,14
13		SDSS J092646.88+132134.5	$210 \pm 25$	$9500 \pm 500$	$0.62 \pm 0.10$	15
14	0945+246	LB11146 <sup>a</sup>	670	$16000 \pm 2000$	0.90 (+0.10, -0.14)	16,17
15	1026+117	LHS 2273	18	$7160 \pm 190$	0.59	18
16	1220+234	PG1220+234	3	26540	0.81	19
17	1300+590	SDSS J13033.48+590407.0	$\approx 6$	$6300 \pm 300$	$0.54 \pm 0.06$	20
18	1328+307	G165-7	0.65	$6440 \pm 210$	$0.57 \pm 0.17$	21
19	1300+015	G62-46	$7.36 \pm 0.11$	6040	0.25	22
20	1350-090	LP 907-037	$\lesssim 0.3$	$9520 \pm 140$	$0.83 \pm 0.03$	23,24

No.	White Dwarf	Aliases	$B_{\text{pol}}/\text{MG}$	$T_{\text{eff}}/\text{K}$	Mass/ $M_{\odot}$	References
21	1440+753	EUVE J1439+750 <sup>a</sup>	14 – 16	20000-50000	1.04 (+0.88, -1.19)	25
22	1503-070	GD 175 <sup>a</sup>	2.3	6990	0.70 ± 0.13	2
23		SDSS J150746.80+520958.0	65.2 ± 0.3	18000 ± 1000	0.99 ± 0.05	15
24		SDSS J150813.24+394504.0	18.9	18000 ± 2000	0.88 ± 0.06	44
25	1533-057	PG 1355-057	31 ± 3	20000 ± 1040	0.94 ± 0.18	26,27,25
26	1639+537	GD 356, GR 329	13	7510 ± 210	0.67 ± 0.07	2,28,29,45
27	1658+440	1658+440, FBS 376	2.3 ± 0.2	30510 ± 200	1.31 ± 0.02	11,30
28	1748+708	G240-72	≥ 100	5590 ± 90	0.81 ± 0.01	2,5
29	1818+126	G141-2 <sup>a</sup>	≈ 3	6340 ± 130	0.26 ± 0.12	18,31
30	1829+547	G227-35	170 – 180	6280 ± 140	0.90 ± 0.07	2,8
31	1900+705	AC +70°8247, GW +70°8247 EG 129, GL 742, LHS 3424	320 ± 20	16000	0.95 ± 0.02	2,32,33,34,35,36
32	1953-011	G92-40, LTT 7879, GL 772 LP 634-001, EG 135, LHS 3501	0.1 – 0.5	7920 ± 200	0.74 ± 0.03	2,37,38
33	2010+310	GD 229, GR 333	300 – 700	16000	1.10-1.20	33,35,39,40,41,42
34	2329+267	PG 2329+267, EG 161	2.31 ± 0.59	9400 ± 240	0.61 ± 0.16	2,43,24

<sup>a</sup> Unresolved DD, <sup>b</sup> Praesepe (M44, NGC 2632)

**References:** (1) Valyavin et al. (2005); (2) Bergeron, Ruiz & Leggett (2001); (3) Bergeron, Ruiz & Leggett (1992); (4) Vennes et al. (2003); (5) Angel (1978); (6) Dufour et al. (2005); (7) Pragal & Bues (1989); (8) Putney & Jordan (1995); (9) Schmidt, Stockman, Smith (1992); (10) Giovannini et al. (1998); (11) Ferrario et al. (1998); (12) Vanlandingham et al. (2005); (13) Angel (1977); (14) Angel, Illing & Landstreet (1972); (15) Dobbie et al. (2012); (16) Glenn et al. (1994); (17) Liebert et al. (1993); (18) Bergeron, Ruiz & Leggett (1997); (19) Liebert, Bergeron & Holberg (2003); (20) Girven et al. (2010); (21) Dufour et al. (2006); (22) Bergeron, Ruiz & Leggett (1993); (23) Schmidt & Smith (1994); (24) Liebert, Bergeron, Holberg (2005); (25) Vennes et al. (1999); (26) Liebert et al. (1985); (27) Achilleos & Wickramasinghe (1989); (28) Ferrario et al. (1997a); (29) Brinkworth et al. (2004); (30) Schmidt et al. (1992); (31) Greenstein (1986); (32) Wickramasinghe & Ferrario (1988); (33) Wickramasinghe & Ferrario (2000); (34) Jordan (1992); (35) Angel, Liebert & Stockman (1985); (36) Greenstein et al. (1985); (37) Maxted et al. (2000); (38) Brinkworth et al. (2005); (39) Green & Liebert (1981); (40) Schmidt, Latter & Folz (1990); (41) Schmidt et al. (1996); (42) Jordan et al. (1998); (43) Moran et al. (1998); (44) Dobbie et al. (2013). (45) Ferrario et al. (1997a).

The comparison of the mass distribution between theory and observations is shown in Fig. 2.4. Most of our models reproduce the observed peak near  $0.8 M_{\odot}$  but are less successful at reproducing the higher and lower mass tails. Interestingly the peak is dominated by giant cores that merge with main-sequence stars. This case was not considered by García-Berro et al. (2012) who focused only on merging DDs. We used a Kolmogorov-Smirnov (K–S) test (Press et al., 1992) to compare the mass distribution of the observed HFMWDs with our synthetic populations. The K–S test determines the statistical probability that two sample sets are drawn from the same population. It uses the CDFs of the two sample sets which naturally agree at the smallest value of an independent variable where they are both zero and again at its maximum where they are both unity. The test then uses the intervening behaviour to distinguish the populations. The test gives a statistic  $D$  which is the maximum of the absolute difference between two CDFs at a given  $M_{\text{WD}}$  and the probability  $P$  that a random selection from the population would lead to a larger  $D$  than that measured.

Fig. 2.5 shows the mass distribution CDFs for the 27 observed HFMWDs (jagged line) and for the 12 803 SDSS DR7 field WDs (smooth curve). A visual inspection shows the two CDFs to be distinctly different. The K–S test gives a  $D = 0.4417$  and  $P = 3 \times 10^{-5}$ . So we deduce that HFMWD masses are not distributed in the same manner as non-magnetic single WDs. When the CDF for the observed HFMWD mass distribution is compared to the CDF for the  $\text{BSE}$  theoretical mass distribution (Fig. 2.6) for  $\alpha = 0.10$  it can be seen that the two curves are remarkably similar. The K–S test gives a smaller  $D$  of 0.1512 with a probability of 0.7095 that indicates success of our model. The results of the K–S test for a range of  $\alpha$ s (Table 2.10) show that the mass distribution is consistent over the wide range  $0.05 \leq \alpha \leq 0.7$ . On the other hand, based on the results in Table 2.8 the observed incidence of magnetism, as observed in the Kawka et al. (2007) volume-limited sample, constrains  $\alpha$  to be in the narrower range  $0.1 \leq \alpha \leq 0.3$ .

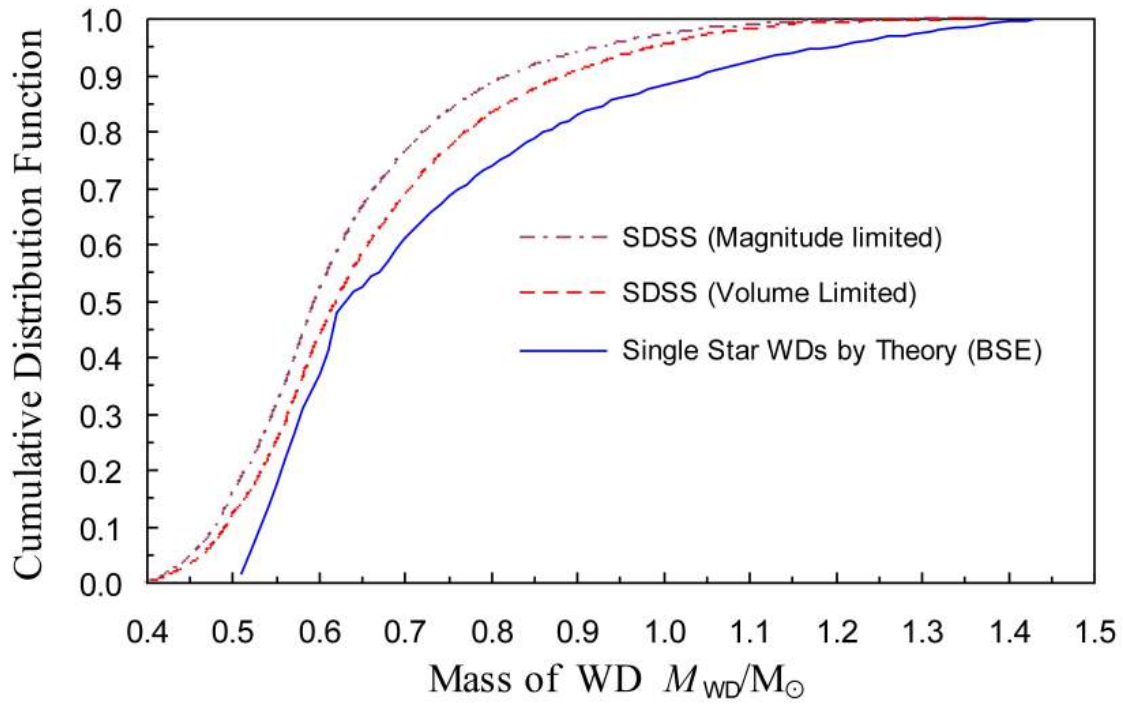


**Figure 2.3:** CDFs of masses of observed SDSS DR7 (Kleinman et al., 2013) non-magnetic, magnitude-limited and converted-volume-limited field WDs and the theoretical (BSE) volume-limited population of non-magnetic WDs from single star evolution for a Galactic disc age of 9.5 Gyr.

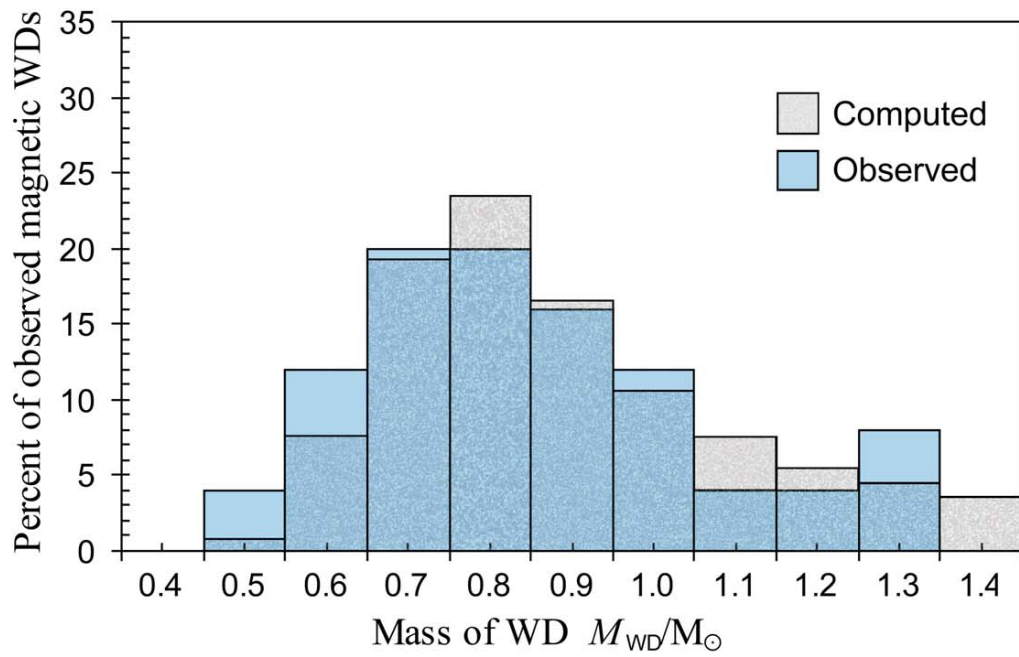


**Figure 2.4:** Mass distribution of 27 observed HFMWDs (objects taken from Table 2.9) compared with the computed sample.

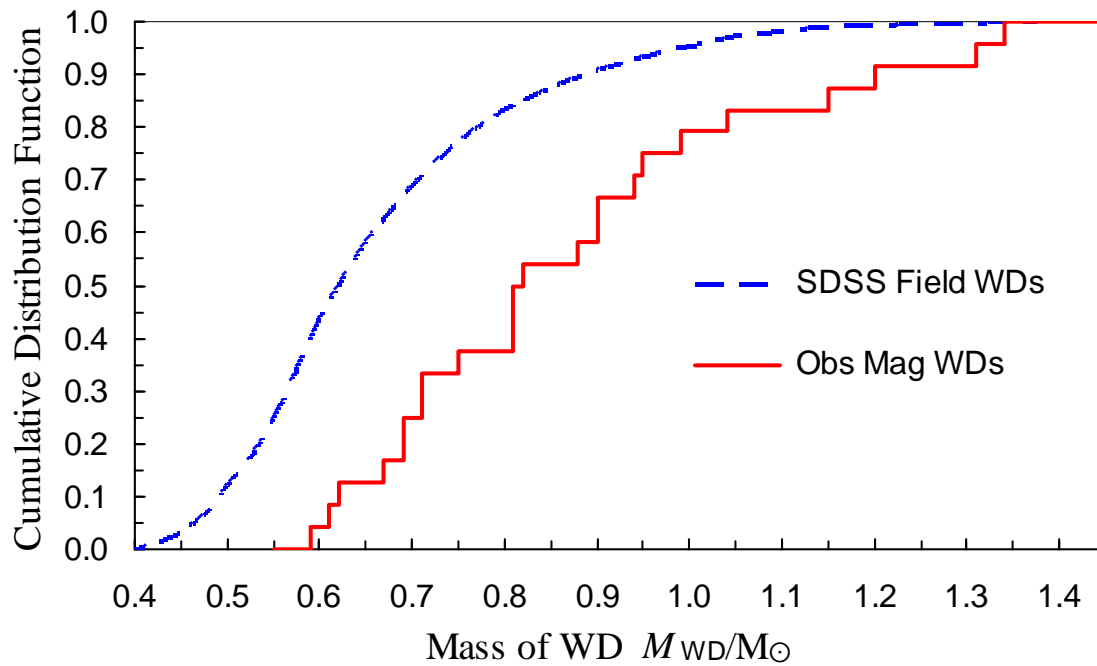


**Figure 2.5:** CDFs of volume-limited-converted masses of observed SDSS DR7 (Kleinman et al., 2013) non-magnetic, field WDs and the observed MWDs. The population of observed MWDs is not strictly a volume limited sample since it comes from various surveys as discussed in the text. A formal application of the K–S test has  $D = 0.4417$  and  $P = 3 \times 10^{-5}$ .



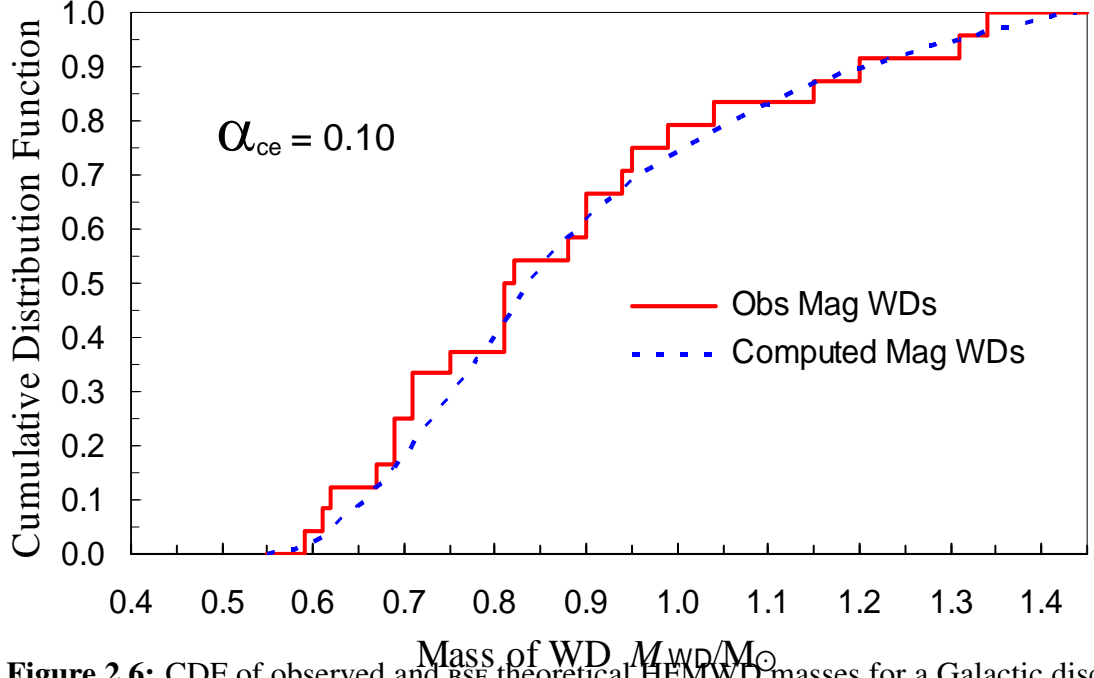


**Figure 2.6:** CDF of observed and bse theoretical HFMWD masses for a Galactic disc age of 9.5 Gyr and  $\alpha = 0.10$ . The K-S test has  $D = 0.1512$  and  $P = 0.7095$ .

**Table 2.10:** Kolmogorov-Smirnov  $D$  statistic and  $P$  of the mass distributions of the theoretical (bse) and observed MWD populations being drawn from the same distribution for various values of  $\alpha$ . The theoretical population is for a Galactic disc age of 9.5 Gyr.

$\alpha$	$D$	$P$
0.05	0.1558	0.6735
0.10	0.1512	0.7095
0.20	0.1565	0.6684
0.25	0.1616	0.6288
0.30	0.1675	0.5824
0.40	0.1827	0.4700
0.50	0.2040	0.3326
0.60	0.2304	0.2039
0.70	0.2580	0.1144
0.80	0.2814	0.0665
0.90	0.2915	0.0518

## 2.7 Discussion and Conclusions

Two competing models for the origin of strong magnetic fields in WDs are broadly the fossil field model and the merging star model. The proponents of the fossil field model have noted that the maximum poloidal flux observed in the magnetic Ap and Bp stars is similar to the maximum poloidal magnetic flux observed in the MWDs. The two groups of stars could therefore be evolutionarily linked. However, to date, there have been no stellar evolution models that have shown how a strong fossil magnetic flux can survive through the various stages of stellar evolution through to the WD phase. It is also not clear if the similarities in the maximum magnetic fluxes between two groups of stars is necessarily a reason to assume a causal link. The dynamo model of Wickramasinghe, Tout & Ferrario (2014) suggests that similar maximum magnetic fluxes may be expected for physical reasons if the fields are generated from differential rotation caused by merging. Here we have explored the consequences of such a hypothesis for the origin of the HFMWDs with binary population synthesis under standard assumptions, discussed in section 4.4. We have found the following.

- (i) While the mass distribution of HFMWDs is not very sensitive to  $\alpha$ , good agreement can be obtained with both the observed mass distribution and the observed incidence of magnetism for models with  $0.1 \leq \alpha \leq 0.3$ . In particular the mean predicted mass of HFMWDs is  $0.88 M_{\odot}$  compared with  $0.64 M_{\odot}$  (corrected to include observational biases) for all WDs while observations indicate respective mean masses of  $0.85 M_{\odot}$  (see also Kepler et al., 2013) and  $0.62 M_{\odot}$  (Kleinman et al., 2013). A K–S test shows that the small number of reliably measured masses of HFMWDs are not distributed in the same way as the masses of non-magnetic single WDs. The probability they are is only  $3 \times 10^{-5}$ . On the other hand our best model fit to the observed mass distribution of HFMWDs has a probability of 0.71.
- (ii) Stars that merge during CEE and then evolve to become WDs outnumber merging post-CE DD systems for all  $\alpha$ . The CEs yield mainly CO WDs with a few He and ONe WDs, while the DDs yield only CO WDs.
- (iii) The major contribution to the observed population of HFMWDs comes from main-sequence stars merging with degenerate cores at the end of CEE. The resulting giants go on to evolve to HFMWDs.
- (iv) The merging DDs tend mostly to populate the high-mass end of the WD mass distribution.

We also note that the study by Zorotovic et al. (2010) of the evolution of a sample of SDSS post-CE binary stars consisting of a WD and a main-sequence star indicates that the best agreement with observational data is achieved when  $\alpha = 0.25$  and this is consistent with our findings. In summary, available observations of the mass distribution and incidence of HFMWDs are compatible with the hypothesis that they arise from stars that merge mostly during CEE with a few that merge during post-CE as DD systems. Our calculations, when taken together with the observation that there are no examples of HFMWDs in wide binary systems, allow us to argue strongly in favour of this hypothesis. In the majority of cases the fields may be generated by a dynamo mechanism of the type recently proposed by Wickramasinghe, Tout & Ferrario (2014). The disc field model of Nordhaus et al. (2011) or the model proposed by García-Berro et al. (2012) may be relevant in the case of merging DD cores depending on mass ratio. The rate of merging of post-CE DDs alone is too low to account for all observed HFMWDs.

## **Acknowledgements**

We would like to thank the Referee, Zhanwen Han, for his suggestions and comments which have helped me improving the quality of this work. GPB gratefully acknowledges receipt of an Australian Postgraduate Award. CAT thanks the Australian National University for supporting a visit as a Research Visitor of its Mathematical Sciences Institute, Monash University for support as a KevinWatford distinguished visitor and Churchill College for his fellowship.



# Chapter 3

## Genesis of the Magnetic Field

This chapter is a reproduction of the paper accepted for publication in Monthly Notices of the Royal Astronomical Society, viz:

*Briggs, Ferrario, Tout & Wickramasinghe, MNRAS (2018), (In publication). Genesis of magnetic fields in isolated white dwarfs*

### 3.1 Abstract

A dynamo mechanism driven by differential rotation when stars merge has been proposed to explain the presence of strong fields in certain classes of magnetic stars. In the case of the HFMWDs, the site of the differential rotation has been variously thought to be the CE, the hot outer regions of a merged degenerate core or an accretion disc formed by a tidally disrupted companion that is subsequently accreted by a degenerate core. We have shown previously that the observed incidence of magnetism and the mass distribution in HFMWDs are consistent with the hypothesis that they are the result of merging binaries during CEE. Here we calculate the magnetic field strengths generated by CE interactions for synthetic populations using a simple prescription for the generation of fields and find that the observed magnetic field distribution is also consistent with the stellar merging hypothesis. We use the Kolmogorov-Smirnov K-S test to study the correlation between the calculated and the observed field strengths and find that it is consistent for low envelope ejection efficiency. We also suggest that field generation by the plunging of a giant gaseous planet on to a WD may explain why magnetism among cool WDs (including DZ WDs) is higher than among hot WDs. In this picture a super-Jupiter residing in the outer regions of the WD's planetary system is perturbed into a highly eccentric orbit by a close stellar encounter and is later accreted by the WDs.

## 3.2 Introduction

The existence of strong magnetic fields in stars at any phase of their evolution is still largely unexplained and very puzzling (see Ferrario et al., 2015a; Wickramasinghe & Ferrario, 2000). HFMWDs have dipolar magnetic field strengths of up to  $10^9$  G. There are no observed HFMWDs with late-type companions found in wide binary systems. Liebert et al. (2005, 2015a) pointed out that this contrasts with non-magnetic WDs, a large fraction of which are found in such systems. This led Tout et al. (2008) to hypothesise that the entire class of HFMWDs with fields  $10^6 < B/G < 10^9$  owe their magnetic fields to binary systems which have merged while in a CE stage of evolution. In this scenario, when one of the two stars in a binary evolves to become a giant or a super-giant its expanded outer layers fill its Roche lobe. At this point unstable mass transfer leads to a state in which the giant's envelope engulfs the companion star as well as its own core. This merging idea to explain the origin of fields in WDs is now favoured over the fossil field hypothesis first suggested by Woltjer (1964) and Landstreet (1967) whereby the the magnetic main-sequence Ap and Bp stars are the ancestors of the HFMWDs if magnetic flux is conserved all the way to the compact star phase (see also Tout et al., 2004; Wickramasinghe & Ferrario, 2005, and references therein).

During CEE, frictional drag forces acting on the cores and the envelope cause the orbit to decay. The two cores spiral together losing energy and angular momentum which are transferred to the differentially revolving CE, part of which at least, is ejected from the system. This process is thought to proceed on a dynamical time scale of less than a few thousand years and hence has never been observed. The original model of Tout et al. (2008) suggested that high fields were generated by a dynamo between the CE and the outer layers of the proto-WD before the CE is ejected. If the cores merge the resulting giant star eventually loses its envelope to reveal a single HFMWD. If the envelope is ejected when the cores are close but have not merged a magnetic CV is formed. Potter & Tout (2010) found problems with this scenario in that the time-scale for diffusion of the field into the WD is significantly longer than the expected CE lifetime. Instead Wickramasinghe, Tout & Ferrario (2014) suggested that a weak seed field is intensified by the action of a dynamo arising from the differential rotation in the merged object as it forms. This dynamo predicts a poloidal magnetic flux that depends only on the initial differential rotation and is independent of the initial field. Nordhaus et al. (2011) suggested another model where magnetic fields generated in an accretion disc formed from a tidally disrupted low-mass companion are advected onto the surface of the proto-WD. However, this would once again depend on the time-scale for diffusion of the field into the surface layers of the WD. García-Berro et al.

(2012) found that a field of about  $3 \times 10^{10}$  G could be created from a massive, hot and differentially rotating corona forming around a merged DD. They also carried out a population synthesis study of merging DDs with a CE efficiency factor  $\alpha = 0.25$ . They achieved good agreement in the observed properties between high-mass WDs ( $M_{\text{WD}} \geq 0.8M_{\odot}$ ) and HFMWDs but their studies did not include degenerate cores merging with non-degenerate companions as I did in chapter 2.

The stellar merging hypothesis may only apply to HFMWDs. Landstreet et al. (2012) point out that weak fields of  $B \leq 1$  kG may exist in most WDs and so probably arise in the course of normal stellar evolution from a dynamo action between the core and envelope.

With population synthesis we showed, in chapter 2 that the origin of HFMWDs is consistent with the stellar merging hypothesis. The calculations presented in chapter 2 could explain the observed incidence of magnetism among WDs and showed that the computed mass distribution fits the observed mass distribution of the HFMWDs more closely than it fits the mass distribution of non-magnetic WDs. This demonstrated that magnetic and non-magnetic WDs belong to two populations with different progenitors. We now present the results of calculations of the magnetic field strength expected from merging binary star systems.

### 3.3 Population synthesis calculations

As described in chapter 2, we create a population of binary systems by evolving them from the zero-age main sequence (ZAMS) to 9.5 Gyr, the age of the Galactic disc (Kilic et al., 2017). Often an age of 12 Gyr is assumed when population synthesis studies are carried out but an integration age of 12 Gyr, that encompasses not only the thin and thick disc but also the inner halo, would be far too large for our studies of the origin of HFMWDs. The HFMWDs belong to the thin disc population, according to the kinematic studies of HFMWDs by Sion et al. (1988) and Anselowitz et al. (1999), who found that HFMWDs come from a young stellar disc population characterised by small motions with respect to the Sun and a dearth of genuine old disc and halo space velocities. The more recent studies of the WDs within 20 pc of the Sun by Sion et al. (2009) also support the earlier findings and show that the HFMWDs in the local sample have significantly lower space velocities than non-magnetic WDs.

We use the rapid binary stellar evolution algorithm `BSE` developed by Hurley, Tout & Pols (2002) that allows modelling of the most intricate binary evolution. This algorithm includes not only all those features that characterise the evolution of single stars (Hurley, Pols & Tout, 2000) but also all major phenomena pertinent to binary evolu-

tion. These comprise Roche lobe overflow, CEE (Paczynski, 1976), tidal interaction, collisions, gravitational radiation and magnetic braking.

As in chapter 2, we have three initial parameters. The mass of the primary star  $0.8 \leq M_1/M_\odot \leq 12.0$ , the mass of its companion  $0.1 \leq M_2/M_\odot \leq 12.0$  and the orbital period  $0.1 \leq P_0/d \leq 10\,000$ . These initial parameters are on a logarithmic scale of 200 divisions. We then compute the real number of binaries assuming that the initial mass of the primary star is distributed according to Salpeter's (1955) mass function and the companion's mass according to a flat mass ratio distribution with  $q \leq 1$  (e.g. Hurley, Tout & Pols, 2002; Ferrario, 2012). The period distribution is taken to be uniform in its logarithm. We use the efficiency parameter  $\alpha$  (energy) formalism for the CE phases with  $\alpha$  taken as a free parameter between 0.1 and 0.9. In our calculations we have used  $\eta = 1.0$  for the Reimers' mass-loss parameter and a stellar metallicity  $Z = 0.02$ . We select a sub-population consisting of single WDs that formed by merging during CEE. Conditions of the selection are that (i) at the beginning of CEE the primary has a degenerate core to ensure that any magnetic field formed or amplified during CE persists in a frozen-in state and (ii) from the end of CE to the final WD stage there is no further nuclear burning in the core of the pre-WD star which would otherwise induce convection that would destroy any frozen-in magnetic field. In addition to stellar merging during CE, we also select double WD binaries whose components merge to form a single WD at any time after the last CEE up to the age of the Galactic disc. This forms the DD merging channel for the formation of HFMWDs.

### 3.3.1 *Theoretical magnetic field strength*

The goal of this chapter is to construct the magnetic field distribution of our synthetic sample of HFMWDs using, as a basis, the results and ideas set out by Tout et al. (2008) and Wickramasinghe, Tout & Ferrario (2014). If the cores of the two stars do not merge during CE, Our assumption is that a fraction of the maximum angular momentum available at the point of the ejection of the envelope causes the shear necessary to generate the magnetic field. The non-merging case, leading to the formation of MCVs, is presented in chapter 4. In the case of coalescing cores, a fraction of the break-up angular momentum of the resulting degenerate core provides the shear required to give rise to the strongest fields. In the following sections and in chapter 4 we show that our models indeed show that the highest fields are generated when two stars merge and give rise to a HFMWD.

Having obtained the actual number of WDs we then assign a magnetic field  $B$  to each. Our prescription is that the field, generated and acquired by the WD during CE



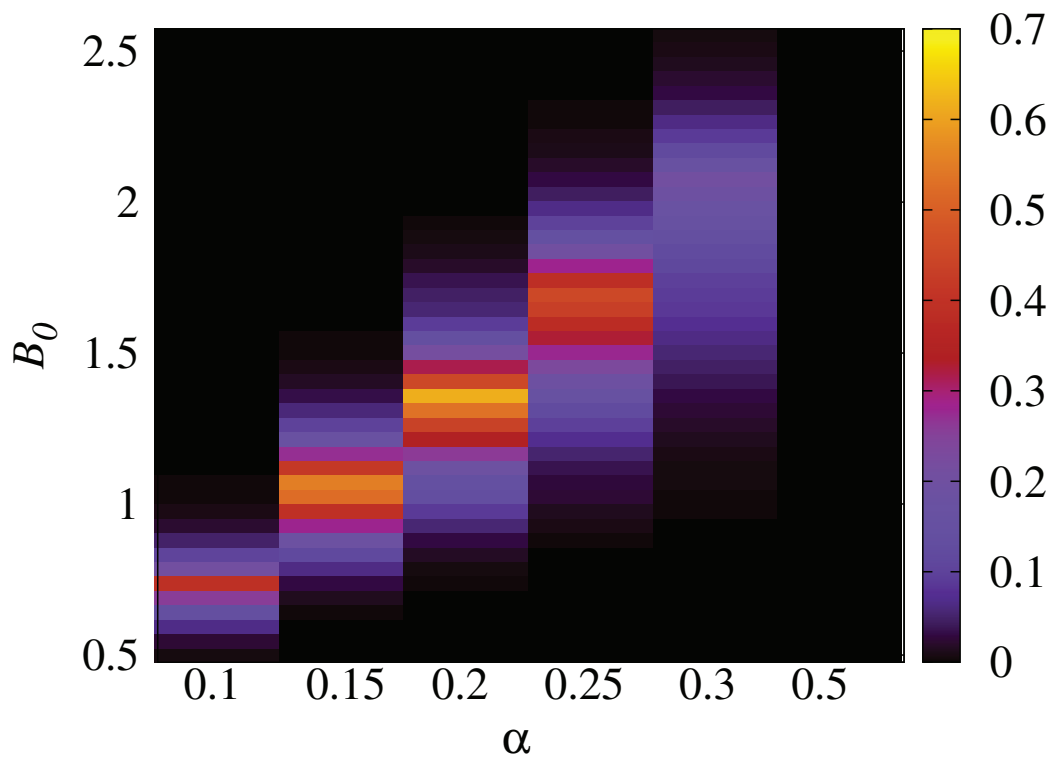


Figure 3.1: Density plot of the probability given by the K–S test that the CDFs of the theoretical and observed magnetic field distributions are drawn from the same population. This was generated for a range of  $\alpha$  and  $B_0$  (see text). The probability is colour-coded according to the palette shown on the right hand side of the figure. The sub-structures in this plot are caused by the discretisation of  $\alpha$  and  $B_0$ .

evolution or DD merging, is proportional to the orbital angular velocity

$$\Omega = \frac{2\pi}{P_{\text{orb}}} \quad (3.1)$$

of the binary at the point the envelope is ejected and write

$$B = B_0 \left( \frac{\Omega}{\Omega_{\text{crit}}} \right) G. \quad (3.2)$$

where

$$\Omega_{\text{crit}} = \sqrt{\frac{GM_{\text{WD}}}{R_{\text{WD}}^3}} = 0.9 \left( \frac{M_{\text{WD}}}{M_{\odot}} \right)^{1/2} \left( \frac{5.4 \times 10^8}{R_{\text{WD}}} \right)^{-3/2} \quad (3.3)$$

is the break-up angular velocity of a WD of mass  $M_{\text{WD}}$  and radius  $R_{\text{WD}}$ .

This model encapsulates the dynamo model of (Wickramasinghe, Tout & Ferrario, 2014) where a seed poloidal field is amplified to a maximum that depends *linearly* on the initial differential rotation imparted to the WD. In view of these results, here we simply assume a linear relationship between the poloidal field and the initial rotation and recalibrate the (Wickramasinghe, Tout & Ferrario, 2014) relation between differential rotation and field using (i) a more recent set of data and (ii) results from our population synthesis calculations that provide  $\Omega$  in equation (4.1). The quantity  $B_0$  in equation (4.1) is also a parameter to be determined empirically. Different  $B_0$ 's simply shift the field distribution to lower or higher fields with no changes to the shape of the field distribution which is solely determined by the CE efficiency parameter  $\alpha$ .

For the radius of the WD we use the Nauenberg (1972) mass-radius formula

$$R_{\text{WD}} = 0.0112R_{\odot} \left[ \left( \frac{M_{\text{Ch}}}{M_{\text{WD}}} \right)^{2/3} - \left( \frac{M_{\text{WD}}}{M_{\text{Ch}}} \right)^{2/3} \right]^{1/2}, \quad (3.4)$$

where  $M_{\text{Ch}} = 1.44 M_{\odot}$  is the Chandrasekhar limiting mass.

### 3.3.2 Parameters calibration

The data set of HFMWDs is affected by many biases, even though some of the surveys that discovered them were magnitude-limited. This is because HFMWDs tend to be more massive than their non-magnetic counterparts, as first noticed by Liebert (1988), and therefore their smaller radii, as expected by equation (3.4), make them dimmer and so less likely to be detected. Volume-limited samples are far better, given that our synthetic population mimics a volume-limited sample, but do not include enough

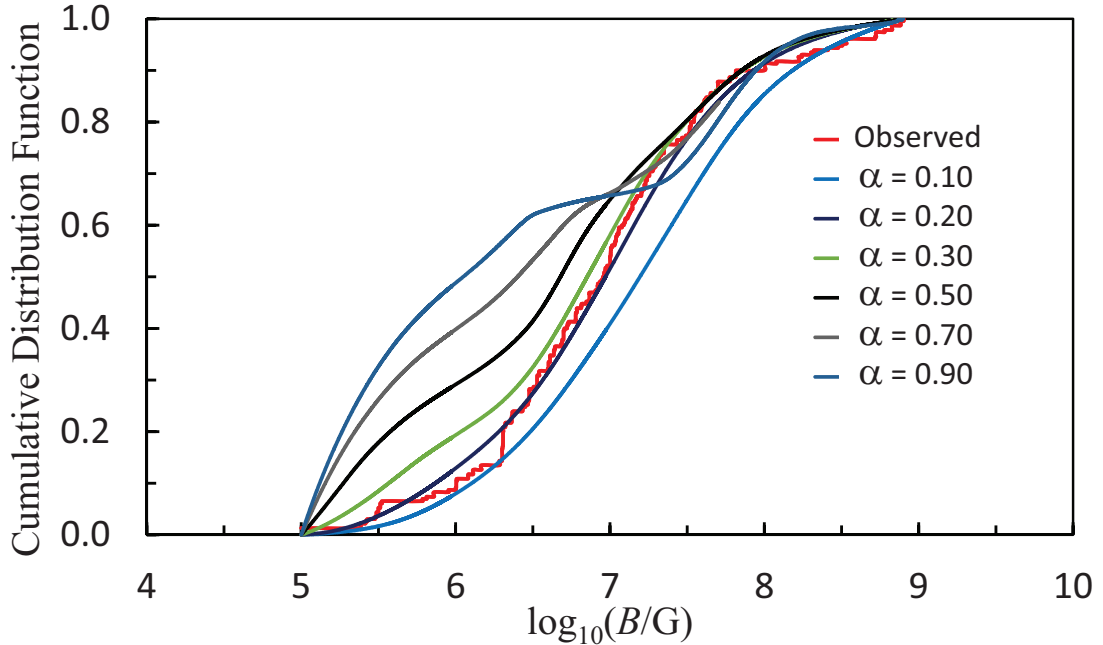


Figure 3.2: CDFs of observed (red) and BSE theoretical magnetic field distributions for a Galactic disc age of 9.5 Gyr and various  $\alpha$ .

HFMWDs to allow us to conduct any statistically meaningful study. In this section we establish the parameter space of relevance to the observations of HFMWDs by comparing the predictions of the magnetic field distribution derived from our population synthesis calculations to the fields of HFMWDs listed in Ferrario et al. (2015b).

In order to achieve this goal we have employed the K–S test (Press et al., 1992) to establish which combination of  $B_0$  and  $\alpha$  yield the best fit to the observed field distribution of HFMWDs. The K–S test compares the cumulative distribution functions (CDFs) of two data samples (in this case the theoretical and observed field distributions) and gives the probability  $P$  that they are drawn randomly from the same population. We have calculated CDFs for seven different  $\alpha$  and 44 different  $B_0$ s for each  $\alpha$ . If we discard all combinations of  $\alpha$  and  $B_0$  for which  $P \leq 0.01$ , we find  $0.5 \times 10^{10} \leq B_0/\text{G} \leq 2.5 \times 10^{10}$  and  $\alpha < 0.5$ . We have depicted in Fig. 3.1 a density plot of our results. The highest probability is for  $B_0 = 1.35 \times 10^{10}$  G and  $\alpha = 0.2$ . We show in Fig. 3.2 the theoretical CDFs for  $B_0 = 1.35 \times 10^{10}$  G and various  $\alpha$ s and the CDF of the observations of the magnetic field strengths of HFMWDs.

In the following sections we will discuss models with  $B_0 = 1.35 \times 10^{10}$  G and a range of  $\alpha$  again noting that a different  $B_0$  would simply move the field distribution to lower or higher fields with no change of shape. Therefore our discussion in the following sections will focus on the effects of varying  $\alpha$ .

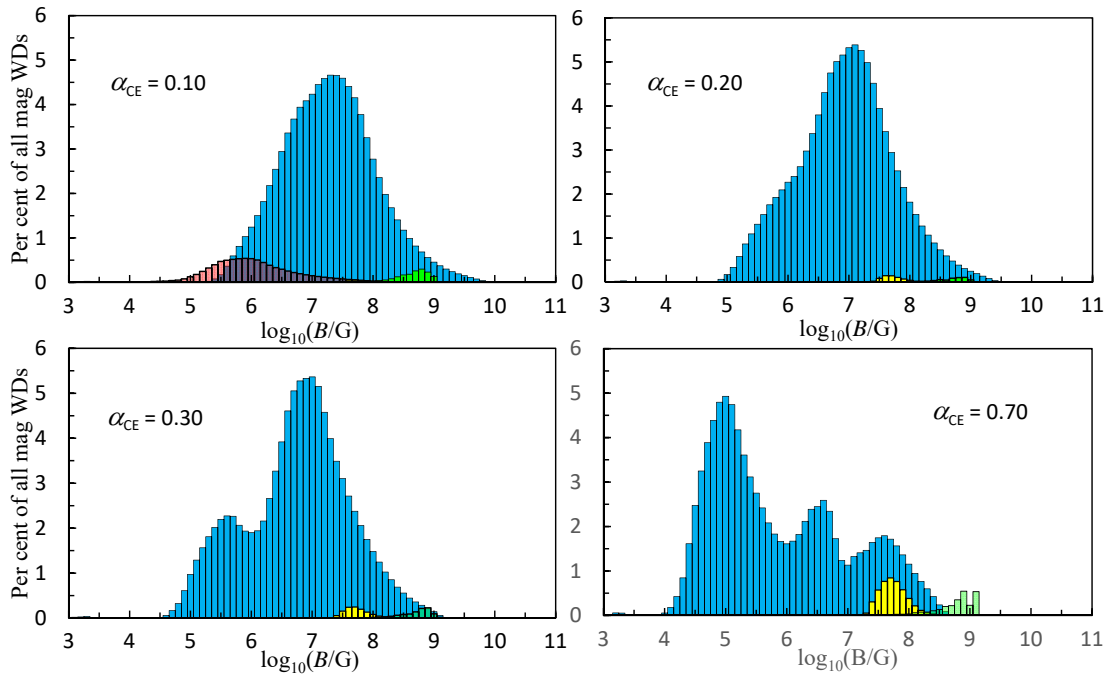


Figure 3.3: Theoretical magnetic field strength for a Galactic disc age of 9.5 Gyr and various  $\alpha$ . The histograms are superimposed, not stacked, to highlight the contribution made by each type of WD to the overall distribution. The blue, red and yellow histograms represent, respectively, CO, ONe, He WDs. The green histograms depict the merged DD systems.

### 3.4 Discussion of results

Fig. 3.3 shows the calculated magnetic field distribution and the breakdown of the WD types for  $\alpha = 0.1$  to  $0.7$ . The maximum field strength is a few  $10^9$  G and is found mostly in systems in which the HFMWD forms either via the merging of two very compact stars on a tight orbit or through the merging of two WDs after CEE (DD path). The reason for this is that these systems have very short periods and when they merge produce very strongly magnetic WDs, as expected from equation 4.1.

We show in Fig. 3.4 the theoretical magnetic field distribution of HFMWDs for  $\alpha = 0.1$  to  $\alpha = 0.7$  with the breakdown of their main formation channels, that is, their pre-CE progenitors. The overwhelming contributors to the HFMWD population are AGB stars merging with MS or CS. At low  $\alpha$ , systems with initially short orbital periods merge as soon as their primaries evolve off the main sequence, either whilst in the Hertzsprung's gap or during their ascent along the RGB. Usually such merging events produce single stars that continue their evolution burning helium in their cores and later on, depending on the total mass of the merged star, heavier elements. Because of core nuclear burning these stars continue their evolution to eventually become single non-magnetic WDs. The only observational characteristic that may distinguish them from other non-magnetic WDs could be an unusual mass that does not fit any reasonable initial to final mass function associated to the stellar cluster to which they belong. On the other hand, if the RGB star has a degenerate core, as for stars with  $M_1 \leq 2.2 M_\odot$  on the ZAMS, and merges with a low-mass CS, then the resulting object is a strongly magnetic He WD. These RGB/CS merging events do occur at all  $\alpha$  but their fraction is higher at large  $\alpha$  owing to fewer overall merging occurrences at high envelope clearance efficiencies.

When systems do not merge when the primary evolves on the RGB, they may merge when they undergo CE evolution on the AGB. In this case those binaries with the shortest orbital periods at the beginning of the CEE are those that form the highest magnetic field tail of the distribution. There are two main types of merging pairs, AGB stars merging with MS stars ( $M \geq 0.7 M_\odot$ ) and AGB stars merging with CS ( $M < 0.7 M_\odot$ ). Each of these combinations exhibits two peaks as seen in Fig. 3.4 for  $\alpha > 0.2$ , although the second peak at lower fields of the merging AGB/CS pair becomes well defined only when  $\alpha = 0.7$ . Because AGB/MS systems have larger orbital periods at the onset of CEE, their merging gives rise to generally more massive but less magnetic WDs as expected from equation (4.1). This is why the bulk of AGB/MS merging pairs occupy the lowest and most prominent peak near  $B = 10^{5.5}$  G with the secondary maximum at  $B = 10^{6.8}$  G. The AGB/CS merging pairs form another

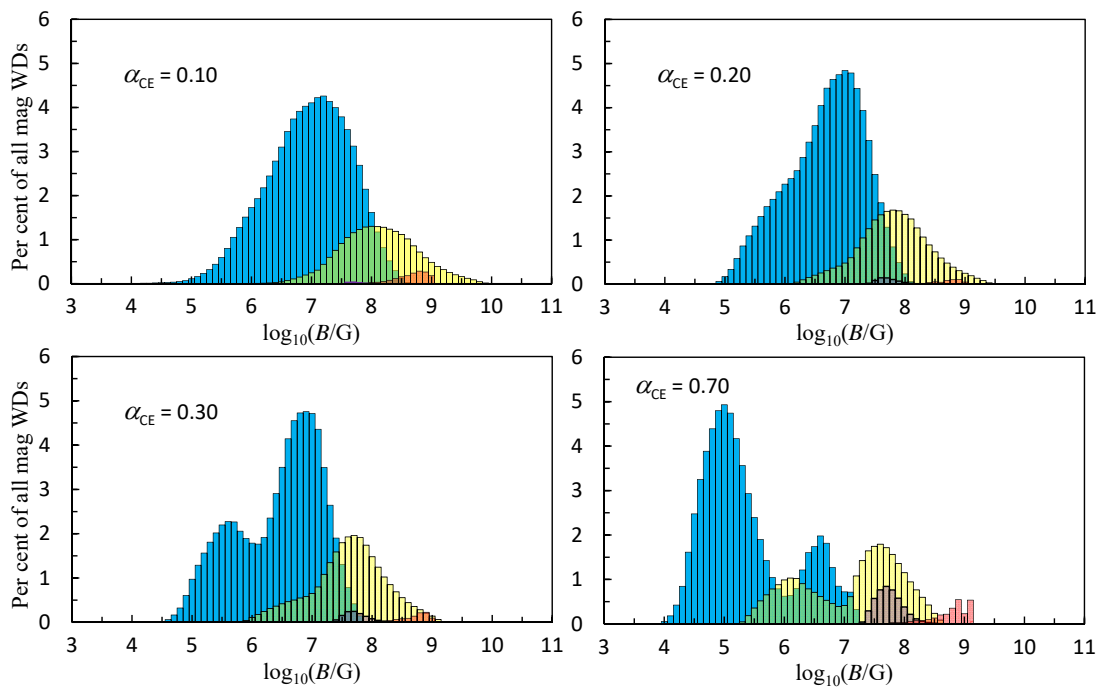


Figure 3.4: Theoretical magnetic field distribution of HFMWDs showing the pre-CE progenitors for various  $\alpha$ . The light blue, yellow and purple histograms represent, respectively, the AGB/MS, AGB/CS and RGB/CS merging pairs. The red histograms depict the merged DD systems.

two peaks, one at  $B = 10^6$  G and the other at  $B = 10^{7.75}$  G. RGB stars merging with CS stars also form a maximum at  $B = 10^{7.75}$  G. The reason for the double peaks in AGB/MS and AGB/CS merging pairs is because high envelope clearance efficiencies (high  $\alpha$ ) require more massive primaries to bring the two stars close enough together to merge during CEE. Thus, these double peaks are caused by a dearth of AGB/MS merging pairs near  $B = 10^6$  G and of AGB/CS pairs near  $B = 10^7$  G. Those systems whose orbital periods would give rise to magnetic fields in these gaps fail to merge because their initial periods are large and their primary stars are not massive enough to bring the two components close enough to merge. These double peaks are not present at low  $\alpha$  because low envelope clearance efficiency always leads to tighter orbits and merging is more likely for a much wider range of initial masses and orbital periods, more effectively smearing the contributions made by specific merging pairs.

### 3.5 Comparison to observations

A prediction of our merging hypothesis for the origin of HFMWDs is that low-mass HFMWDs, mostly arising from AGB/CS merging pairs, should display fields on average stronger than those of massive HFMWDs which predominantly result from the merging of AGB/MS pairs. The HFMWDs formed through the merging of two WDs (DD channel) are excluded from this prediction. These are expected to produce objects that are on average more massive, more strongly magnetic, and may be spinning much faster than most HFMWDs (e.g. RE J0317-853, Barstow et al., 1995; Ferrario et al., 1997b; Vennes et al., 2003). Given the very small number of HFMWDs for which both mass and field are known, it is not possible to verify whether this trend is present in observed in HFMWDs. The problem is that it is very difficult to measure masses of HFMWDs when their field is above a few  $10^6$  G. In the low field regime one can assume that each Zeeman component is broadened as in the zero field case. That is, the field does not influence the structure of the WD's atmosphere. Thus, the modelling of Zeeman spectra has allowed the determination of masses and temperatures of lower field WDs such as 1RXS J0823.62525 ( $B = 2.8 - 3.5$  MG and  $M=1.2 M_{\odot}$ ; Ferrario et al., 1998), PG 1658+441 ( $B = 3.5$  MG and  $M=1.31 M_{\odot}$ ; Schmidt et al., 1992; Ferrario et al., 1998), and the magnetic component of the double degenerate system NLTT 12758 ( $B = 3.1$  MG and  $M = 0.69 M_{\odot}$ ; Kawka et al., 2017). The masses of high field objects can only be determined when their trigonometric parallax is known (e.g. Grw +70°8247 with  $B = 320 \pm 20$  MG and  $M = 0.95 \pm 0.02 M_{\odot}$ , Greenstein et al., 1985; Wickramasinghe & Ferrario, 1988). Nevertheless, it is encouraging to see that all the most massive (near the Chandrasekhar's limit) currently known HFMWDs do

indeed possess low field strengths and that the merged DD RE J0317-853 is a strongly magnetic WD. A test of our prediction of an inverse relation between field strength and mass will become possible with the release of the accurate astrometric data of a billion stars by the ESA satellite *Gaia*. This new set of high quality data will not only allow one to test the (non-magnetic) WD mass–radius relation but will also provide precise mass and luminosity measurements of most of the currently known WDs, including the HFMWDs (Jordan, 2007).

The theoretical distribution for  $\alpha = 0.2$  overlapped to the observations of HFMWDs is displayed in Fig. 3.5. This figure shows that the maxima of the theoretical and observed distributions occur near the same field strength with the theoretical distribution extending from  $10^5$  G to  $10^9$  G, as observed. The overwhelming contribution to the theoretical field distribution is from CO WDs (see Fig. 3.3). ONe WDs are the next most common but at much lower frequency and with field strengths  $4 \leq \log_{10} B/G \leq 8$ . Merged DD WDs present field strengths  $8 \leq \log_{10} B/G \leq 9$  at an even lower frequency than the ONe WDs. Finally, He WDs are present in very small numbers with field strengths centred at  $B = 10^{7.75}$  G. This is in contrast to observations of HFMWDs that show the presence of very low-mass objects (see table 1 of Ferrario et al., 2015b) that the BSE formalism is unable to form. This mismatch between theory and observations may be corrected through the use of, e.g., different superwind assumptions (see Han et al., 1994; Meng et al., 2008, and references therein).

We note that the models shown in Fig. 3.3 with  $\alpha > 0.2$  predict the existence of a large fraction of low-field magnetic WDs with a bump appearing near  $B = 10^{5.5}$  G for  $\alpha = 0.3$ . This bump shifts toward lower fields and becomes increasingly more prominent as  $\alpha$  increases. For  $\alpha = 0.7$  this low-field hump is the most prominent feature of the magnetic field distribution. In the past suggestions were made that the incidence of magnetism in white dwarfs may be bimodal, sharply rising below  $10^5$  G with an incidence that was predicted to be similar to or exceeding that of HFMWDs (Wickramasinghe & Ferrario, 2000). However, recent low-field spectropolarimetric surveys of WDs have not found anywhere near the number of objects that had been forecast to exist in this low-field regime (Landstreet et al., 2012). Therefore, there is enough observational evidence to allow us to exclude the bimodality of the magnetic field distribution that is theoretically predicted for large  $\alpha$ 's.

### 3.6 Incidence of magnetism among cool white dwarfs

Because WDs have very high gravities, all chemical elements heavier than hydrogen, helium and dredged-up carbon or oxygen, quickly sink to the bottom of their atmosphere. Nonetheless, up to 30 per cent of WDs exhibit traces of Ca, Si, Mg, Fe, Na



and other metals (DZ WDs, Zuckerman et al., 2003). This metal pollution has been attributed to the steady accretion of debris from the tidal disruption of large asteroids and rocky planets (Jura, 2003) making these WDs important tools for the study of the chemical composition of exosolar planets. Interestingly, the incidence of magnetism among cool ( $T_{\text{eff}} < 8\,000\text{ K}$ ) DZ WDs is about thirteen per cent (Kawka & Vennes, 2014; Hollands et al., 2015) which is much higher than between two and five per cent in the general WD population (Ferrario et al., 2015a). Although our modelling does not include the merging of sub-stellar companions, we speculate that the moderately strong magnetic fields observed in metal-polluted WDs ( $0.5 \leq B/10^7\text{ G} \leq 1.1$ , Hollands et al., 2017) may be caused by giant gaseous planets plunging into the star. The accretion of other minor rocky bodies would then produce the observed atmospheric pollution. This mechanism could be applicable to all WDs, although it is not clear what the fraction of HFMDs that may have undergone this process is. Currently only ten out of about 240 HFMDs are metal-polluted (Hollands et al., 2017).

Such merging events may occur during the latest stages of AGB evolution when the outer envelope of the star engulfs the innermost planets and the drag forces exerted on them as they move through the stellar envelope cause them to drift toward the degenerate stellar core (Li et al., 1998). Whilst this mechanism is plausible, it does not explain why the incidence of magnetism is much higher among *cool* DZ WDs. Another possibility involves close stellar encounters able to significantly disturb the orbits of outer planets and asteroid belts. Such encounters can trigger dynamical instabilities that cause the inward migration, and accretion by the WD, of a massive gaseous planet and other rocky planets and asteroids. Because it takes hydrogen-rich WDs with  $0.5 \leq M/M_{\odot} \leq 1.0$  about 1.5 – 9 billion years to reach effective temperatures between 5 000 and 8 000 K (Tremblay et al., 2011; Kowalski & Saumon, 2006), such stellar encounters are possible, as discussed in detail by Farihi et al. (2011) to explain the origin of the very cool ( $T_{\text{eff}} = 5310\text{ K}$ ) and polluted magnetic WD G77–50.

A similar explanation may be invoked to explain the high incidence of magnetism among cool WDs of all types, as first reported by Liebert (1979). The study of Fabrika & Valyavin (1999) showed that whilst the incidence of magnetism among hot WDs is only around 3.5 per cent, it increases above twenty per cent among cool WDs. The volume-limited sample of Kawka et al. (2007) also shows a high incidence of magnetism (greater than ten per cent) which is consistent with the fact that volume-limited samples are dominated by cooler objects (Liebert, Bergeron & Holberg, 2003). Even the Palomar-Green magnitude-limited sample study of Liebert, Bergeron, Holberg (2005) shows a higher incidence of magnetism among cooler WDs than hotter ones. Over the years this topic has been a cause of concern. It is difficult to think of

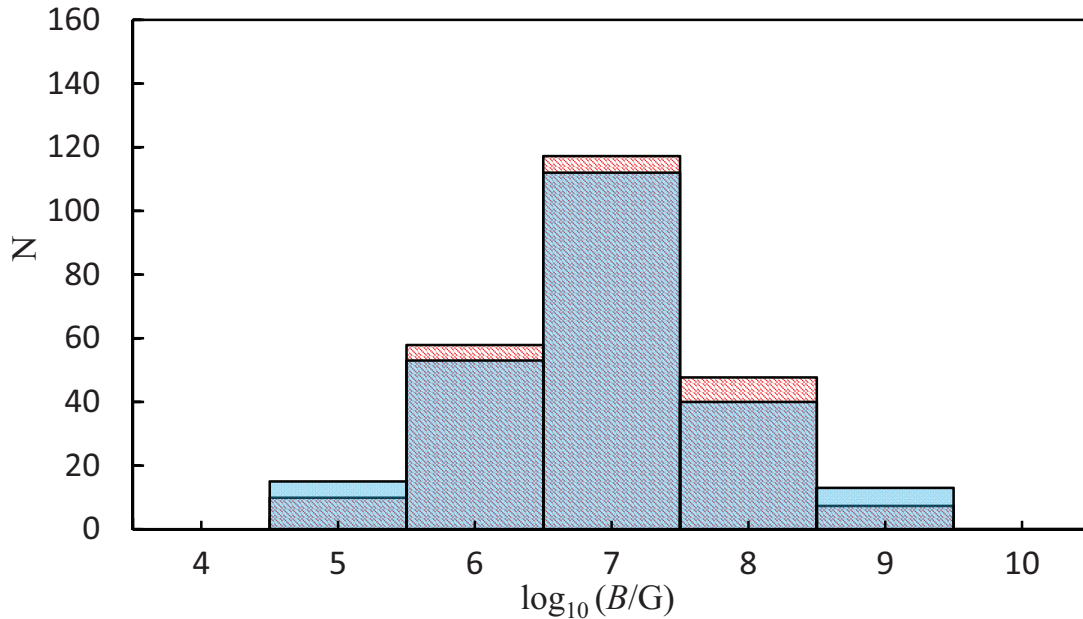


Figure 3.5: Theoretical field distribution for  $\alpha = 0.2$  of the total of the four types of HFMWDs (pink histogram) compared to the field distribution of the observed HFMWDs (blue histogram).

how fields could be generated once the star has already evolved into a WD because, if anything, fields decay over time. Alternatively, one could argue that the formation rate of HFMWDs was higher when the Galactic disc was younger, another hypothesis that is difficult to justify. Wickramasinghe & Ferrario (2000) and Ferrario et al. (2015a) have shown that the field strength is independent of effective temperature as expected by the very long ohmic decay time scales of WDs. The cumulative distribution function of the effective temperatures of the sample of HFMWDs of Ferrario et al. (2015a, see their Figure 5) appears to be smooth over the full range of effective temperatures ( $4\,000 \leq T_{\text{eff}}/\text{K} \leq 45\,000$  K) suggesting that the birthrate of HMWDs has not altered over the age of the Galactic disc. However, the sample of HFMWDs at our disposition is neither volume nor magnitude-limited and biases easily come into play.

Thus, should a future enlarged and less biased sample of HFMWDs confirm that the incidence of magnetism among cool WDs is indeed substantially higher than among hot WDs, then the possibility of field generation by accretion of giant gaseous planets on to an originally non-magnetic WD may provide a solution to this puzzle.

Nordhaus et al. (2011) found that discs formed from tidally disrupted companions with masses in the range 0.1–500 Jupiter masses can explain the presence of high fields in WDs. Thus, the central issue is, once again, how the magnetic field can diffuse into the core of a WD over an appropriate timescale. This is a key question that still needs to be quantitatively answered.

The other question concerns the likelihood for an old and presumably stable planetary system to be sufficiently perturbed to send planets inward to plunge into the WD. Farihi et al. (2011) have shown that the number of close stellar encounters that can have an appreciable effect on the outer regions of a planetary system by sending objects into highly eccentric orbits is around  $0.5 \text{ Gyr}^{-1}$ . That is, the probability is about 50 per cent every  $0.5 \text{ Gyr}^{-1}$ . Considering typical cooling times between 1.5 and 9 Gyr, these close encounters become likely during the life of a WD. If this hypothesis is correct, we should expect all WDs hosting a large gaseous planet to develop a magnetic field at some point in their lifetime.

### 3.7 Conclusions

In chapter 2 we discussed the evolution of HFMWDs resulting from two stellar cores (one of which is degenerate) that merge during a phase of CEE. We fitted the observed mass distribution of the HFMWDs and the incidence of magnetism among Galactic field WD and found that the HFMWDs are well reproduced by the merging hypothesis for the origin of magnetic fields if  $0.1 \leq \alpha \leq 0.3$ . However in chapter 2 we did not propose a prescription that would allow me to assign a magnetic field strength to each WD. This task has been carried out and the results presented here. We have assumed that the magnetic field attained by the core of the single coalesced star emerging from CEE is proportional to the orbital angular velocity of the binary at the point the envelope is ejected. The break-up angular velocity is the maximum that can be achieved by a compact core during a merging process and this can only be reached if the merging stars are in a very compact binary, such as a merging DD system.

In our model there are two parameters that must be empirically estimated. These are  $B_0$ , that is linked to the efficiency with which the poloidal field is regenerated by the decaying toroidal field (see Wickramasinghe, Tout & Ferrario (2014)) and the CE efficiency parameter  $\alpha$ . We carried out K-S test on the CDFs of the observed and theoretical field distributions for a wide range of  $B_0$  and  $\alpha$  and we found that the observed field distribution is best represented by models characterised by  $B_0 = 1.35 \times 10^{10} \text{ G}$  and  $\alpha = 0.2$ . Population synthesis studies of MCVs that make use of the results obtained here and chapter 2 show that the same  $B_0$  can also explain observations of magnetic binaries.

We have also speculated that close stellar encounters can send a giant gaseous planet from the outer regions of a WD's planetary system into a highly eccentric orbit. The plunging of this super-Jupiter into the WD can generate a magnetic field and thus provide an answer to why magnetism among cool WDs, and particularly among cool DZ WDs, is higher than among hot WDs.

## **Acknowledgements**

GPB gratefully acknowledges receipt of an Australian Postgraduate Award. CAT thanks the Australian National University for supporting a visit as a Research Visitor of its Mathematical Sciences Institute, Monash University for support as a Kevin Watford distinguished visitor and Churchill College for his fellowship.

# Chapter 4

## Origin of magnetic fields in cataclysmic variables

This chapter is a reproduction of the paper submitted for publication in Monthly Notices of the Royal Astronomical Society, viz:

*Briggs, Ferrario, Tout & Wickramasinghe, MNRAS (2018) (Submitted for publication), Origin of Magnetic Fields in Cataclysmic Variables*

### 4.1 Abstract

In a series of recent papers it has been proposed that HFMDs are the result of close binary interaction and merging. Population synthesis calculations have shown that the origin of isolated highly magnetic white dwarfs is consistent with the stellar merging hypothesis. In this picture the observed fields are caused by an  $\alpha - \Omega$  dynamo driven by differential rotation. The strongest fields arise when the differential rotation equals the critical break up velocity and result from the merging of two stars (one of which has a degenerate core) during CEE or from the merging of two white dwarfs. We now synthesise a population of binary systems to investigate the hypothesis that the magnetic fields in the MCVs also originate during stellar interaction in the CE phase. Those systems that emerge from CE more tightly bound form the CVs with the strongest magnetic fields. We vary the CE efficiency parameter  $\alpha$  and compare the results of our population syntheses with observations of magnetic cataclysmic variables. We find that CE interaction can explain the observed characteristics of these magnetic systems immediately after CE if  $\alpha < 0.4$ .

Keywords: Stars: cataclysmic variables – stars: white dwarfs – stars: magnetic fields – stars: binaries.

### 4.2 Introduction

Cataclysmic variables (CVs) are close interacting binaries generally consisting of a low-mass main-sequence (MS) star transferring matter to the WD primary via Roche lobe overflow (Warner, 1995). In non-magnetic or weakly magnetic systems, which

make up the majority of observed CVs, the hydrogen-rich material leaving the secondary star from the inner Lagrangian point forms an accretion disc around the WD. It is estimated that some 20 – 25 per cent of all CVs host a magnetic WD (MWDs, Wickramasinghe & Ferrario, 2000; Ferrario et al., 2015a). These systems are the MCVs. Among MCVs we have the strongly magnetic AM Herculis variables or polars. In polars the high magnetic field of the WD can thread and channel the material from the secondary star directly from the ballistic stream to form magnetically confined accretion funnels, so preventing the formation of an accretion disc. In these systems the two stars are locked in synchronous rotation at the orbital period. The radiation from the accretion funnels (e.g. Ferrario & Wehrse, 1999) and the cyclotron radiation from the shocks located at the funnels' footpoints of closed magnetic field lines dominate the emission of these systems from the X-rays to the infrared bands (e.g. Meggitt & Wickramasinghe, 1982; Wickramasinghe & Ferrario, 1988). Cyclotron and Zeeman spectroscopy and spectropolarimetry have revealed the presence of strong fields in the range of a few  $10^7 - 10^8$  G (see, e.g., Ferrario, Bailey & Wickramasinghe, 1993; Ferrario et al., 1996). Weaker fields of about  $10^6$  to  $3 \times 10^7$  G are found in the DQ Herculis variables or Intermediate Polars (IPs) where the WD's magnetic field cannot totally prevent the formation of an accretion disc (e.g. see Ferrario, Wickramasinghe & King, 1993). In these systems the material is magnetically threaded from the inner regions of a truncated accretion disc and channelled on to the primary forming magnetically confined accretion curtains (Ferrario & Wickramasinghe, 1993). In the IPs the white dwarf is not synchronously locked with the orbital period but is spun up to a spin period shorter than the orbital period of the system.

Liebert et al. (2005) noticed the enigmatic lack of MWDs from the 501 detached binaries consisting of a WD with a non-degenerate companion found in the DR1 of the Sloan Digital Sky Survey (SDSS, York et al., 2000). They also noticed that among the 169 MWDs known at the time, none had a non-degenerate detached companion. This was puzzling because such a pairing is very common among non-magnetic WDs (see, e.g. Hurley, Tout & Pols, 2002; Ferrario, 2012). A similar study conducted on the much larger DR7 sample of SDSS detached binaries consisting of a WD with a non-degenerate companion Kleinman et al. (2013) led to the same conclusion (Liebert et al., 2015). Over the years, not a single survey conducted to ascertain the incidence of magnetism among WDs has yielded a system consisting of a magnetic WD with a non-degenerate companion (e.g., Schmidt et al., 2001a; Kawka et al., 2007). It is this curious lack of pairing that led Tout et al. (2008) to propose that the existence of magnetic fields in WDs is intimately connected to the duplicity of their progenitors and that they are the result of stellar interaction during CEE. In this picture, as the cores

of the two stars approach each other, their orbital period decreases and the differential rotation that takes place in the convective CE generates a dynamo mechanism driven by various instabilities. Regős & Tout (1995a) argued that it is this dynamo mechanism that is responsible for the transfer of energy and angular momentum from the orbit to the envelope which is eventually, all or in part, ejected.

Wickramasinghe, Tout & Ferrario (2014) have shown that strong magnetic fields in WDs can be generated through an  $\alpha - \Omega$  dynamo during CEE where a weak seed poloidal field is wound up by differential rotation to create a strong toroidal field. However toroidal and poloidal fields are unstable on their own (Braithwaite, 2009). Once the toroidal field reaches its maximum strength and differential rotation subsides the decay of toroidal field leads to the generation of a poloidal field with the two components stabilising each other and limiting field growth until they reach a final stable configuration. Thus, a poloidal seed field can be magnified during CEE by an amount that depends on the initial differential rotation but is independent of its initial strength. According to this scenario the closer the cores of the two stars are dragged at the end of CEE, before the envelope is ejected, the greater the differential rotation and thus the stronger the expected frozen-in magnetic field. If CEE leads to the merging of the cores the result is a highly magnetic isolated WD. If the two stars do not coalesce they emerge from the CE as a close binary that evolves into a MCV. The viability of such model, in terms of incidence of magnetism among single WDs and their mass and magnetic field distribution, have been shown in chapters 2 and 3 respectively.

In this chapter we continue our study of the origin of fields in MWDs to explain the parentage of MCVs. To this end we carry out a comprehensive population synthesis study of binaries for different CE efficiencies  $\alpha$ . we examine all paths that lead to a system consisting of a WD with a low-mass companion star. We show that the observed properties of the MCVs are generally consistent with their fields originating through CEE for  $\alpha < 0.4$ .

### 4.3 Evolution and space density of MCVs

Observed MCVs consist of a WD that accretes matter from a secondary star that has not gone through any significant nuclear evolution when the transfer of mass begins. The mass ratio of an MCV is given by  $q = M_{\text{sec}}/M_{\text{WD}} < 1$  where  $M_{\text{WD}}$  is the mass of the WD primary and  $M_{\text{sec}}$  is the mass of the companion star. The mass accretion process in MCVs is relatively stable over long periods of time, although the polars suffer from high and low states of accretion. It is not known what sparks the change in accretion mode but, because polars do not have a reservoir of matter in an accretion disc,

they can switch very quickly from high to low states. IPs have never been observed in low states of accretion. Stable mass transfer can be driven by nuclear-timescale expansion of the secondary (not generally applicable to MCVs) and/or by loss of angular momentum, driven by magnetic braking above the CV period gap (caused by the disrupted magnetic braking mechanism, see Spruit & Ritter, 1983; Rappaport, Verbunt & Joss, 1983; Verbunt, 1984) and gravitational radiation below the gap. Loss of angular momentum shrinks the orbit keeping the companion star filling its Roche lobe and so drives mass transfer. Therefore, as MCVs evolve, the orbital period diminishes until it reaches a minimum when the secondary star becomes a substellar-type object whose radius increases as further mass is lost. Systems that have reached the minimum period and have turned back to evolve toward longer periods are often called period bouncers (e.g. Patterson, 1998)

The evolution of MCVs is expected to be similar to that of non-magnetic CVs. However, Li et al. (1994) have shown that angular momentum loss may not be as efficient in polars as it is in non-magnetic or weakly magnetic CVs in bringing the two stars together because the wind from the secondary star is trapped within the magnetosphere of the WD. This phenomenon slows down the loss of angular momentum, reduces the mass transfer rate and leads to longer evolutionary timescales. This mechanism provides a simple explanation for the observed high incidence of magnetic systems among CVs (Araujo-Betancor et al., 2005).

We show in Fig. 4.1 the period distribution of CVs and MCVs where the MCVs have been subdivided into polars and intermediate polars. The space density of CVs is not well known and, over the years, there has been some considerable disagreement between observations and theoretical predictions. The recent study of *Swift* X-ray spectra of an optically selected sample of nearby CVs conducted by Reis et al. (2013) has unveiled a number of very low emission X-ray systems. Hard X-ray surveys of the Galactic ridge have shown that a substantial amount of diffuse emission can be resolved into discrete low-luminosity sources. Because the MCVs are generally strong X-ray emitters, Munro et al. (2004) and Hong (2012) have propounded that IPs could be the main components of these low-luminosity hard X-ray sources. The SDSS has also revealed a substantial number of low-accretion rate CVs near the CV period minimum (Gänsicke et al., 2009).

Pretorius et al. (2013) have conducted a study of the X-ray flux-limited *ROSAT* Bright Survey (RBS) to determine the space density of MCVs. They assume that the 30 MCVs in the RBS are representative of the intrinsic population. They also allow for a 50 per cent high-state duty cycle for polars under the assumption that polars are below the RBS detection threshold while they are in low states of accretion. They



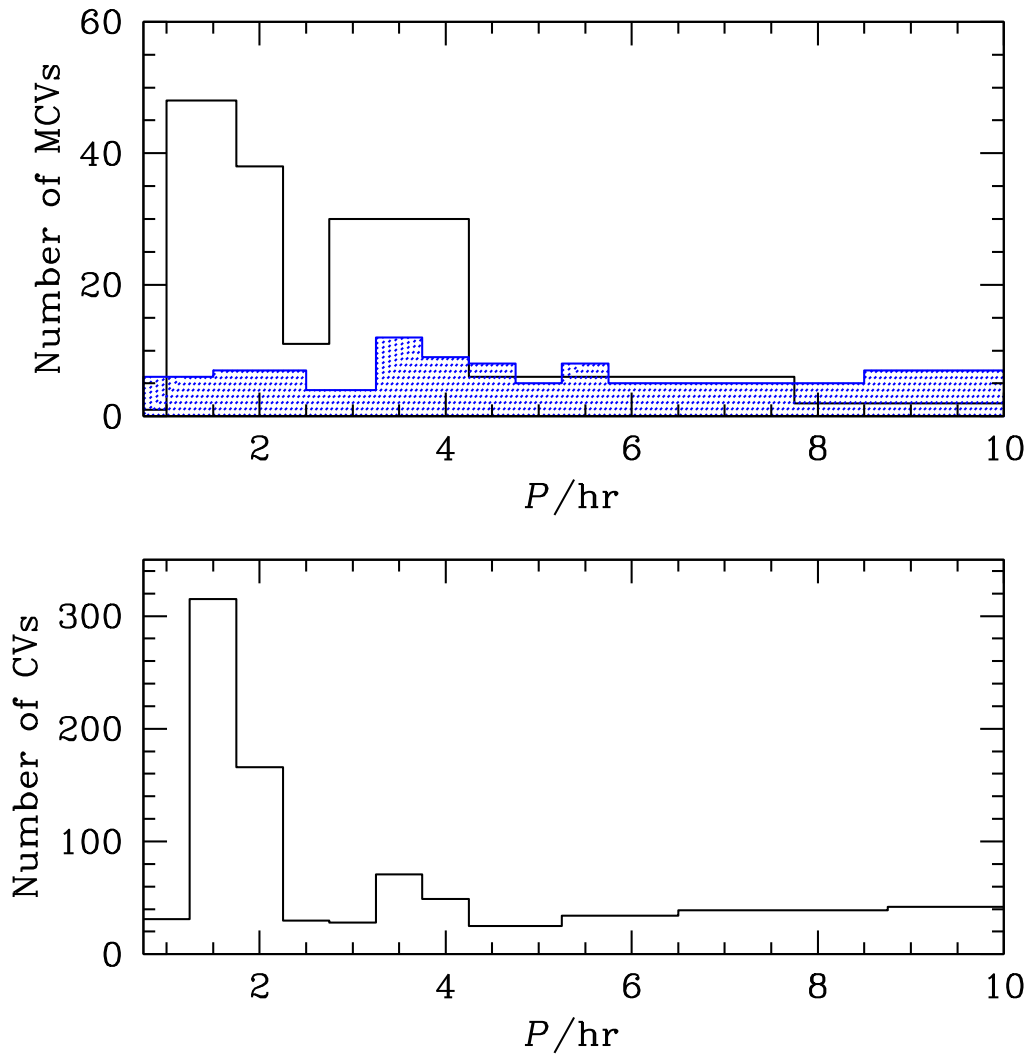


Figure 4.1: The orbital period distribution of MCVs (top) and of the CVs (bottom). The MCVs are subdivided into Polars (solid black line histogram) and IPs (shaded histogram). We have used the latest version (v7.20) of the Ritter & Kolb (2003) CV catalogue to create this figure.

find that the total space density of MCVs is  $1.3_{0.4}^{+0.6} \times 10^6 \text{ pc}^{-3}$  with about one IP per 200 000 stars in the solar neighbourhood. They conclude that IPs are indeed a possible explanation for most of the X-ray sources in the Galactic Centre. These new findings seem to suggest that the space density of CVs is somewhat larger than initially forecast and thus in closer agreement with theoretical expectations.

#### 4.3.1 *Where are the progenitors of the MCVs?*

Liebert et al. (2005, 2015) asked, “Where are the magnetic white dwarfs with detached, non-degenerate companions?” This question is awaiting an answer and thus the progenitors of the MCVs still need to be identified. As already noted, the proposal by Tout et al. (2008), that the existence of high magnetic fields in all WDs, isolated and in binaries, is related to their duplicity prior to CEE is gaining momentum. Observational support for the binary origin of magnetic fields in MCVs is also strengthening. Zorotovic et al. (2010) listed about 60 post CE binaries (PCEBs) from the SDSS and other surveys consisting of a WD with an M-dwarf companion. The periods of these PCEBs range from about 0.08 to 20 d and the WD effective temperatures in the range 7 500 to 60 000 K. According to current binary evolution theory, one third of these systems should lose angular momentum from their orbits by magnetic braking and gravitational radiation and are expected to come into contact within a Hubble time. However none of these 60 binaries contains a MWD, even if observations indicate that 20 to 25 per cent of all CVs harbour one. Furthermore, magnitude limited samples of WD have shown an incidence of magnetism of about 2 to 3 per cent and thus some pre-MCVs should be present among the objects listed by Zorotovic et al. (2010). This finding indicates that magnetic white dwarf primaries are only present in those binaries that are already interacting or are close to interaction. The magnetic systems originally known as Low-Accretion Polars (LARPS, Schwöpe et al., 2002) have been proposed to be the progenitors of the polars (Schwöpe et al., 2009). The first LARPS were discovered in the Hamburg/ESO Quasar Survey (HQS, Wisotzki et al., 1991) and then by the SDSS by virtue of their unusual colours arising from the presence of strong cyclotron harmonic features in the optical band together with a red excess owing to the presence of a low-mass red companion star. The MWDs in LARPS are generally quite cool ( $T_{\text{eff}} \lesssim 10\,000 \text{ K}$ ) and have low-mass MS companions which underfill their Roche lobes (e.g. Reimers et al., 1999; Schwöpe et al., 2009; Parsons et al., 2013). The MWDs in these systems accrete mass from the wind of their companion at a rate substantially larger than that observed in detached non-magnetic PCEBs (Parsons et al., 2013). These systems were thus renamed pre-polars (PREPs) by Schwöpe et al.

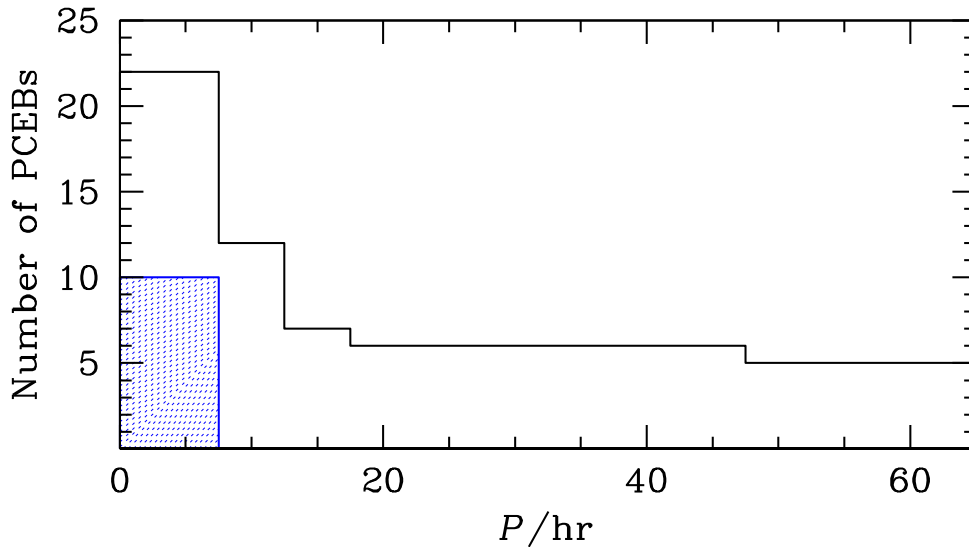


Figure 4.2: The orbital period distribution of PCEBs (solid black line histogram, Nebot Gómez-Morán et al., 2011) and PREPs (shaded histogram, Ferrario et al., 2015a).

(2009) to avoid confusion with polars in a low state of accretion. PREPs have orbital periods which are, on average, only marginally longer than those of polars. The ages of the WDs in PREPs, as indicated by their effective temperatures, are generally above a billion years. The absence of PREPs with hot WDs is puzzling but maybe still not alarming, if one considers the small number of PREPs currently known and the initial rapid cooling of WDs. Thus, the hypothesis that the progenitors of MCVs are expected to emerge from CE when they are close to transferring mass via Roche Lobe overflow is well warranted. We show in Fig. 4.2 the period distribution of PCEBs and PREPs.

#### 4.4 Population synthesis calculations

Each binary is assigned three initial parameters. These are the mass  $1.0 \leq M_1/M_\odot \leq 10.0$  of the primary star, the mass  $0.1 \leq M_2/M_\odot \leq 2.0$  of the secondary star, and the orbital period  $1 \leq P_0/d \leq 10\,000$  at the zero-age main sequence (ZAMS). We set the eccentricity to zero. Each parameter was sampled uniformly on a logarithmic scale with 200 divisions. This sampling gives a synthetic population of about 70 million binary systems. The actual number of binary systems is then calculated on the premise that  $M_1$  follows Salpeter’s mass function distribution (Salpeter, 1955) and  $M_2$  is according to a flat mass ratio distribution with  $q \leq 1$ . The initial period distribution is assumed to be uniform in the logarithm.

Table 4.1: We have indicated with  $N$  (second column) the fraction of PREPs that emerge from CE for different efficiency parameters  $\alpha$  (first column) in a single generation of binaries. The other columns give the smallest and the largest progenitor masses and initial orbital periods.

$\alpha$	$N$ (per cent)	$M_{1_{\min}}/M_{\odot}$	$M_{2_{\min}}/M_{\odot}$	$M_{1_{\max}}/M_{\odot}$	$M_{2_{\max}}/M_{\odot}$	$P_{0_{\min}}/d$	$P_{0_{\max}}/d$
0.10	1.518	1.08	0.10	8.16	1.42	369.7	3144.0
0.15	1.672	1.08	0.10	8.16	1.42	293.3	2800.5
0.20	1.663	1.08	0.10	8.16	1.42	246.6	2354.3
0.25	1.213	1.08	0.10	8.16	1.36	207.3	2097.0
0.30	1.163	1.08	0.10	8.16	1.14	184.6	2221.9
0.50	0.808	1.08	0.10	8.16	0.58	123.2	2221.9
0.70	0.804	1.08	0.10	8.16	0.19	87.0	1867.9
0.90	0.859	1.08	0.10	8.16	0.13	69.1	1762.9

We have used the rapid binary star evolution algorithm, *BSE*, developed by Hurley, Tout & Pols (2002), to evolve each binary system from the ZAMS to 9.5 Gyr (age for the Galactic Disc, Kilic et al., 2017). *BSE* is an extension of the single star evolution code written by Hurley, Pols & Tout (2000). It allows for stellar mass loss, interaction between the two stars as mass transfer, Roche lobe overflow, CEE (Paczynski, 1976), tidal interaction, supernova kicks, and angular momentum loss caused by gravitational radiation and magnetic braking.

We use the  $\alpha$  (energy) formalism for CE phases where  $\alpha$  is a free parameter ranging between 0.1 and 0.9 (see chapters 2 and 3 for more details). Single star mass loss rates are described by Hurley, Pols & Tout (2000). In our calculations we have adopted a solar metallicity  $Z = 0.02$  and  $\eta = 1.0$  for the Reimers' mass-loss parameter.

Our theoretical sample of PCEBs consists of systems that (i) have undergone CEE, (ii) have a primary that evolves into a WD, (iii) have a companion that remains largely unevolved and (iv) have a mass ratio  $q \leq 1$ . A subset of these systems come into contact over the age of the Galactic Disc and become classical CVs. Those systems with a WD that develops a strong magnetic field become MCVs.

Of our sample of PCEBs, we then select the subset consisting of the PREPs (the progenitors of the MCVs). PREPs must fulfil two additional criteria: (i) the primary star must have a degenerate core before entering the last CE phase and (ii) no further core burning occurs. The reason for the first criterion is that a degenerate core is essential for a stellar magnetic field to persist, in a frozen-in state, after its formation. The reason for the second is that nuclear burning in the core would ignite convection that would destroy any frozen-in magnetic field. Systems that violate either criterion but come into contact over the age of the Galactic Disc are expected to evolve into classical non-magnetic CVs. We show in Table 4.1 the limits of the parameter space within which PREPs are formed. The minimum ZAMS masses of the systems that give rise to PREPs are listed in the columns with headings  $M_{1\min}$  and  $M_{2\min}$  and the maximum masses are under the headings  $M_{1\max}$ ,  $M_{2\max}$ . Minimum and maximum initial periods are in the columns under  $P_{0\min}$  and  $P_{0\max}$  respectively.

Once we have obtained our theoretical PREP sample, we assign a magnetic field  $B$  to each of their WD primaries following the prescription described in chapter 3 to model the field distribution of high field magnetic WDs (HFMWDs). That is

$$B = B_0 \left( \frac{\Omega}{\Omega_{\text{crit}}} \right) \text{G}. \quad (4.1)$$

where  $\Omega$  is the orbital angular velocity and  $\Omega_{\text{crit}} = \sqrt{GM_{\text{WD}}/R_{\text{WD}}^3}$  is the break-up

Table 4.2: The number of PCEBs born, the fraction of PREPs from PCEBs and of MCVs (magnetic systems already exchanging mass) from PREP as a function of the CE efficiency parameter  $\alpha$  over the age of the Galactic Disc. The number of PREPs is maximum close to  $\alpha = 0.15$  while the number of MCVs is maximum at  $\alpha = 0.10$ .

$\alpha$	Number of PCEBs	$\frac{\text{PREPs}}{\text{PCEBs}} \times 100$	$\frac{\text{MCV}}{\text{PREPS}} \times 100$
0.10	30517472	20.9	61.0
0.15	36099023	18.9	56.4
0.20	38666876	15.3	49.9
0.30	41197674	8.7	45.0
0.40	43654871	5.6	48.0
0.50	46289395	4.5	51.0
0.60	49010809	4.1	52.0
0.70	51888317	3.8	52.4
0.80	54664759	3.3	52.4

angular velocity of a WD of mass  $M_{\text{WD}}$  and radius  $R_{\text{WD}}$ . The parameter  $B_0$  is a free parameter that was determined empirically in chapter 3, that is,  $B_0 = 1.35 \times 10^{10}$  G. The parameter  $B_0$  does not influence the shape of the field distribution which is only determined by  $\alpha$ . Lower (or higher)  $B_0$  shift the field distribution to lower (or higher) field strengths. Unlike HFMWDs, both stars emerge from CEE but on a much tighter orbit that will allow them to come into contact over a Hubble time and appear as MCVs.

#### 4.5 Synthetic population statistics

We have time integrated each population, characterised by  $\alpha$ , to the Galactic Disc age under the assumption that the star formation rate is constant. We have listed in Table 4.2 the percentage by type of all binaries that emerge from CE over the age of the Galactic Disc.

Column 2 in Table 4.2 shows that while the number of PCEBs increases when  $\alpha$  increases, the percentage of PREPs (progenitors of the MCVs) decreases. This is because as  $\alpha$  increases the envelope's clearance efficiency increases causing the two stars to emerge from CE at wider separations and thus less likely to become PREPs and thence MCVs. On the other hand, the overall number of PCEBs increases because stellar merging events become rarer at high  $\alpha$ , as shown in chapter 2. Fewer merging events are also responsible for the high incidence of systems with low mass He WDs (He WDs) whose ZAMS progenitors were born at short orbital periods and entered

CEE when the primary star became a Hertzsprung gap or a RGB star. At larger initial orbital periods CEE may occur on the AGB. However as  $\alpha$  increases only stars in those systems that harbour massive enough WDs can come sufficiently close to each other to allow stable mass transfer to occur within the age of the Galactic Disc (see section 4.5.2). In contrast, at low  $\alpha$  the clearance efficiency is low and so there is a longer time for the envelope to exert a drag force on the orbit. This results in (i) more merging events, (ii) tighter final orbits for all WD masses and (iii) a larger number of systems coming into contact over the age of the Galactic Disc. Point (i) reduces the overall number of PCEBs while both (ii) and (iii) increase the number of PREPs.

Table 4.3: Evolutionary history of an example binary system that becomes a MCV after CEE with  $\alpha = 0.1$ . Here RLO = Roche Lobe Overflow.

Stage	Time/Myr	$M_1/M_\odot$	$M_2/M_\odot$	$P/d$	$a/R_\odot$	$B/G$	Remarks
1	0.000	4.577	0.230	2244.627	1218.030	0.000E+00	ZAMS
2	128.515	4.577	0.230	2244.627	1218.030	0.000E+00	S1 is a Hertzsprung gap star
3	129.078	4.577	0.230	2245.210	1218.188	0.000E+00	S1 is a RGB star. Separation increases slightly.
4	129.445	4.574	0.230	2247.427	1218.790	0.000E+00	S1 starts core He burning. Some mass loss occurs.
5	149.930	4.466	0.230	2352.896	1247.059	0.000E+00	S1 is an AGB star. Further mass loss occurs.
6	150.947	4.390	0.230	2173.184	1176.321	0.000E+00	S1 is a late AGB star. Separation decreases significantly
7	150.989	4.364	0.230	861.296	633.510	0.000E+00	RLO & CE start. Separation decreases dramatically.
8	150.989	0.918	0.230	0.117	1.053	1.218E+07	S1 emerges from CE as a COMWD and RLO ceases.
9	326.073	0.918	0.230	0.099	0.945	1.218E+07	Separation decreases and MCV phase starts
10	9 500.000	0.918	0.037	0.139	1.112	1.218E+07	Separation reaches a minimum between stages 9 and 10 and increases again. S2 is a brown dwarf.



Table 4.4: Evolutionary history of a second example binary system that becomes a MCV after CE with  $\alpha = 0.4$ .

Stage	Time/Myr	$M_1/M_\odot$	$M_2/M_\odot$	$P$ (d)	$a/R_\odot$	$B/G$	Remarks
1	0.000	1.612	0.257	190.661	171.774	0.000E+00	ZAMS
2	2197.329	1.612	0.257	190.661	171.774	0.000E+00	S1 is a Hertzsprung gap star
3	2239.430	1.611	0.257	190.743	171.811	0.000E+00	S1 is a RGB star, loses mass. Separation increases slightly.
4	2343.048	1.580	0.257	110.351	118.629	0.000E+00	S1 loses more mass, separation decreases.
5	2343.048	0.386	0.257	0.149	1.020	3.577E+07	RLO & CE start. Separation decreases dramatically.
6	2343.048	0.386	0.257	0.149	1.020	3.577E+07	S1 emerges from CE as a He MWD and RLO ceases.
7	3389.278	0.386	0.257	0.102	0.792	3.577E+07	Separation decreases and MCV phase starts
8	9500.000	0.386	0.052	0.100	0.687	3.577E+07	Separation reaches a minimum between stages 7 and 8 and increases again. S2 is a brown dwarf.

### 4.5.1 Magnetic CV evolution examples

The evolutionary history of a binary system depends on the parameters that characterise it. The number of CE events can vary from one to several (Hurley, Tout & Pols, 2002). Whether a classical CV becomes magnetic or not depends on the evolution before and after the common envelope. Here we give two typical examples of systems that evolve into a MCV. In the first the initially rather massive primary star evolves into a CO WD after CEE as a late AGB star. In the second example the primary evolves into a He WD after CE evolution while ascending the RGB.

*Example 1:* Table 4.3 illustrates the evolution of a system that becomes a close binary after CE with  $\alpha = 0.1$ . The progenitors are a primary star (S1) of  $4.58 M_{\odot}$  and a secondary star (S2) of sub-solar mass  $0.230 M_{\odot}$ . At ZAMS the initial period is 2 240 d with a separation of  $1\,220 R_{\odot}$ .

S1 evolves off the ZAMS and reaches the early AGB stage at 149 Myr having lost  $0.111 M_{\odot}$  on the way. After a further 1.02 Myr S1 has become a late AGB star. Further evolution brings the stars closer together at a separation of  $634 R_{\odot}$ . Soon after dynamically unstable Roche lobe overflow from S1 to S2 takes place and CE begins. At the end of the short period of CEE the two stars emerge with a separation of only  $1.05 R_{\odot}$  because of the large orbital angular momentum loss during this stage. The ejection of the envelope exposes the core of S1 that has now become a magnetic  $0.918 M_{\odot}$  CO WD. After a further 175 Myr the separation has further contracted to  $0.945 R_{\odot}$  via magnetic braking and gravitational radiation. Roche lobe overflow begins and the system becomes a bona fide mass-exchange MCV. During the CEE evolutionary phase the mass of the donor star, separation and orbital period steadily decrease until the mass of the companion star becomes too low to maintain hydrogen burning and S2 becomes a degenerate object. At this point separation and orbital period reach a minimum. Further evolution sees these two quantities increase again over time. At an age of 9 500 Myr S2 has lost most of its mass and has become a  $0.037 M_{\odot}$  brown dwarf with the separation from its WD primary increased to  $0.112 R_{\odot}$ .

*Example 2:* Table 4.4 shows the evolution of a second system that becomes a close binary after CE. This time we have  $\alpha = 0.4$ . The progenitors are a MS primary star (S1) of  $1.61 M_{\odot}$  and a secondary star (S2) of mass  $0.257 M_{\odot}$ . At ZAMS the initial period is 191 d and the separation  $172 R_{\odot}$ .

S1 evolves off the ZAMS through the Hertzsprung gap to reach the RGB after 2 240 Myr having lost  $0.001 M_{\odot}$  on the way. Still on the RGB at 2 340 Myr S1 has lost  $0.031 M_{\odot}$  and the separation has decreased to  $119 R_{\odot}$ . Roche lobe overflow from S1 to S2 and CEE begin. S1 emerges from CE as a magnetic He WD with a mass of

0.386  $M_{\odot}$ . The orbital separation has drastically decreased to 1.02  $R_{\odot}$ . S2 maintains its mass and remains an M-dwarf star. From this time onwards magnetic braking and gravitational radiation cause the orbit to shrink further until at 3 390 Myr the separation is 0.792  $R_{\odot}$  and Roche lobe overflow commences. The system is now a MCV. Further evolution leads S2 to lose mass, owing to accretion on to S1, until, at 9 500 Myr, S2 has become a brown dwarf of mass 0.052  $M_{\odot}$  and the separation is 0.687  $R_{\odot}$ .

#### 4.5.2 *Property distributions of the synthetic population*

We create our population of putative PREPs by integration over time from  $t = 0$  to  $t = 9.5$  Gyr. The star formation rate is taken to be constant over the age of the Galactic Disc. Whereas Table 4.1 shows the relative numbers of PREPs obtained from a single generation of binaries, continuous star formation over the age of the Galactic Disc builds up a population of PCEBs, PREPs, CVs, and MCVs that, as birth time increases, favours systems with progressively higher mass primaries because lower mass primaries, especially in later generations, do not have enough time to evolve to the WD stage.

#### **Period distribution**

Figs 4.3 and 4.4 show the theoretical period distribution of the PREPs just before the beginning of Roche lobe overflow (RLOF) in a present day population formed over the age of the Galactic Disc for various  $\alpha$ . The contributions to the period distribution by WD primaries of a certain type are depicted in Fig. 4.3 while the contributions to the period distribution by the secondaries of a given type are displayed in Fig. 4.4.

The period distribution peaks around 3 hr with a long tail extending to about 10 hr for low  $\alpha$ . We note that at low  $\alpha$  our synthetic population tends to have orbital periods clustering around the 1 to 4 hr region while at higher  $\alpha$  they are confined to the 1 to 3 hr region.

Fig. 4.3 shows that when  $\alpha = 0.1$  the main contributors to the whole range of periods are systems with CO WD primaries characterised by orbital periods from about 1 to 7 hr and a peak near 3 hr. Systems with He WDs are also present but are fewer and their periods are below 3 hr. Massive ONe WD primaries form a much smaller fraction of the distribution, as expected from a Salpeter initial mass function, but make some contribution to the full range of periods when  $\alpha < 0.4$ .

As  $\alpha$  increases the fraction of CO WD systems decreases until these all but disappear for  $\alpha > 0.6$  while the percentage of He WDs increases dramatically. For  $\alpha \geq 0.4$ ,

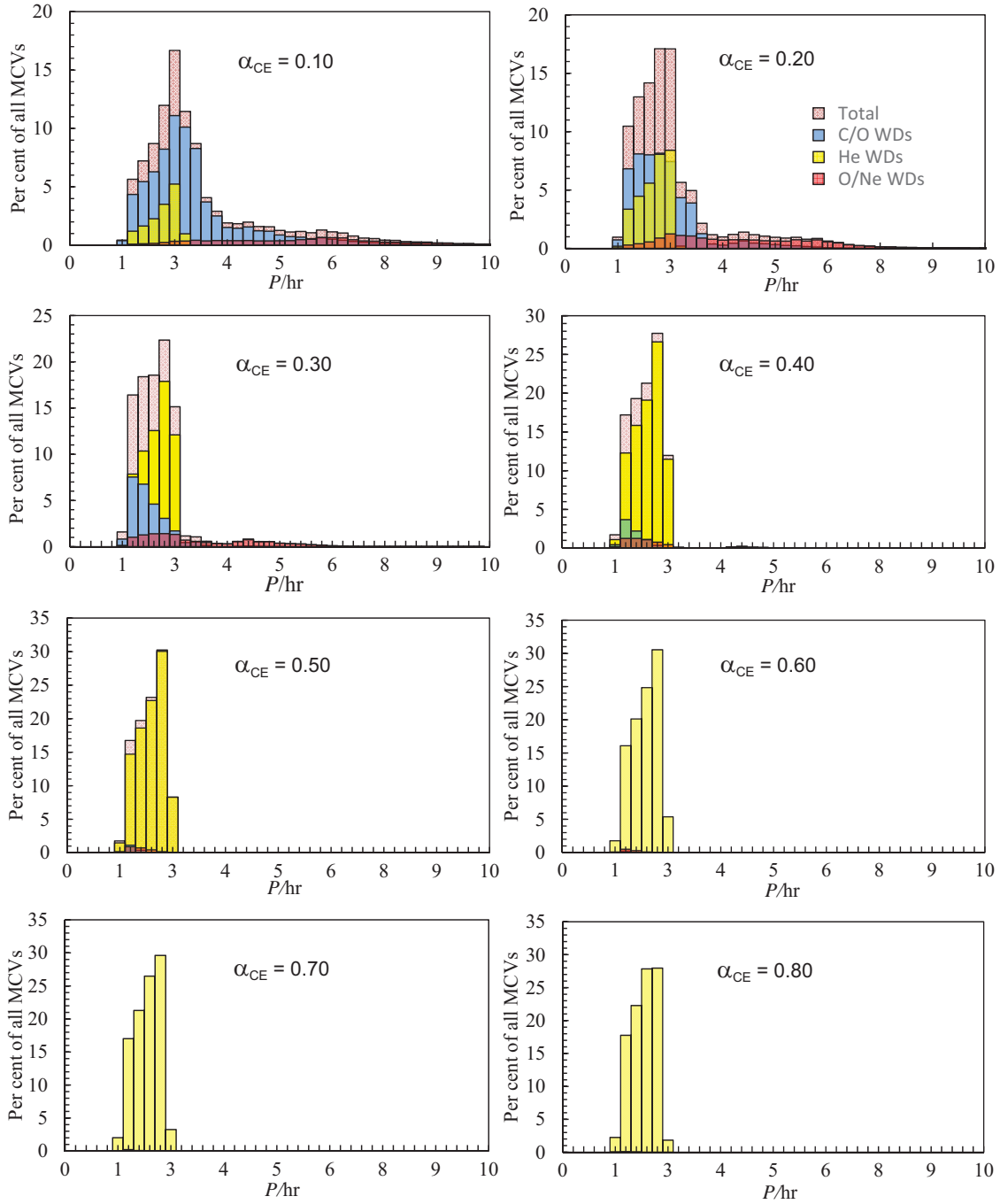


Figure 4.3: Theoretical period distribution of magnetic systems just before they start RLOF for various  $\alpha$ 's. The period distribution of the primary WD types is shown as the superimposed coloured categories. The total of the distribution is shown as the pink background histogram peaking around 2.8 to 3.0 hrs. This is to be compared with the observed distribution for PREPs in Fig. 4.2

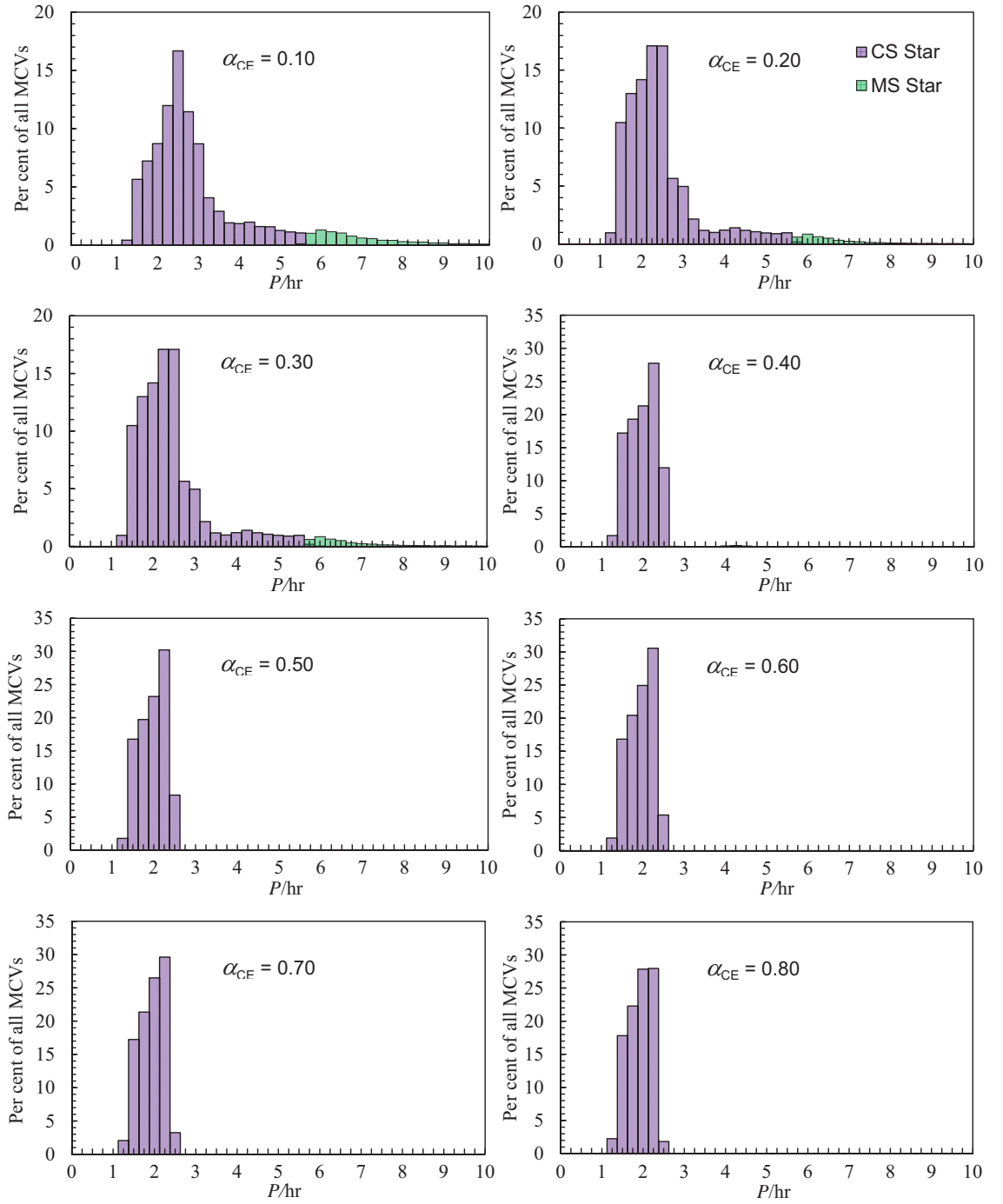


Figure 4.4: Same as Fig.4.3 but with the secondary star types shown as the superimposed coloured categories. Both secondary star types are MS stars. The CS type is a deeply or fully convective MS star with  $M < 0.7 M_{\odot}$ .

the orbital periods are always below 3 hr and He WD systems well and truly dominate the period distribution. For  $\alpha > 0.6$  the only systems that are predicted to exist are those with He WDs. The fraction of ONe WD systems reaches a maximum near  $\alpha = 0.2$  and then decreases.

We note that systems with He WDs tend to populate the lowest period range at all  $\alpha$ . These systems are generally characterised by initially lower-mass primaries, and thus lower-mass companions because  $q \leq 1$ , and shorter orbital periods and initiate common envelope evolution before helium ignition. Usually systems characterised by short initial periods are unlikely to survive at low  $\alpha$  because the stronger drag force exerted on the two stars during WD evolution causes them to merge.

Fig. 4.4 shows that most companions, particularly at shorter orbital periods, are low-mass deeply convective stars. More massive secondaries are generally found at longer periods for three reasons. First, longer orbital periods require high-mass white dwarfs to initiate stable mass transfer over the age of the Galactic Disc and these massive WDs can have secondaries with masses all the way up to  $1.44 M_{\odot}$ , provided  $q \leq 1$ . Second, during CEE for a fixed primary initial mass and orbital period, systems with more massive secondaries have more orbital energy and so a smaller portion of this energy is necessary to eject the envelope. This leads to longer orbital periods. Third, for a fixed WD mass, more massive secondaries fill their Roche lobes at longer orbital periods and so systems with more massive companions are more likely to evolve into PREPS.

### Stellar pair distribution

Table 4.5 lists fractions of the various combinations of types of WD primaries and secondary types just before RLOF commences. At low  $\alpha$  the predominant combination is a CO WD primary with a low-mass M-dwarf secondary. Second in abundance are systems comprised of a He WD with a low-mass M-dwarf secondary. Other combinations are also found but in much smaller numbers. At high  $\alpha$  the two major categories are swapped and those systems with He WD primaries become the predominant type. The observed fraction of He WDs ( $f_{\text{He}}$ ) is generally low among classical CVs ( $f_{\text{He}} \lesssim 10$  per cent) and pre-CVs ( $f_{\text{He}} \lesssim 17 \pm 8$  per cent as shown by Zorotovic et al. (2011)). The results in Table 4.5 indicate that in order to reproduce the observed low fraction of He WDs our models need to be restricted to  $\alpha < 0.3$ .

Table 4.5: The fraction of the combinations of types of WD primaries and secondary types just before RLOF commences for various  $\alpha$ . The stellar type CS is a deeply or fully convective low-mass MS star with  $M < 0.7 M_{\odot}$ .

$\alpha$	MCV progenitor pairs, fraction per cent					
	He WD/CS	CO WD/CS	ONe WD/CS	He WD/MS	CO WD/MS	ONe WD/MS
0.10	14.86	69.63	5.72	0.00	3.77	6.03
0.20	30.27	52.27	12.99	0.00	0.38	4.10
0.30	61.36	25.69	12.49	0.00	0.00	0.46
0.40	96.44	7.78	5.78	0.00	0.00	0.00
0.50	95.85	1.72	2.44	0.00	0.00	0.00
0.60	98.75	0.28	0.98	0.00	0.00	0.00
0.70	99.67	0.01	0.32	0.00	0.00	0.00
0.80	99.92	0.00	0.00	0.00	0.00	0.00

### Mass distribution

Fig. 4.5 shows that all our models predict that, on average, longer orbital period systems contain CO WDs while shorter-period systems tend to have He WD primaries. At low  $\alpha$  the primaries are predominantly CO WDs with masses in the range 0.5 to 1.1  $M_{\odot}$  followed in lesser numbers by He WDs with masses in the range 0.4 to 0.5  $M_{\odot}$  while ONe WDs, with masses in the range 1.2 to 1.4  $M_{\odot}$ , are rarer with their incidence reaching a maximum near  $\alpha = 0.2$ .

We note that there is a curious dip in the WD mass distribution near  $M_{\text{WD}} = 0.8 M_{\odot}$  which widens as  $\alpha$  increases until all CO and ONe WDs disappear for  $\alpha > 0.5$ . This is because as  $\alpha$  increases, systems emerge from CE at progressively longer periods, because large  $\alpha$  means a high envelope clearance efficiency which leads to larger stellar separation at the end of the common envelope stage. However the longer the orbital period, the higher the WD mass needs to be for stable mass transfer to commence. Thus the gap in the WD mass distribution is caused by those systems that emerge from CE at large separations but with WD primaries that are not massive enough to allow RLOF to take place. Another, albeit much narrower, gap occurs near 0.5  $M_{\odot}$  for all  $\alpha$  but becomes wider for  $\alpha \geq 0.2$ . This gap also persists until all CO and ONe WDs disappear at  $\alpha > 0.5$ . It divides systems with He WDs primaries from those with CO WDs and is linked to whether the stars enter CEE on the RGB, and so produce a He WD primary with  $M_{\text{WD}} \lesssim 0.5 M_{\odot}$ , or on the AGB, and so produce a CO WD primary with  $M_{\text{WD}} > 0.5 M_{\odot}$ .

Once again Fig. 4.6 shows that the secondaries are predominantly low-mass deeply or fully convective M-dwarf stars. The distribution has a broad peak around 0.1 to 0.3  $M_{\odot}$  at  $\alpha = 0.1$  to 0.2 with a long tail extending to 1.2  $M_{\odot}$ . As  $\alpha$  increases, the peak in the secondary mass distribution shifts to slightly lower masses (around 0.1 to 0.25  $M_{\odot}$ ) but the high-mass tail shrinks quite dramatically. At  $\alpha \geq 0.4$  the distribution is confined to secondary masses of less than about 0.3  $M_{\odot}$ . As already noted in section 4.5.2, the majority of these very low-mass donor stars belong to systems that underwent CEE during the Hertzsprung gap or RGB phases and thus have He WD primaries with  $M_{\text{WD}} \lesssim 0.5 M_{\odot}$ . We also note that systems with low-mass secondaries ( $M_{\text{sec}} \lesssim 0.35 M_{\odot}$ ) remain detached for longer because magnetic braking is inefficient in these stars and gravitational radiation is the main source of loss of angular momentum.

### Magnetic field distribution

Fig. 4.7 shows the theoretical magnetic field distribution and the breakdown of the primary WD types for our range of  $\alpha$ . The maximum field strength is a few  $10^8$  G and is found mostly in systems whose primary is a He WD. The reason for this is that systems that undergo CEE during the RGB evolution have shorter initial orbital



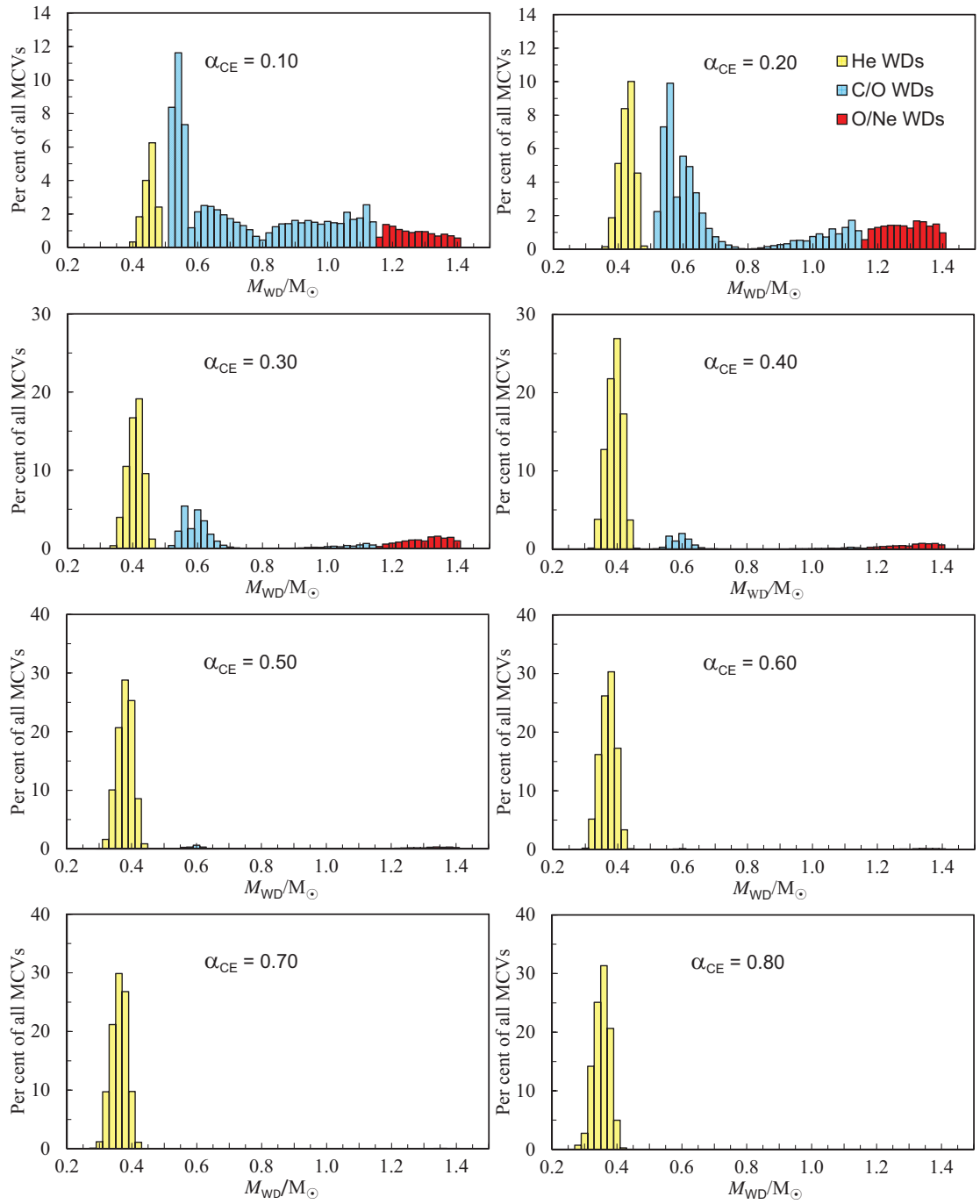


Figure 4.5: Theoretical mass distribution of the WD primary star of magnetic systems just before they start RLOF for various  $\alpha$ . The distributions of the three WD types are shown as three superimposed coloured categories.

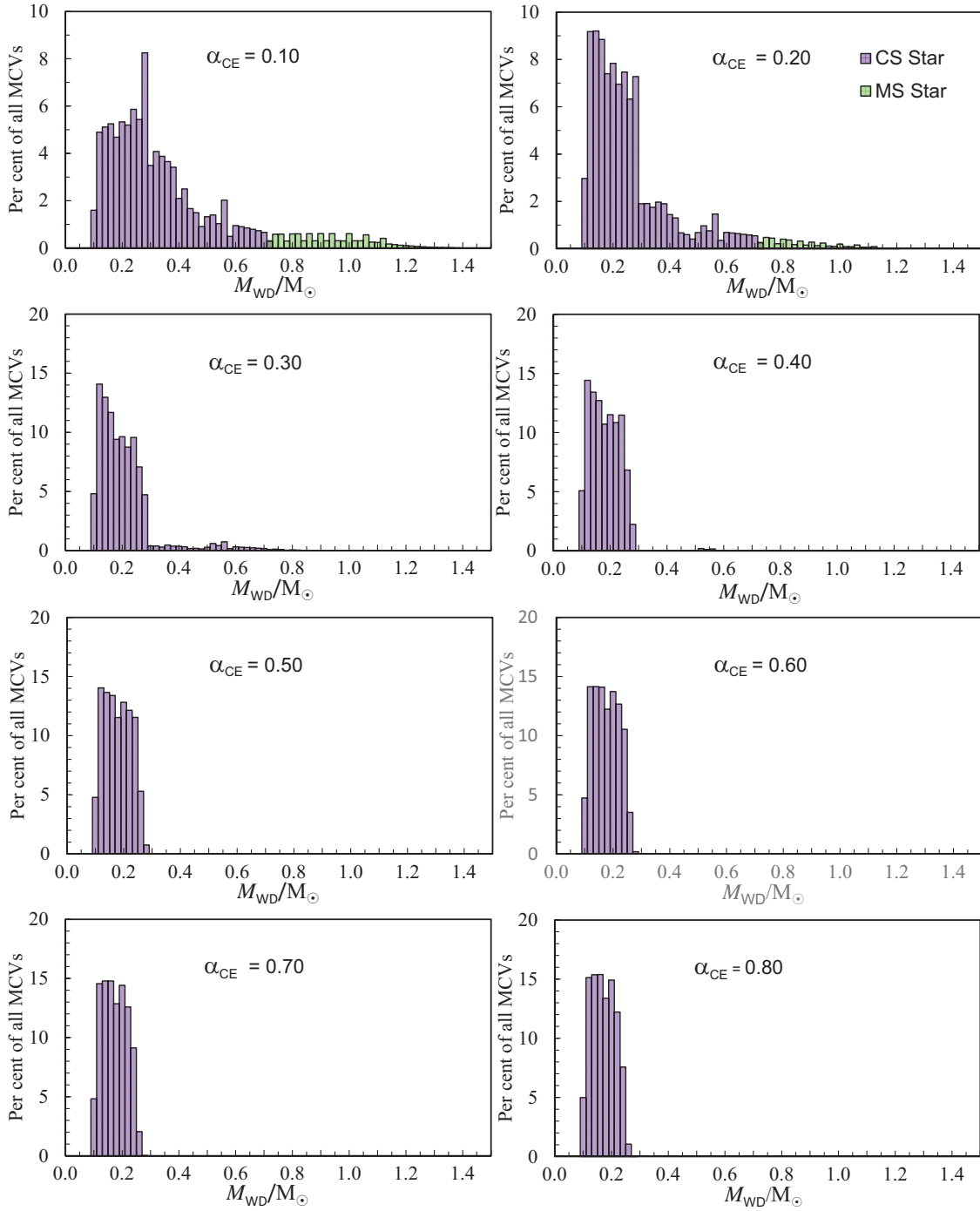


Figure 4.6: As in Fig 4.5 but for the secondary star types shown as the coloured categories. Both secondary star types are MS stars. The CS type is a deeply or fully convective MS star with  $M < 0.7 M_{\odot}$ .

periods and create very short period binaries with a highly magnetic WD, as expected from equation 4.1.

The magnetic field distribution is dominated by systems with CO WD primaries when  $\alpha \leq 0.2$ . When  $\alpha \geq 0.4$  the field distribution becomes narrower and its peak shifts to higher field strengths. For  $\alpha \geq 0.6$  the field distribution only contains very highly magnetic He WD primaries with a peak near  $3.2 \times 10^8$  G at  $\alpha = 0.8$ . This shift to high fields is because those systems that go through CEE while their primaries are on the RGB merge for low  $\alpha$  but can survive for high  $\alpha$  giving rise to very short orbital period systems with strongly magnetic, low-mass WDs.

We note that the magnetic field distribution has a dip near  $8 \times 10^6$  G appearing at  $\alpha \geq 0.2$  and persisting until all CO and ONe WDs disappear from the distribution. This is reminiscent of the dip we encountered in the WD mass distribution (see 4.5.2) and has the same explanation. The similar behaviour is because the magnetic field strength is a function of WD mass (by virtue of equations 4.1). The field dip is thus caused by the dearth of systems with WD masses around  $0.8 M_{\odot}$  (see Fig. 4.5).

## 4.6 Comparison to observations

The optimal observational sample with which to compare our results would be that formed by the known magnetic PREPs. However, this sample is exceedingly small and observationally biased. To make things worse, not all PREPS have well determined parameters, such as masses and magnetic field strengths. Hence, for some of these studies we use the observed sample of MCVs, noting the following important points (i) the MCV sample is magnitude-limited, (ii) MCVs suffer from prolonged high and low states of accretion and (iii) MCVs include systems at all phases of evolution. Some of them began Roche lobe overflow billions of years ago while others have only recently begun mass exchange. Therefore, one should take such a comparison with some degree of caution particularly when it comes to compare quantities that change over time, such as orbital periods and masses. When comparing masses we will also use the observed sample of non-magnetic Pre-CVs (Zorotovic et al., 2011).

The tables of Ferrario et al. (2015a) show that the observed orbital periods of MCVs are in the range 1 to 10 hr, masses are between about  $0.4$  and  $1.1 M_{\odot}$  and that the magnetic field distribution is relatively broad with a peak near  $3.2 \times 10^7$  G. A quick glance at Figs 4.3, 4.5 and 4.7 immediately reveals that models with  $\alpha > 0.3$  are all unable to reproduce the general characteristics expected from the progenitors of the observed population of MCVs and we elaborate on this in more detail below. Generally we see that generally models with  $\alpha > 0.3$  are not realistic and evolutionary effects

Table 4.6: Kolmogorov–Smirnov  $D$  statistic and probability  $P$  of the magnetic field distributions of the observed and synthetic populations of MCVs for a range of  $\alpha$ .

$\alpha$	$D$	$P$
0.10	0.17476	0.36069
0.15	0.19349	0.24632
0.20	0.25141	0.05845
0.30	0.22962	0.10500
0.40	0.26939	0.04298
0.50	0.35186	0.00429
0.60	0.38035	0.00006
0.70	0.61987	0.00000
0.80	0.94366	0.00000

cannot account for the large degree of discrepancy between theory and observations.

We begin our analysis with the magnetic field distribution. There is no evidence for field decay among MCVs (Ferrario et al., 2015a; Zhang et al., 2009) so we can assume that the magnetic field strength remains unchanged over the entire life of the magnetic binary.

We have used a K–S test (Press et al., 1992) to compare the magnetic field distribution of the observed population with the theoretical results. This test establishes the likelihood that two samples are drawn from the same population by comparison of the cumulative distribution functions (CDFs) of the two data samples. The CDFs of the two distributions vary between zero and one and the test is on the maximum of the absolute difference  $D$  between the two CDFs. It gives the probability  $P$  that a random selection would produce a larger  $D$ . Five model CDFs for five different  $\alpha$ 's and the CDF for the known observed magnetic fields of 81 MCV systems are compared in Fig. 4.8.

The observed samples of MCVs and magnetic PREPs are very biased, particularly at the low and high ends of the magnetic field distribution. At low fields ( $B \lesssim 10$  MG) the observed radiation is dominated by the truncated accretion disc. In these low-field systems the photosphere of the WD is never visible and Zeeman splitting cannot be used to determine field strengths. Nor can cyclotron lines be used to measure fields because they are too weak and invisible in the observed spectra. In the high field regime ( $B \gtrsim 100$  MG) mass accretion from the companion star is inhibited (Ferrario et al., 1989; Li et al., 1994) and so high field MCVs are very dim wind accretors often below the detection limits of most surveys (AR UMa, Hoard et al., 2004). Because of these biases the observed samples in these regimes are far from complete and theoretical fits are

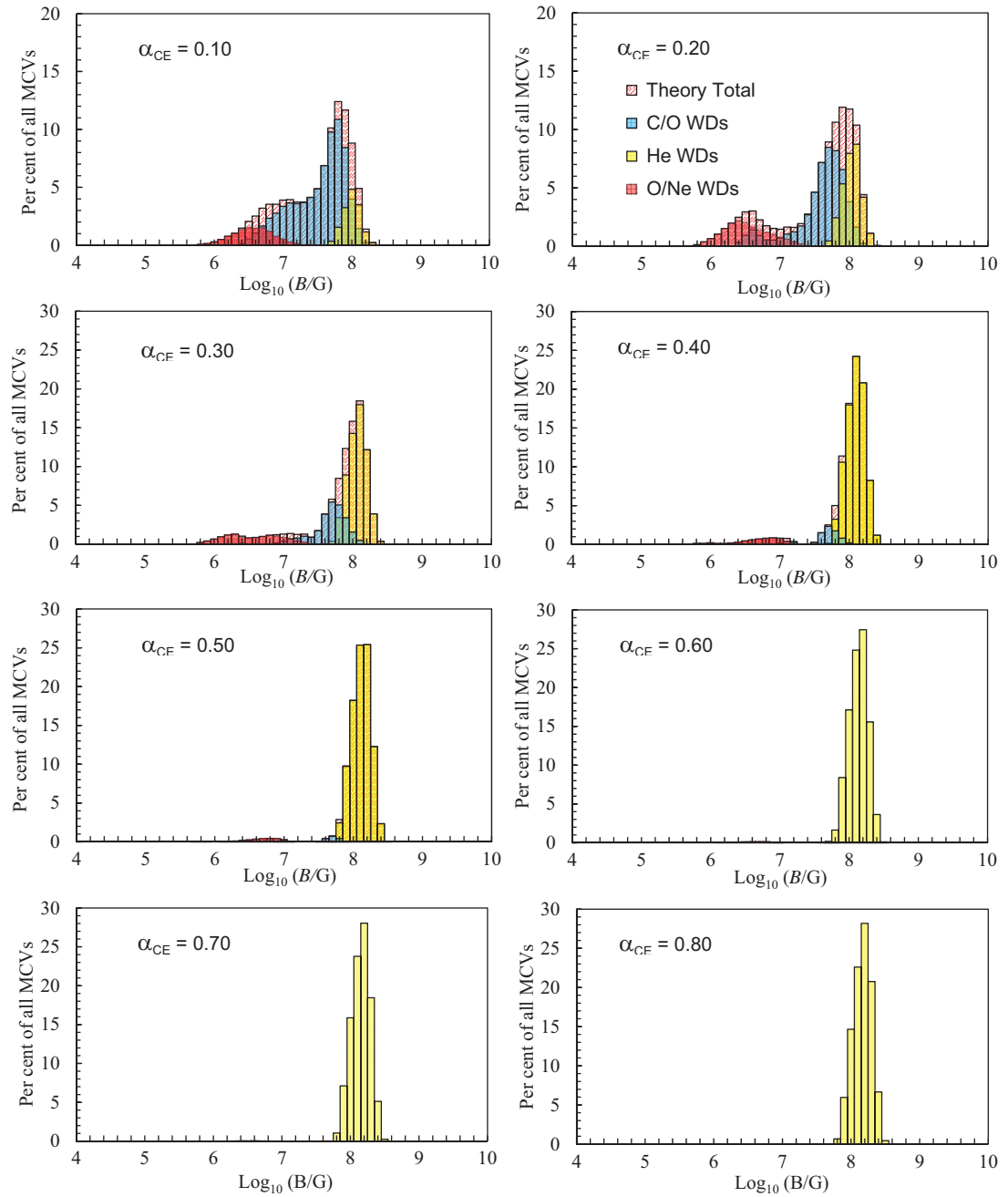


Figure 4.7: Pink shaded histogram: Total theoretical magnetic field distribution of the WD primary stars in magnetic systems just before they start RLOF for the indicated  $\alpha$ . The histograms of the three types of WDs making up the total theoretical magnetic field distribution are shown as the foreground coloured histograms. These three are made partially transparent so that details of the other histograms can be seen through them.

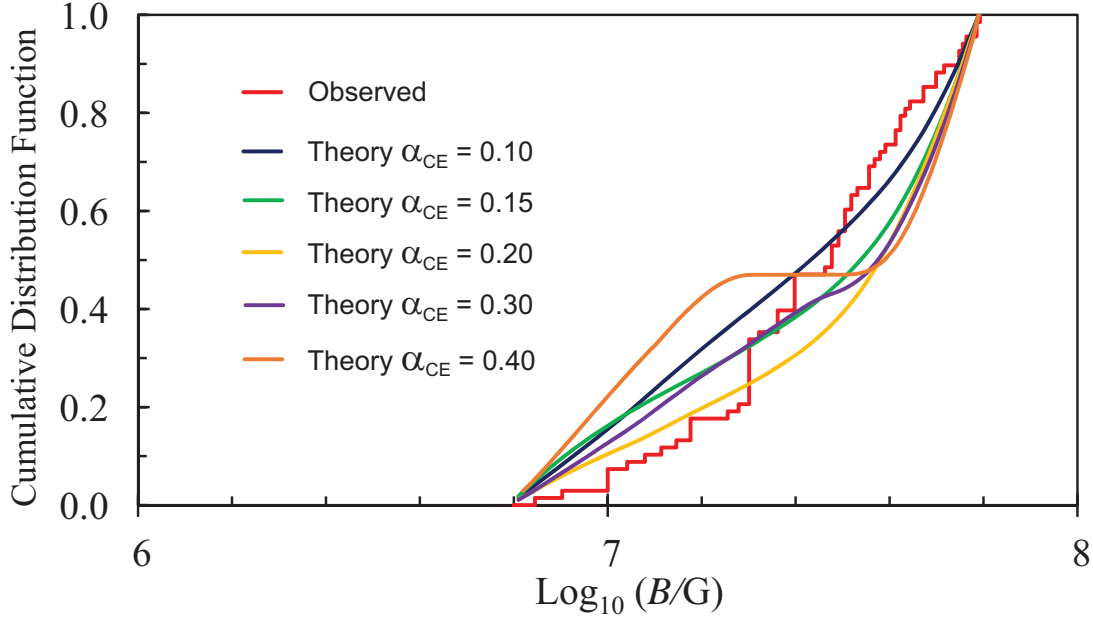


Figure 4.8: Theoretical cumulative distribution functions for the magnetic fields of MCV WDs at RLOF for  $\alpha = 0.10, 0.15, 0.20, 0.30$  and  $0.40$  and the CDF of the observed magnetic field of 81 systems taken from Ferrario et al. (2015a)

unreliable. We therefore restrict our comparison between theory and observations to field strengths in the range 10 to 70 MG.

The results of the K–S test for our range of  $\alpha$  are displayed in Table 4.6 and show that although no  $\alpha$  can be ruled out the field distribution is a better match to the observations at low  $\alpha$ . The comparison of the magnetic field distribution between theory and observations is shown in Fig. 4.9 for  $\alpha = 0.1$ .

We stress that for  $\alpha > 0.3$  all the theoretical magnetic field distributions shown in Fig. 4.7 are very unrealistic because only very high field ( $B > 60$  MG) He WDs ( $M \lesssim 0.5 M_{\odot}$ ) are predicted to exist. This is contrary to observations that show that fields cover a much wider range of strengths (a few  $10^6$  to a few  $10^8$  G) and WD masses ( $0.4$  to  $1.2 M_{\odot}$ ) as seen in Tables 2 and 3 of Ferrario et al. (2015a).

We have performed a K–S study between the synthetic WD mass distribution and that of WD masses in MCVs taken from Ferrario et al. (2015a). In principle such a comparison can be justified if we make the usual assumption that the mass of the white dwarf does not grow in CVs because nova eruptions tend to expel all material that is accreted. However, we found that the K–S test applied to the WD masses of the theoretical and observed population of MCVs yields poor results, as shown in the second and third columns of Table 4.7. However, such a conflict is not surprising because our

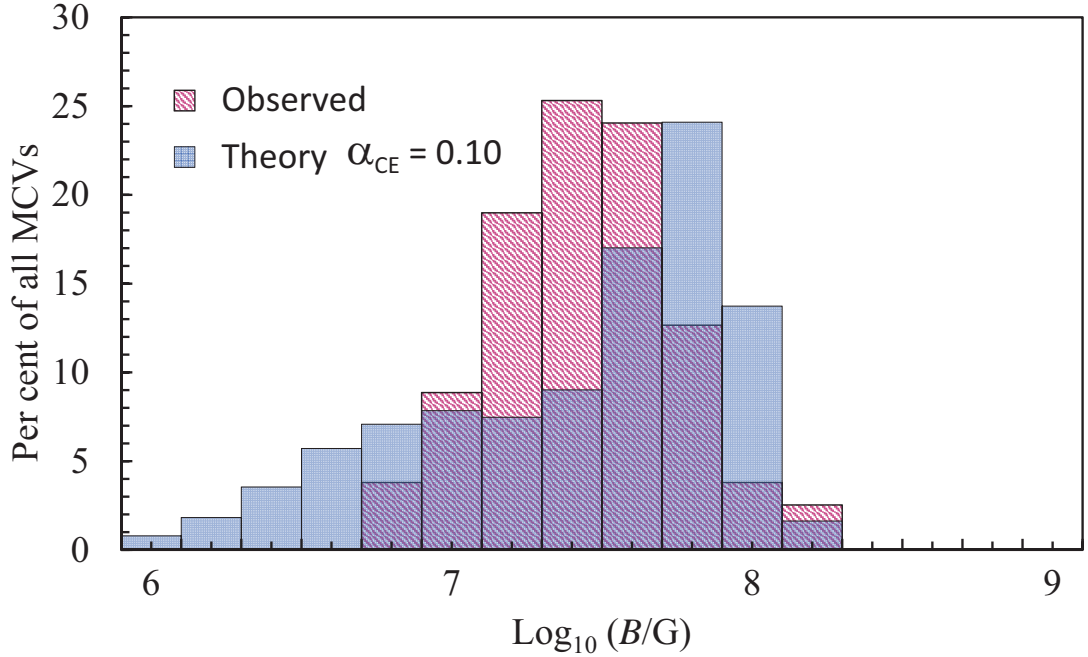


Figure 4.9: Comparison of the theoretical magnetic field strength for  $\alpha = 0.1$  and the observed magnetic field strength of the 81 MCVs taken from Ferrario et al. (2015a)

assumption that the mass of the WD does not grow because of nova eruptions may not be correct.

In this context, I note that Zorotovic et al. (2011) noticed a curious discrepancy in their observational data of CVs and Pre-CVs. That is, they found that the mean WD mass in CVs ( $0.83 \pm 0.23 M_{\odot}$ ) significantly exceeds that of pre-CVs ( $0.67 \pm 0.21 M_{\odot}$ ) and they excluded that this difference could be caused by selection effects. The two possible solutions advanced by Zorotovic et al. (2011) were that either the mass of the WD increases during CV evolution, or a short phase of thermal time-scale mass transfer comes before the formation of CVs during which the WD acquires a substantial amount of mass via stable hydrogen burning on the surface of the WD (as first suggested by Schenker et al., 2002). During this phase the system may appear as a super-soft X-ray source (Kahabka & van den Heuvel, 1997). Using this assumption Wijnen et al. (2015) could build a large number of massive WDs. However their model still created too many low-mass He WDs and too many evolved companion stars contrary to observations. Another possibility has recently been advanced by Zorotovic & Schreiber (2017). In order to achieve a better agreement between their binary population synthesis models and observations of CVs they adopted the ad-hoc mechanism proposed by Schreiber et al. (2016) which surmises the existence of additional angular

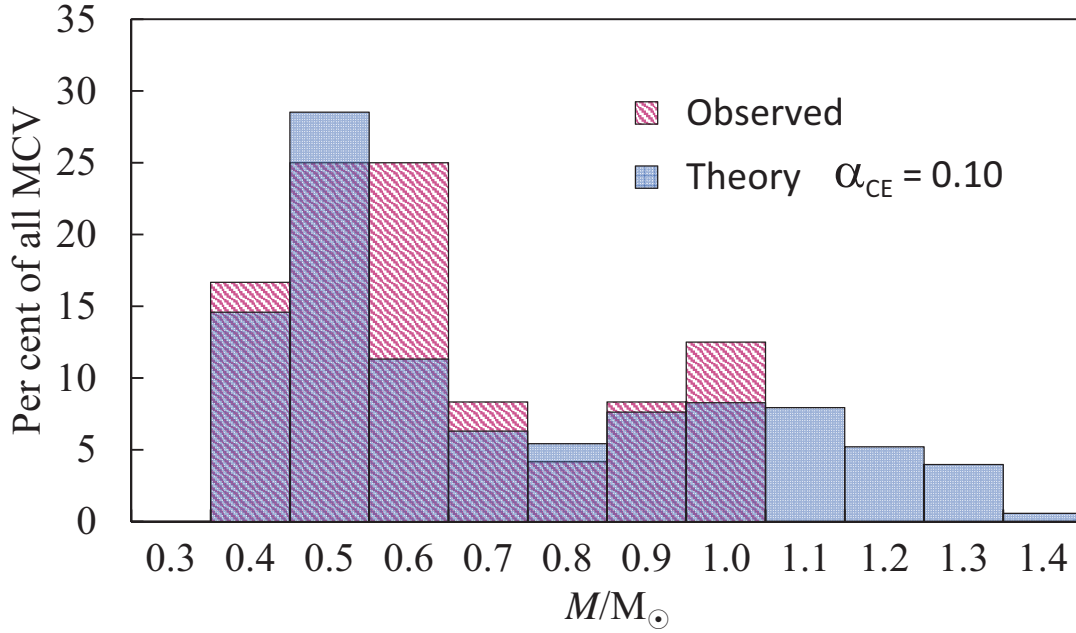


Figure 4.10: Comparison of the mass distributions for the observed pre-CV white dwarf masses taken from Zorotovic et al. (2011) and the theoretical mass distribution of the WDs as the systems start RLOF for  $\alpha = 0.10$ .

momentum losses generated by mass transfer during the CV phase. Such losses are assumed to increase with decreasing WD mass and would cause CVs with low-mass WDs to merge and create an isolated WD. By removing these merged systems from the synthetic CV sample the average WD mass increases. Furthermore such a mechanism would explain the existence of isolated low-mass WDs ( $M_{WD} < 0.5 M_{\odot}$ ) that constitute around 10 per cent of all single WDs observed in the solar neighbourhood (e.g. Kepler et al., 2007).

Going back to our studies, if a comparison between WD masses in MCVs and our synthetic population may not be meaningful, the next best sample to use for our K–S test is the observed WD masses of pre-CVs (Zorotovic et al., 2011). The results are reported in the fourth and fifth columns of Table 4.7 and show that the agreement between observations and theory is greatly improved. The comparison of the synthetic and observed Pre-CV WD mass distribution is shown in Fig. 4.10 for the largest K–S probability when  $\alpha = 0.10$ .

We note that the Pre-CV observational sample shows a dearth of systems in the WD mass distribution centred around  $0.8 M_{\odot}$ . This mass gap was already noted in the theoretical BSE models and the reasons for its existence were explained in section 4.5.2. The smaller size of this gap for models with  $\alpha \leq 0.2$  explains why we achieve a better fit with observations for  $\alpha = 0.1$ , as indicated by the K–S test.



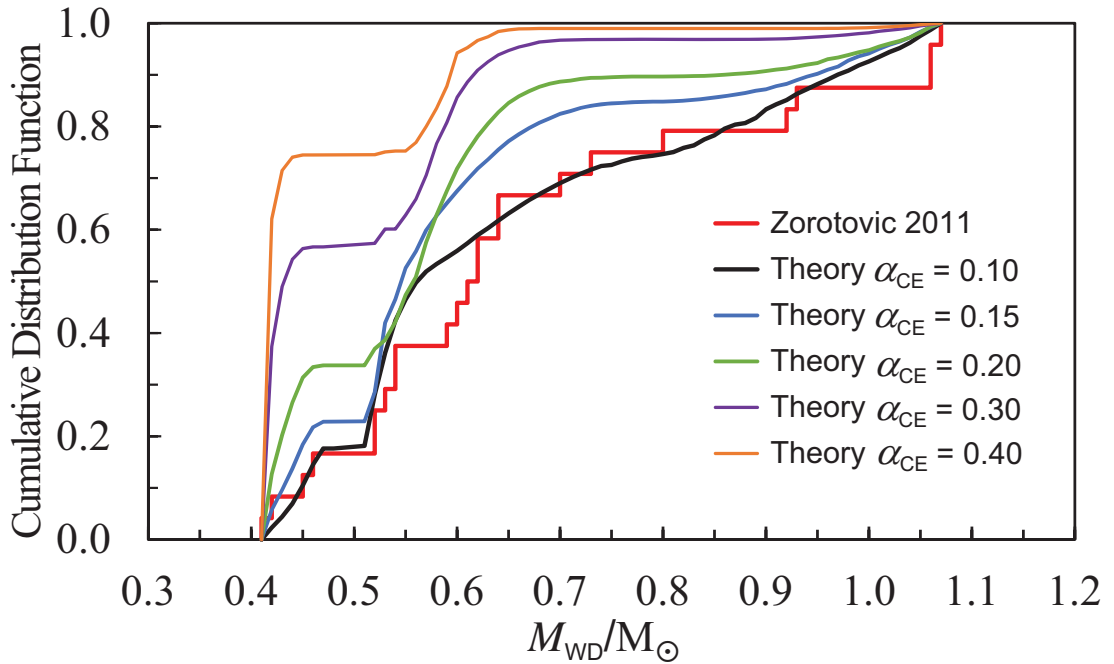


Figure 4.11: Cumulative Distribution Functions of the mass distributions for the observed pre-CV WD masses taken from Zorotovic et al. (2011) and the theoretical distribution of the WDs as the systems start RLOF for  $\alpha = 0.10, 0.15, 0.20, 0.30$  and  $0.40$ . The K-S statistics for this plot are shown in the fourth and fifth columns of table 4.7

Table 4.7: K–S  $D$  statistic and probability  $P$  of the WD mass distributions of the observed MCVs listed by Ferrario et al. (2015a, second and third columns) and our synthetic populations for  $\alpha$  given in the first column. We show the K–S results of the observed Pre-CV masses of Zorotovic et al. (2011) and our synthetic populations at the start of RLOF (fourth and fifth columns).

$\alpha$	$D$	$P$	$D$	$P$
0.10	0.37687	0.02023088	0.12954	0.95281557
0.15	0.49861	0.00064407	0.23478	0.34844783
0.20	0.56677	0.00006150	0.26010	0.23507547
0.30	0.62615	0.00000622	0.48014	0.18713800
0.40	0.69590	0.00000032	0.66148	0.00106500

We stress that if  $\alpha > 0.3$  the theoretical WD mass distribution shown in Fig. 4.5 is very unrealistic because only He WDs ( $M < 0.5 M_{\odot}$ ) are predicted to exist by these models. This is contrary to observations that show that masses cover the much wider range 0.4 to  $1.2M_{\odot}$  (see Tables 2 and 3 in Ferrario et al., 2015a).

Next, we look at the secondary mass distribution, keeping in mind that a comparison between our synthetic `bse` mass sample and the observed secondary masses in MCVs is definitely not appropriate because secondary masses decrease over time as mass is transferred to the WD. Nonetheless it may still be pertinent to use the observed Pre-CV sample to study and compare the overall characteristics of these samples so that we can, at the very least, discard some of the most extreme theoretical models.

Fig. 4.6 shows that if  $\alpha > 0.3$  then  $M_{\text{sec}} < 0.3 M_{\odot}$ , which is inconsistent with observations of pre-CVs (see Zorotovic et al., 2011). Furthermore, we can see that when  $\alpha > 0.2$ , the decline towards higher masses becomes far too steep. This straightforward comparison seems again to indicate that models with  $\alpha > 0.3$  are very unrealistic and therefore low  $\alpha$  is a better fit.

## 4.7 Discussion and Conclusions

The origin of large-scale magnetic fields in stars is still a puzzling question (see Ferrario et al., 2015b). However, the results from recent surveys such as the SDSS (Kepler et al., 2013), BinaMIcS (Alecian et al., 2015) and MiMes (Wade et al., 2016) have provided us with a much enlarged sample of magnetic stars that have allowed investigators to conduct studies like this one. There are two main competing scenarios to explain the existence of magnetic fields in WDs. In 1981, Angel et al. first proposed that the magnetic Ap and Bp stars are the most likely progenitors of the highly MWDs under the assumption of magnetic flux conservation (see also Tout et al., 2004; Wickramasinghe & Ferrario, 2005). According to this scenario the weak fields recently observed in a number of WDs (e.g. Landstreet et al., 2016) could be either dynamo generated in late stages of stellar evolution or these WDs may be the descendants of MS stars with fields below the current detection limit. However, not much is known about the weak magnetic field regime. For instance, it is still not known whether all white dwarfs are magnetic at some level because the weakest measured fields are just about at the limit of detectability.

The best clue so far on the origin of fields in WDs (isolated and in binaries) has come from the study of their binary properties (Liebert, Bergeron, Holberg, 2005; Liebert et al., 2015), as outlined in section 4.3.1. This is why the proposal by Tout et al. (2008), that the origin of magnetic fields in WDs is related to their duplicity and

stellar interaction during CEE, is becoming more and more appealing.

We have extended our population synthesis study of binary systems carried out in chapters 2 and 3 for the HFMWDs to explain the origin of fields in the accreting WDs in MCVs. Similarly to the investigations conducted in chapters 2 and 3, we varied the CE efficiency parameter  $\alpha$  to investigate its effects on the resulting synthetic population of MCVs. We have shown that models with  $\alpha \geq 0.4$  are not able to reproduce the large range of WD masses, field strengths, and secondary types and masses that are observed in MCVs and therefore models with  $\alpha < 0.4$  best represent the observed data. K–S tests conducted to compare our synthetic WD mass and magnetic field distributions with the observed populations have given us some quantitative support in favour of models with  $\alpha < 0.4$ .

However, we need to stress again some of the shortcomings of our work and in particular those that arise from our comparison to observations. Many of the parameters (e.g., WD mass, magnetic field, secondary star mass and type, orbital period) that characterise the Galactic populations of MCVs and PREPs and are needed for comparison studies are often hard to ascertain owing to evolutionary effects and observational biases that are difficult to disentangle. For instance, we mentioned in section 4.6 magnetic WDs in PREPs would be the best objects with which to compare my theoretical results and in particular the mass distribution, because mass is not then contaminated by accretion processes. On the other hand there are far too few members of this population. The WD mass distribution provided by the much larger sample of MCVs cannot be used either for comparison purposes because masses vary over time, owing to accretion and nova explosions. So instead we have used the sample provided by the non-magnetic Pre-CVs of Zorotovic et al. (2011).

The situation is somewhat ameliorated when we consider the magnetic field distribution because fields are not expected to change over time (see Ferrario et al., 2015a). However, the true magnetic field distribution of MCVs is not well known because it is plagued by observational biases. For example, at field strengths below a few  $10^7$  G most systems (the intermediate polars) have an accretion disc from which continuum emission and broad emission lines swamp the Zeeman and cyclotron features arising from the WD surface (Ferrario et al., 1992) and so hide those spectral signatures that are crucial to determine their field strengths. Very high field polars are also likely to be under-represented in the observational set because mass accretion from the companion star is impeded by the presence of strong fields (Ferrario et al., 1989; Li et al., 1994) making these systems very dim wind accretors.

Despite the limitations highlighted above, we have shown that the characteristics of the MCVs are generally consistent with those of a population of binaries that is born

already in contact (exchanging mass) or close to contact, as first proposed by Tout et al. (2008). This finding is also in general agreement with the hypothesis first advanced by Schwöpe et al. (2009) that the binaries known as PREPs, where a MWD accretes matter from the wind of a low-mass companion, are the progenitors of the MCVs.

### **Acknowledgements**

GPB gratefully acknowledges receipt of an Australian Postgraduate Award. CAT thanks the Australian National University for supporting a visit as a Research Visitor of its Mathematical Sciences Institute, Monash University for support as a Kevin Watford distinguished visitor and Churchill College for his fellowship.

# Chapter 5

## A Double Degenerate White Dwarf System

This chapter is a reproduction of the paper published in Monthly Notices of the Royal Astronomical Society, viz:

*Kawka, Briggs, Vennes, Ferrario, Paunzen & Wickramasinghe, MNRAS (2017), 466(1): 1127–1139. A fast spinning magnetic white dwarf in the double-degenerate, super-Chandrasekhar system NLTT 12758<sup>1</sup>*

### 5.1 Abstract

We present an analysis of the close double degenerate NLTT 12758, which is comprised of a magnetic white dwarf with a field of about 3.1 MG and an apparently non-magnetic white dwarf. We measured an orbital period of 1.154 days and found that the magnetic white dwarf is spinning around its axis with a period of 23 minutes. An analysis of the atmospheric parameters has revealed that the cooling ages of the two white dwarfs are comparable, suggesting that they formed within a short period of time from each other. Our modelling indicates that the non-magnetic white dwarf is more massive ( $M = 0.83 M_{\odot}$ ) than its magnetic companion ( $M = 0.69 M_{\odot}$ ) and that the total mass of the system is higher than the Chandrasekhar mass. Although the stars will not come into contact over a Hubble time, when they do come into contact, dynamically unstable mass transfer will take place leading to either an accretion induced collapse into a rapidly spinning neutron star or a Type Ia supernova.

### 5.2 Introduction

The majority of stars will evolve into a white dwarf and a significant fraction of white dwarfs harbours a magnetic field that ranges from a few kG to about 1000 MG (Liebert,

---

<sup>1</sup>Based on observations made with ESO telescopes at the La Silla Paranal Observatory under programmes 083.D-0540, 084.D-0862, 089.D-0864 and 090.D-0473. Based in part on data collected with the Danish 1.54-m telescope at the ESO La Silla Observatory.

Bergeron & Holberg, 2003; Kawka et al., 2007). Spectroscopic and spectropolarimetric surveys (e.g., Schmidt & Smith, 1995; Schmidt et al., 2001a; Aznar Cuadrado et al., 2004; Kawka et al., 2007; Kawka & Vennes, 2012a; Landstreet et al., 2012; Kepler et al., 2013) of white dwarfs have been able to place constraints on the incidence of magnetism among white dwarfs. The incidence of magnetic white dwarfs in the local neighbourhood has been estimated by Kawka et al. (2007) to be around 20 %. The local sample, as well as various surveys, have shown that the incidence of magnetism as a function of field strength is constant, although Landstreet et al. (2012) suggested a possible field resurgence at the extremely low-field ( $< 1$  kG) end of the distribution. A higher incidence of magnetism is also observed in cool polluted white dwarfs. Kawka & Vennes (2014) found an incidence of  $\approx 40$  % in cool ( $T_{\text{eff}} < 6000$  K) DAZ<sup>2</sup> white dwarfs. A higher incidence of magnetism was also observed among cool DZ<sup>3</sup> white dwarfs (Hollands et al., 2015). A recent review on the properties of magnetic white dwarfs can be found in Ferrario et al. (2015a).

The origin of large scale magnetic fields in stars is still one of the main unanswered questions in astrophysics, although recent data, particularly from surveys such as the Sloan Digital Sky Survey (SDSS, York et al., 2000), the Magnetism in Massive Stars (MiMes, Wade et al., 2016) and the Binarity and Magnetic Interactions in various classes of stars (BinaMIcS, Alecian et al., 2015) may have finally thrown some light into this matter (Ferrario et al., 2015b). Magnetism in white dwarfs has been explained with two main evolutionary scenarios. For a long time the leading theory was that the progenitors of magnetic white dwarfs are magnetic Ap and Bp stars (Angel et al., 1981). Under the assumption of magnetic flux conservation, the magnetic field strengths observed in Ap stars would correspond to magnetic fields in white dwarfs in excess of 10 MG (Kawka & Vennes, 2004; Tout et al., 2004; Wickramasinghe & Ferrario, 2005). The progenitors of white dwarfs with weaker fields may be other main-sequence stars whose magnetic fields are below our current detection limits or could be dynamo-generated in later stages of stellar evolution.

More recently, proposals that strong magnetic fields are created in evolving interacting binaries via a dynamo mechanism during a common envelope (CE) phase (Tout et al., 2008; Potter & Tout, 2010; Nordhaus et al., 2011; García-Berro et al., 2012; Wickramasinghe, Tout & Ferrario, 2014) have gained momentum as a possible origin for strong magnetic fields in white dwarfs. The main reason for this proposal is that all magnetic white dwarfs appear to be either single or in interacting binaries (the magnetic cataclysmic variables). That is, magnetic white dwarfs are never found paired

---

<sup>2</sup>DAZ type white dwarfs show photospheric hydrogen (DA) and metal lines.

<sup>3</sup>DZ type white dwarfs show metal lines only.

with a non-interacting, non-degenerate star, which is at odds with the fact that approximately 30% of all non-magnetic white dwarfs are found in non-interacting binaries with a non-degenerate companion (usually an M-dwarf) (Liebert et al., 2005; Ferrario, 2012; Liebert et al., 2015a). This result is hard to explain and leaves the magnetic cataclysmic variables without obvious progenitors. Because of this observational peculiarity, the existence of magnetic fields in white dwarfs has been linked to fields generated during CE binary interactions or mergers. The merger scenario during the CE also successfully explains the higher than average mass of isolated magnetic white dwarfs (Briggs et al., 2015). The complex magnetic field structure usually observed in rotating high field magnetic white dwarfs would also be in support of a merging hypothesis.

However, a few common-proper motion (CPM) magnetic plus non-magnetic double degenerate systems are now known (Ferrario et al., 1997b; Girven et al., 2010; Dobie et al., 2012, 2013). In some of these cases, the more massive magnetic white dwarf is hotter and hence younger than its non-magnetic companion, which seems to imply that the more massive star evolved later. This apparent paradox can be resolved by postulating that systems of this kind were initially triple systems and that the magnetic white dwarf resulted from the merger of two of the three stars (e.g., EUVE J0317–855, Ferrario et al., 1997b).

The study of the magnetic field structure in white dwarfs may also give us important clues on how they formed. Normally, a simple dipole is assumed for the field structure, but the study of rotating magnetic white dwarfs have all shown variability, hence revealing much more complex structures. One of the most extreme examples of a rotating magnetic white dwarf is the hot ( $T \approx 34\,000$  K) and massive ( $M \approx 1.35 M_{\odot}$ ) EUVE J0317-855, which has a rotation period of 12 minutes (Barstow et al., 1995; Ferrario et al., 1997b). The rotation of the white dwarf reveals a two component magnetic field structure: A high field magnetic spot ( $B \geq 425$  MG) with an underlying lower field (Vennes et al., 2003). Another example of a rotating white dwarf with a complex magnetic field structure is WD 1953-011 (Maxted et al., 2000; Valyavin et al., 2008). In this case, the rotation is slower ( $P_{\text{rot}} = 1.448$  days Brinkworth et al., 2005) and the magnetic field strength is much weaker (180 kG - 520 kG) than that of EUVE J0317-855.

NLTT 12758 was discovered to be a magnetic white dwarf by Kawka & Vennes (2012a). They showed that the circular polarization spectra are variable and that there is also variability in the  $H\alpha$  core suggesting that NLTT 12758 is a close double degenerate system. Here, we present our analysis of spectroscopic, spectropolarimetric and photometric data of NLTT 12758. The observations are presented in Section 5.3. The

orbital and rotation period analyses are described in Sections 5.4.1 and 5.4.2, respectively. The stellar and atmospheric parameters are presented in 5.4.3, and we discuss the evolutionary scenarios in subsection 5.4.4. We discuss the case of NLTT 12758 in comparison to other known double degenerate systems containing a magnetic white dwarf in section 5.5 and we conclude in section 5.6.

## 5.3 Observations

### 5.3.1 Spectroscopy and Spectropolarimetry

NLTT 12758 was first observed with the R.-C. spectrograph attached to the 4m telescope at Cerro Tololo Inter-American Observatory (CTIO) on UT 2008 February 24. We used the KPGL2 (316 lines per mm) grating with the slit-width set to 1.5 arcsec providing a resolution of about 8 Å. We obtained a second set of low-dispersion spectra with the EFOSC2 spectrograph attached to the New Technology Telescope (NTT) at La Silla. Two consecutive spectra were obtained on UT 2009 08 27. We used grism number 11 and set the slit-width to 1.0 arcsec providing a resolution of about 14 Å. Both sets of spectra revealed Zeeman splitting in the Balmer lines. Figure 5.1 shows the low dispersion spectra.

We obtained a first set of spectropolarimetric observations using the FOcal Reducer and low dispersion Spectrograph (FORS2) attached to the 8m telescope (UT1) of the European Southern Observatory (ESO) in 2009. We obtained another set of observations using the same set-up in 2013. We used the 1200 lines  $\text{mm}^{-1}$  grism (1200R+93) centred on  $H\alpha$  providing a spectral dispersion of  $0.73 \text{ \AA pixel}^{-1}$ . We set the slit-width to 1 arcsec providing a spectral resolution of  $3.0 \text{ \AA}$ . Each spectropolarimetric observation consisted of two individual exposures, the first having the Wollaston prism rotated to  $-45^\circ$  immediately followed by the second exposure with the prism rotated to  $+45^\circ$ .

We also obtained five spectra of NLTT 12758 with the EFOSC2 spectrograph in September 2012. These spectra were obtained with grism number 20 which provides a spectral dispersion of  $1.09 \text{ \AA}$  per binned pixel. The slit-width was set to 0.7 arcsec providing a resolution of  $3.0 \text{ \AA}$ .

Finally we obtained a set of five consecutive spectra of NLTT 12758 with the X-shooter spectrograph (Vernet et al., 2011) attached to the VLT at Paranal Observatory on UT 2014 August 26. The spectra were obtained with the slit width set to 0.5, 0.9 and 0.6 arcsec for the UVB, VIS and NIR arms, respectively. This setup provided a resolution of  $R = 9000, 7450$  and  $7780$  for the UVB, VIS and NIR arms, respectively.

The log of the spectroscopic observations is presented in Table 5.1 below.



**Table 5.1:** Spectroscopic observation log.

UT date	UT start	Exposure time (s)	Instrument & Telescope
24 Feb 2008	02:04:42	1200	RC/CTI04m
24 Feb 2008	02:26:56	1200	RC/CTI04m
27 Aug 2009	09:39:21	600	EFOSC2/NTT
27 Aug 2009	09:49:57	600	EFOSC2/NTT
23 Oct 2009	06:35:09	900	FORS2/UT1
23 Oct 2009	06:51:18	900	FORS2/UT1
23 Oct 2009	07:16:20	900	FORS2/UT1
23 Oct 2009	07:32:28	900	FORS2/UT1
23 Oct 2009	07:55:18	900	FORS2/UT1
23 Oct 2009	08:11:35	900	FORS2/UT1
24 Nov 2009	02:40:00	900	FORS2/UT1
24 Nov 2009	02:56:08	900	FORS2/UT1
24 Nov 2009	03:24:14	900	FORS2/UT1
24 Nov 2009	03:40:22	900	FORS2/UT1
02 Sep 2012	08:41:00	900	EFOSC2/NTT
02 Sep 2012	09:04:14	900	EFOSC2/NTT
03 Sep 2012	08:09:10	900	EFOSC2/NTT
03 Sep 2012	08:33:13	900	EFOSC2/NTT
03 Sep 2012	09:18:43	900	EFOSC2/NTT
04 Jan 2013	03:49:14	700	FORS2/UT1
04 Jan 2013	04:02:02	700	FORS2/UT1
04 Jan 2013	04:15:06	700	FORS2/UT1
04 Jan 2013	04:27:55	700	FORS2/UT1
04 Jan 2013	04:41:01	700	FORS2/UT1
04 Jan 2013	04:53:49	700	FORS2/UT1
07 Jan 2013	02:39:34	700	FORS2/UT1
07 Jan 2013	02:52:22	700	FORS2/UT1
07 Jan 2013	03:05:26	700	FORS2/UT1
07 Jan 2013	03:18:14	700	FORS2/UT1
07 Jan 2013	03:31:18	700	FORS2/UT1
07 Jan 2013	03:44:06	700	FORS2/UT1

<sup>41</sup> Exposure times for the VIS/UVB arms, respectively.**Table 5.1:** continues on the next page.

**Table 5.1:** Spectroscopic observation log - continued

UT date	UT start	Exposure time (s)	Instrument & Telescope
07 Jan 2013	03:57:28	700	FORS2/UT1
07 Jan 2013	04:10:17	700	FORS2/UT1
07 Jan 2013	04:33:02	700	FORS2/UT1
07 Jan 2013	04:46:02	700	FORS2/UT1
03 Feb 2013	03:01:49	700	FORS2/UT1
03 Feb 2013	03:14:38	700	FORS2/UT1
03 Feb 2013	03:27:35	700	FORS2/UT1
03 Feb 2013	03:40:24	700	FORS2/UT1
03 Feb 2013	03:53:22	700	FORS2/UT1
03 Feb 2013	04:06:10	700	FORS2/UT1
26 Aug 2014	08:18:30	450/540 <sup>1</sup>	Xshooter/UT3
26 Aug 2014	08:28:43	450/540 <sup>1</sup>	Xshooter/UT3
26 Aug 2014	08:37:51	450/540 <sup>1</sup>	Xshooter/UT3
26 Aug 2014	08:47:00	450/540 <sup>1</sup>	Xshooter/UT3
26 Aug 2014	08:56:08	450/540 <sup>1</sup>	Xshooter/UT3

<sup>1</sup> Exposure times for the VIS/UVB arms, respectively.

### 5.3.2 Photometry

We collected available photometric measurements from the Galaxy Evolutionary Explorer (*GALEX*) sky survey, optical photometry from Eggen (1968) and the AAVSO Photometric All-Sky Survey, Deep Near Infrared Survey (DENIS) of the southern sky, the Two Micron All Sky Survey (2MASS) and the Wide-field Infrared Survey Explorer (*WISE*). These measurements are listed in Table 5.2.

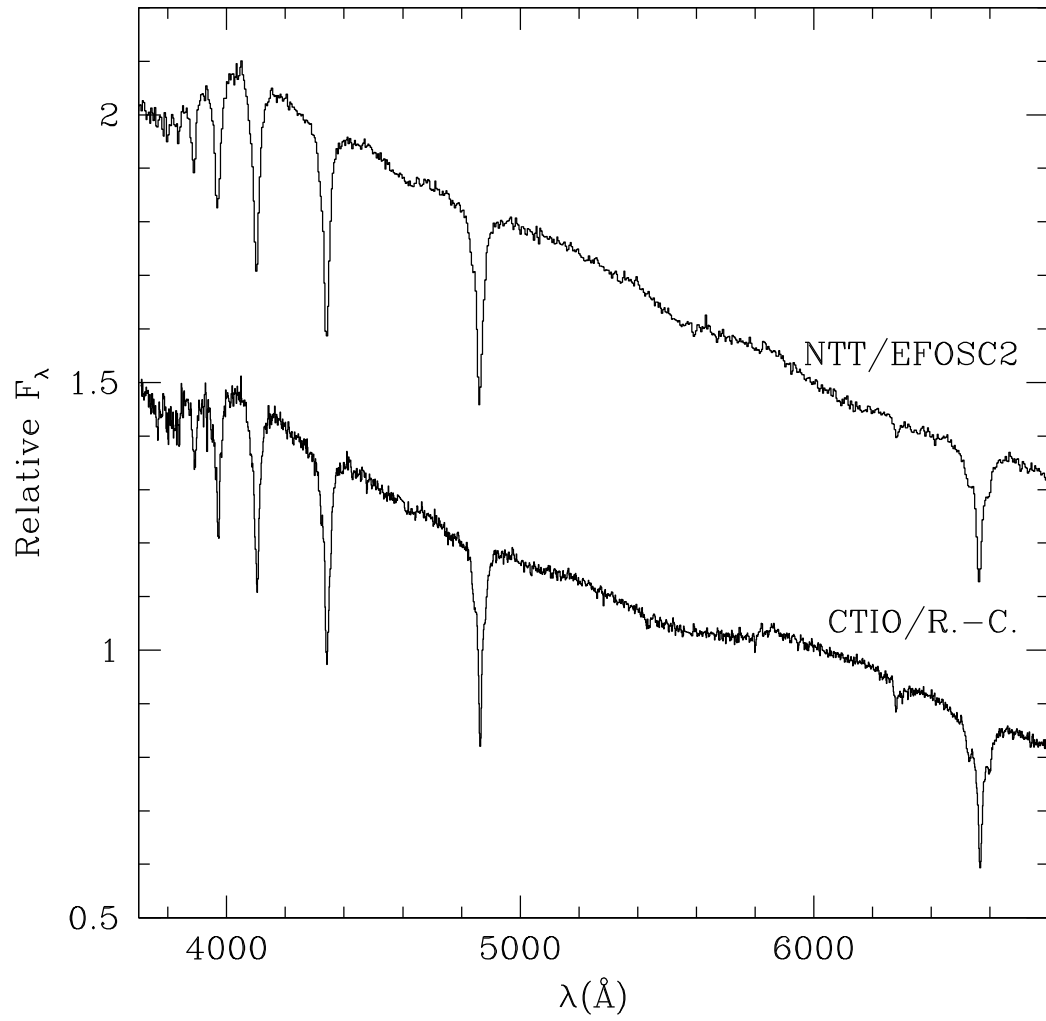


**Figure 5.1:** Low dispersion CTIO/R.-C. and NTT/EFOSC2 spectra of NLTT 12758 revealing Zeeman splitted Balmer lines.

**Table 5.2:** Photometric measurements of NLTT 12758

Band	Magnitude	Reference
<i>GALEX FUV</i>	not detected	1
<i>GALEX NUV</i>	$17.401 \pm 0.016$	1
<i>V</i>	$15.46, 15.483 \pm 0.071$	2,3
<i>B - V</i>	+0.31	2
<i>U - B</i>	-0.71	2
<i>B</i>	$15.855 \pm 0.094$	3
<i>g</i>	$15.607 \pm 0.037$	3
<i>r</i>	$15.417 \pm 0.074$	3
<i>i</i>	$15.443 \pm 0.132$	3
DENIS <i>I</i>	$14.976 \pm 0.07$	4
DENIS <i>J</i>	$14.713 \pm 0.15$	4
2MASS <i>J</i>	$14.809 \pm 0.032$	5
2MASS <i>H</i>	$14.723 \pm 0.071$	5
2MASS <i>K</i>	$14.683 \pm 0.096$	5
WISE <i>W1</i>	$14.703 \pm 0.034$	6
WISE <i>W2</i>	$14.781 \pm 0.069$	6

**References:** (1) Morrisey et al. (2007); (2) Eggen (1968); (3) Henden et al. (2016); (4) Fouqué et al (2000); (5) Skrutskie et al. (2006); (6) Cutri et al. (2012)

We obtained new CCD photometric measurements with the 1.54-m Danish telescope at the La Silla Observatory in Chile on UT 26th December 2014, 30th January 2015 and 11th March 2016. On 26th December 2014, we alternated between the *V* and *R* filter and on 30th January 2015 11th March 2016 we observed NLTT 12758 with the *R* filter only. The integration time was set to 40 seconds for all observations. The data reduction and differential photometry were performed using the C-Munipack package<sup>6</sup>. Since several comparison stars were available, and these were checked individually to exclude variable objects. We compared the results of the final differential light curves using the aperture photometry routine from IRAF (Stetson, 1987). We found no differences above the photon noise.

<sup>6</sup><http://c-munipack.sourceforge.net/>

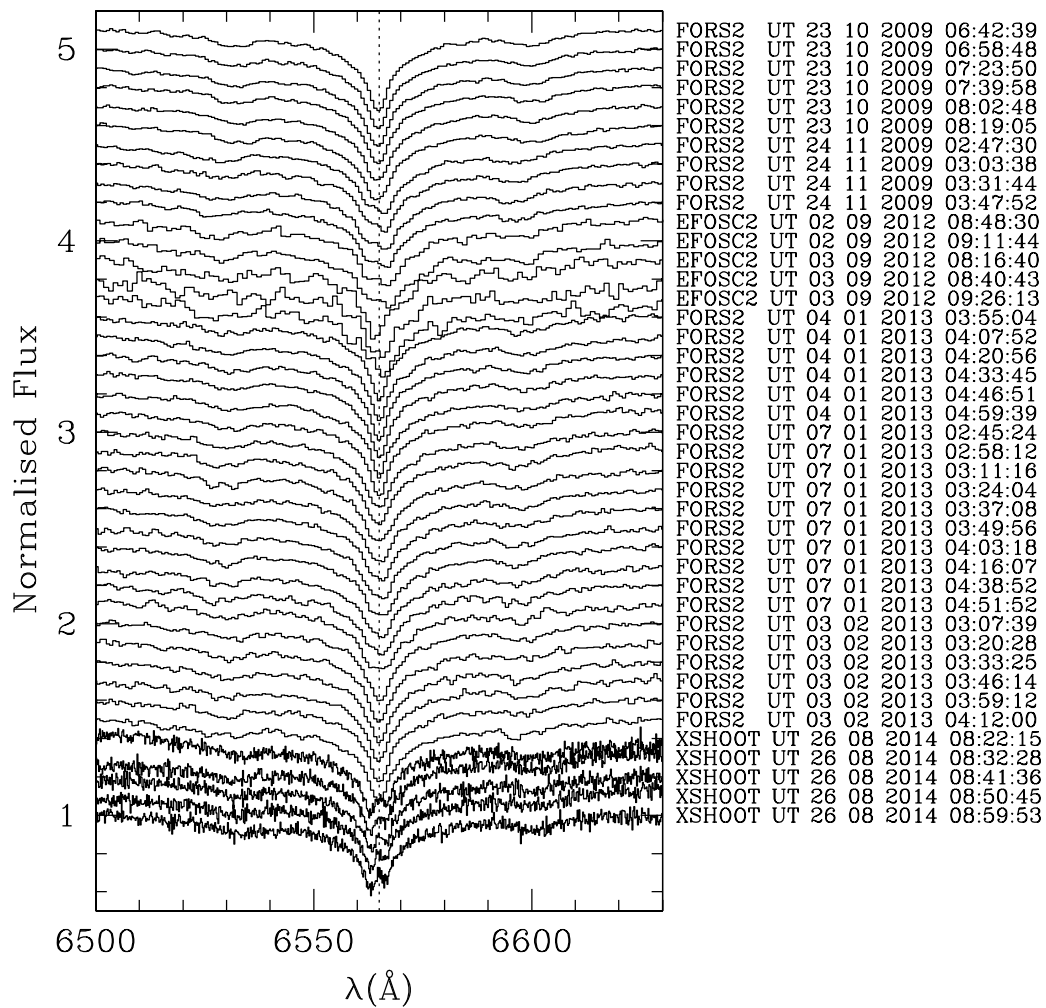


**Figure 5.2:** EFOSC2, FORS2 and X-shooter spectra of NLTT 12758 showing variations in the H $\alpha$  core. The mid-exposure UT time is listed for each spectrum.

## 5.4 Analysis

During the first spectropolarimetric observations of NLTT 12758, we found that the  $\sigma$  components of H $\alpha$  varied with a reversal in the polarisation spectra, thus revealing itself as a new member of the DAP white dwarf class<sup>7</sup>. We also found that the width of the core of the  $\pi$  component is structured and variable, thus suggesting the presence of a close companion. The FORS2, EFOSC2 and X-shooter spectra displayed in Figure 5.2 clearly show the variations in the central H $\alpha$  core. The resolution of the X-shooter spectra and timing of the observations allowed us to discern the individual cores of the two components.

### 5.4.1 Binary parameters

We measured the radial velocity of the magnetic white dwarf by first subtracting a template representing the DA white dwarf and then cross-correlating the DAP white dwarf FORS/EFOSC2 spectra ( $\sigma$  components only) with the X-shooter spectrum. The DA radial velocity could only be measured at quadrature, i.e., at maximum line core separation, and with a sufficient signal-to-noise ratio. Only three sets of spectra met these criteria. Consecutive exposures (2 to 4) were co-added to increase the signal-to-noise and improve the reliability of the velocity measurements while minimizing orbital smearing. Table 5.3 lists the barycentric julian date (BJD) with the measured radial velocities of the magnetic and non-magnetic white dwarfs in NLTT 12758. All velocities are barycentric corrected.

We searched for a period in the measurements using  $\chi^2$  minimization techniques by fitting the sinusoidal function  $v = \gamma + K \times \sin(2\pi(t - T_0)/P)$  to the measured radial velocities where  $t$  is time (BJD). The initial epoch ( $T_0$ ), period ( $P$ ), mean velocity ( $\gamma$ ) and velocity semi-amplitude ( $K$ ) were determined simultaneously and we normalized the  $\chi^2$  function by setting the minimum reduced  $\chi^2$  to 1.

Figure 5.3 shows the period analysis of the FORS2, EFOSC2 and X-shooter data sets and Table 5.4 lists the new binary parameters. Using the FORS2 and EFOSC2 data combined with the X-shooter data we determined a period of  $1.15401 \pm 0.00005$  days and a velocity semi-amplitude for the DAP star of  $89.7 \pm 3.8 \text{ km s}^{-1}$  with an average residual of only  $7.7 \text{ km s}^{-1}$  and commensurate with measurement errors (Table 5.3). The corresponding mass function is  $f(M_{\text{DA}}) = 0.0863 \pm 0.0110 M_{\odot}$ . Since the X-shooter spectra were taken near quadrature and clearly show the cores of both

---

<sup>7</sup>DAP white dwarfs show hydrogen lines with detectable polarisation. The DAH classification is reserved for Zeeman splitted line spectra, but without confirmed polarization.

**Table 5.3:** Radial velocity measurements

BJD (2450000+)	$v_{DAP}$ (km s <sup>-1</sup> )	$v_{DA}$ (km s <sup>-1</sup> )
5127.78952	157 ± 6	...
5127.81811	165 ± 5	...
5127.84523	196 ± 5	...
5159.62676	2 ± 8	...
5159.64212	...	156 ± 20
5159.65748	18 ± 8	...
6172.87606	18 ± 7	196 ± 20
6173.86764	35 ± 8	...
6296.67107	112 ± 6	...
6296.68904	120 ± 7	...
6296.70703	124 ± 6	...
6299.62701	47 ± 7	...
6299.65848	38 ± 8	...
6299.69457	29 ± 9	...
6326.64042	100 ± 6	...
6326.66725	79 ± 6	...
6895.86223	193 ± 5	12 ± 5

components, we were able to estimate a semi-amplitude of  $81.9 \pm 17.3$  km s<sup>-1</sup> for the non-magnetic white dwarf. The orbital mass ratio  $M_{DA}/M_{DAP} = 0.85 - 1.35$  is not sufficiently accurate to constrain the evolution of the system, and additional constraints will be provided by the spectroscopic analysis (Section 5.4.3).

#### 5.4.2 Rotation

The spectropolarimetric data have revealed a modulation that we attribute to the rotation of the magnetic white dwarf.

We measured the integrated polarization for both  $\sigma$  components and conducted a period search. Two significant periods at 22.6 minutes and 9 minutes stand out. Since some of the exposure times were longer than 9 minutes, it is unlikely that the 9 minutes period is real. Figure 5.4 shows line polarization measurements obtained by integrating  $V/I$  over the wavelength range ( $\approx \pm 20\text{\AA}$ ) covered by the individual  $\sigma$  components phased on the 22.6 minute period. Both  $\sigma$  components show sinusoidal behaviour and a symmetry about the null polarization axis which imply that the magnetic poles spend nearly equal time in the field-of-view.

Figure 5.5 shows the co-added FORS2 circular polarization spectra over three separate ranges of a rotation cycle ( $P = 22.6$  min) highlighting the flipping of the sigma

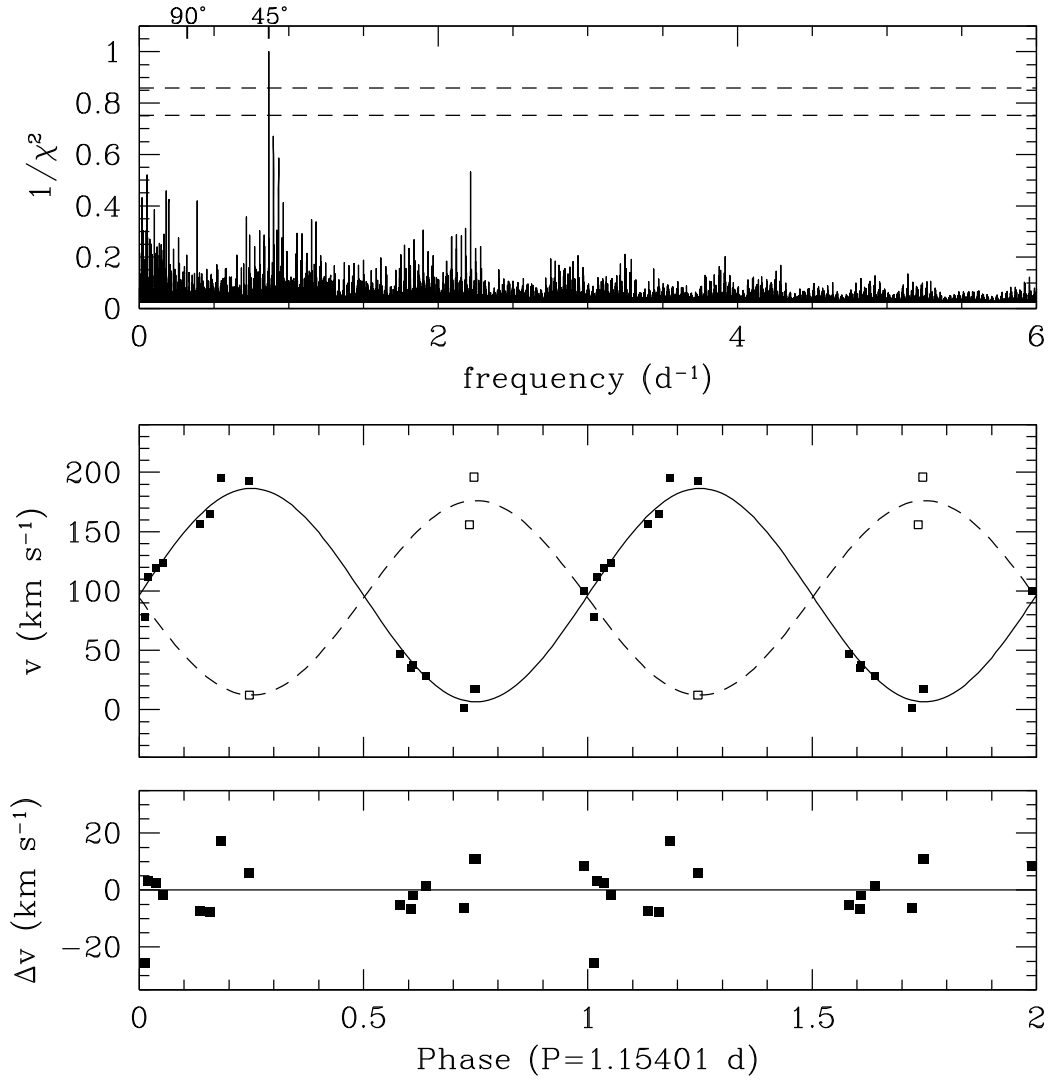


**Figure 5.3:** (Top panel) period analysis of the FORS2, EFOC2 and X-shooter data with 66 and 90% confidence level (dashed lines). (Middle panel) radial velocity measurements (Table 5.3) of the DA (open squares) and DAP stars (full squares) phased on the orbital period and the best-fitting sine curves (Table 5.4) and (bottom panel) velocity residuals for the DAP star. The longest period is marked at  $90^\circ$  on the top horizontal axis along with the actual period at  $45^\circ$ .



components. The flip in the sign of the H $\alpha$   $\sigma$  components at phases 0.1-0.4 and 0.6-0.9 and their anti-symmetric behaviour around the zero polarization spectrum of phases 0.4-0.6, indicate that the magnetic axis must be nearly perpendicular to the rotation axis of the white dwarf.

Figure 5.6 illustrates the geometry of the system with  $\alpha$  set at its minimum value ( $90 - i$ ). Assuming  $i = 45^\circ$  (see Section 5.4.3), the angle  $\alpha$  will vary between  $90^\circ - 45^\circ$  and  $90^\circ + 45^\circ$ . When  $\alpha \approx 90^\circ$ , the positive and negative polarization contributions cancel each other and give rise to the unpolarized, featureless spectrum observed in the phase range 0.4-0.6. This can be explained by the change, due to stellar rotation, between the magnetic field direction and the line of sight to the observer averaged over the visible hemisphere of the star (Wickramasinghe & Martin, 1979). The  $\pi$  component in the circular polarisation spectra shows the presence of narrow antisymmetric circular polarisation features. These are caused by Faraday mixing due to magneto-optical effects which converts linear polarisation into circular polarisation (Martin & Wickramasinghe, 1981, 1982) during the radiation transfer.

### Photometric variations

The photometric observations were analysed using three different methods described in detail by Paunzen & Vanmunster (2016). First, we employed periodic orthogonal polynomials which are particularly useful for the detection of non-sinusoidal oscillations. We fitted the observations to identify the period and employed the analysis of the variance (ANOVA) statistic to evaluate the fit quality (Schwarzenberg-Czerny, 1996).

Next, we employed the string-length methods which simply minimize the separation between consecutive phased data points at trial periods. The best-fitting period corresponds to a minimum in the "string-length" which consists of the sum of data separations. The methods are useful for sparse data sets.

Finally, The Phase Dispersion Minimization (PDM) method is similar to the string-length method (Stellingwerf, 1978). In this method, the data are sorted into phase bins at trial periods and the variance within each bin is calculated. The sum of the variances is minimized at the best-fitting period.

We found that the photometric observations in the  $R$  band show variations. The calculated frequencies and their errors for the three different nights are  $65.4 \pm 1.3$ ,  $65.3 \pm 0.6$ , and  $65.6 \pm 1.2$  cycles per day, respectively. The errors depend on the individual data set lengths and the overall quality of the nights. Within the errors, these values transform to a period of  $22 \pm 0.5$  min. The semi-amplitude of the variations is 6.2 mmag. Figure 5.7 shows the photometric magnitudes phased on the best rotation period of 22.0 minutes with the periodogram.

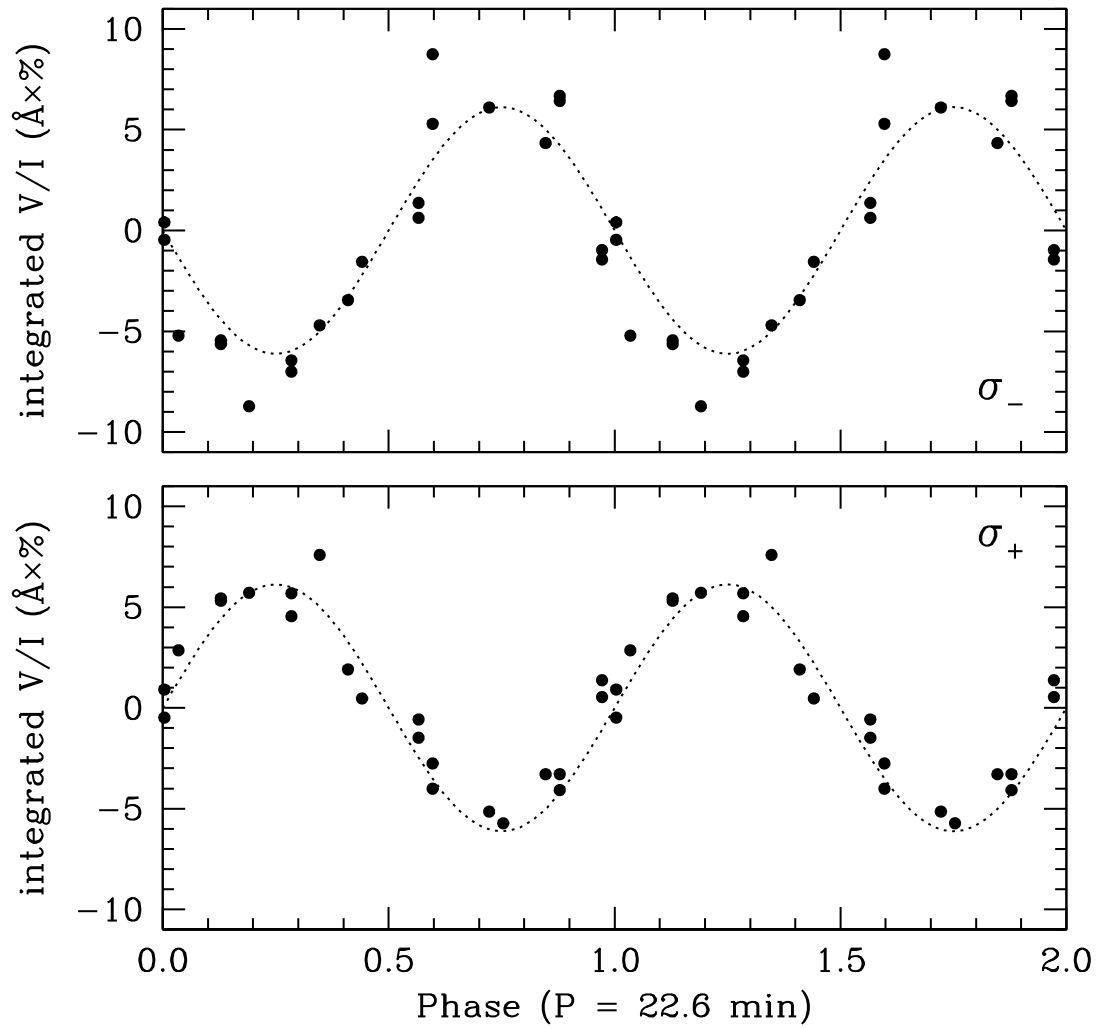


**Figure 5.4:** Integrated polarization measurements of the two individual  $\sigma$  components phased on the rotation period of 22.6 minutes revealing a complete reversal of the field vector. The top panel shows the measurements for the blue-shifted  $\sigma_-$  component and the bottom panel shows the measurements of the red-shifted  $\sigma_+$  component.

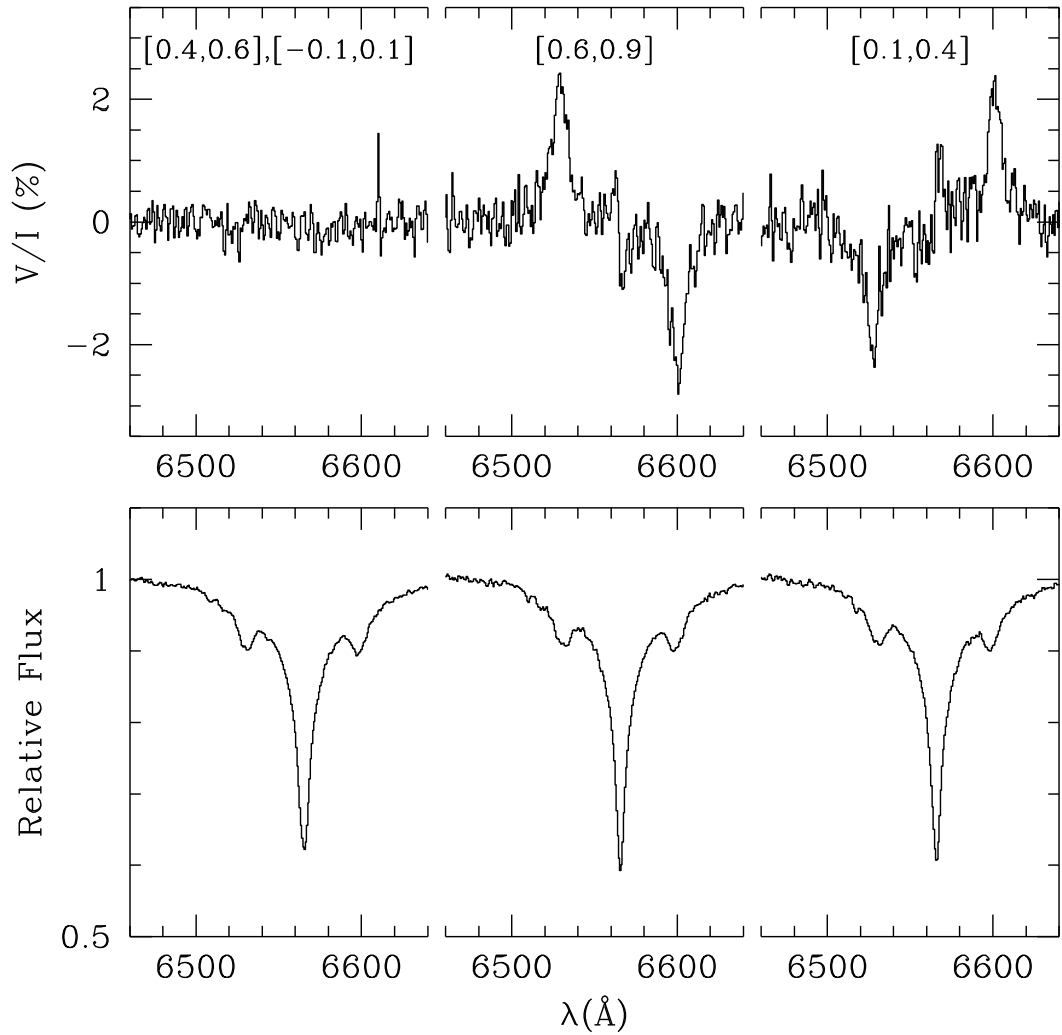


**Figure 5.5:** Co-added FORS2 circular polarization spectra (top panel) and flux spectra (bottom panel) at three phase ranges showing the flip in the sign of the  $\sigma$  components of H $\alpha$ . The spectrum with zero polarization corresponds to a nearly orthogonal viewing angle to the magnetic axis.

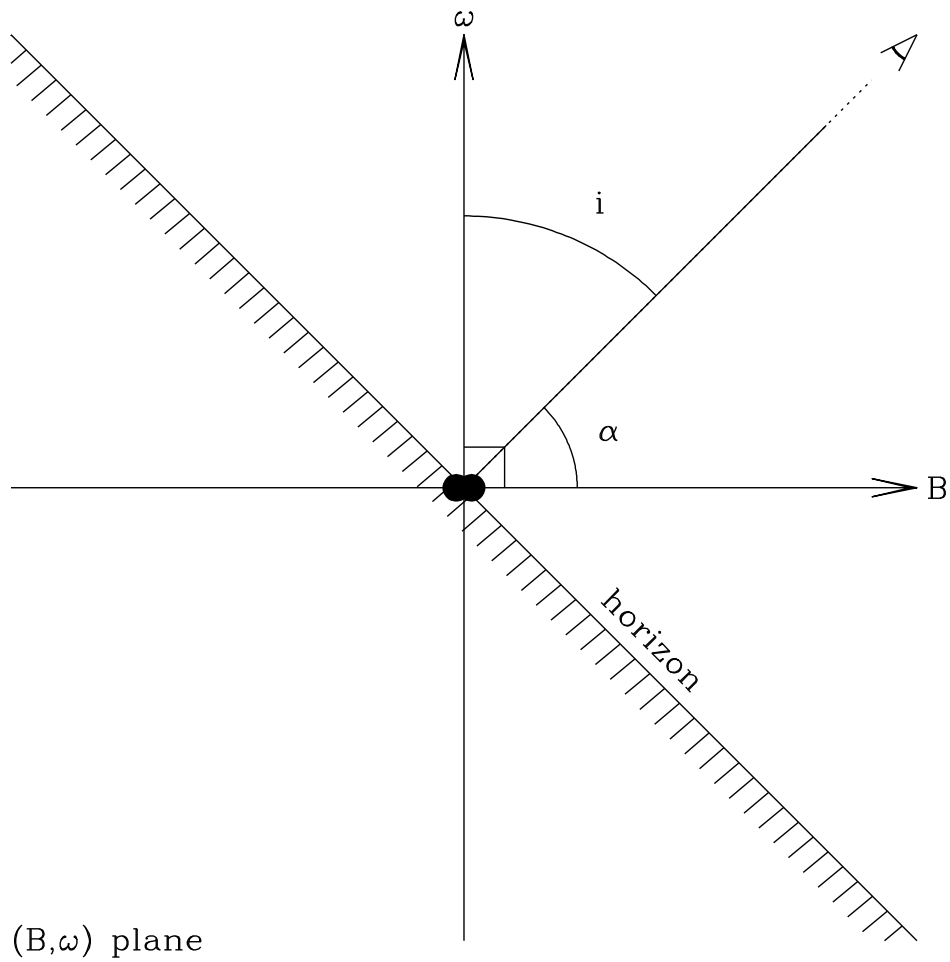


**Figure 5.6:** Schematic view of the geometry of the double degenerate system NLTT 12758. The rotation plane of the magnetic white dwarf is assumed to coincide with the orbital plane, and the spin axis is marked  $\omega$ . The spin axis is at an angle  $i$  with respect to the observer and the magnetic field axis  $B$  is at an angle  $\alpha$  with respect to the observer.

We conclude that the variations in spectropolarimetry and photometry coincide and are phased on the rotation period of the magnetic white dwarf. The photometric variation may be explained in terms of magnetic dichroism which is caused by the different absorption coefficients of left and right handed circularly polarised radiation. A formulation for magnetic dichroism of hydrogen in magnetic white dwarfs was first obtained by Lamb & Sutherland (1974) and used to explain the photometric variations of the high field magnetic white dwarf EUVE J0317-855 (Ferrario et al., 1997b). However the magnetic field of the DAP component of NLTT 12758 is relatively low ( $B < 20$  MG) for this effect to be important. An alternate explanation for the photometric variations could be stellar spots (Brinkworth et al., 2005). Such a spot could be formed by the inhibition of convection in the atmosphere by the magnetic field. Tremblay et al. (2015) show that convection is inhibited at the surface of objects such as the magnetic component of NLTT 12758, however their models are not able to explain flux variations like those observed in NLTT 12758 and other cool white dwarfs with low magnetic fields observed by Brinkworth et al. (2013).

### 5.4.3 *Stellar and atmospheric parameters*

#### **Modelling the field structure**

The appearance of the spectra of magnetic white dwarfs changes dramatically as the field increases in strength. If we indicate with  $(n, l, m_l)$  the zero field quantum numbers, the linear Zeeman regime arises through the removal of the  $m_l$  degeneracy, which for the Balmer series occurs at a field strength of  $\sim 1 - 4$  MG. As the field increases, or the principal quantum number  $n$  increases, the quadratic effect becomes more important until the  $l$  degeneracy is also removed. This is called the quadratic Zeeman regime. In this regime, the wavelength shift depends on the electron excitation level and the  $\pi$  and  $\sigma$  Zeeman components are all displaced from their zero field positions by different amounts. The quadratic shift is of similar importance to the linear shift at  $B \sim 4$  MG for the higher components of the Balmer series (e.g.  $H\delta$ ). The spectra of NLTT 12758 indicate that the magnetic component of this system belongs to the low field regime, as first reported by Kawka & Vennes (2012a).

Before outlining our modelling methods, we need to stress that an important and as yet unsolved problem regarding the modelling of magnetic atmospheres, particularly in the high magnetic field regime, is that concerning line broadening. However in the low field regime, which is appropriate to the study of the spectrum of NLTT 12758, it is possible to assume, as a first approximation, that each Zeeman component is broadened

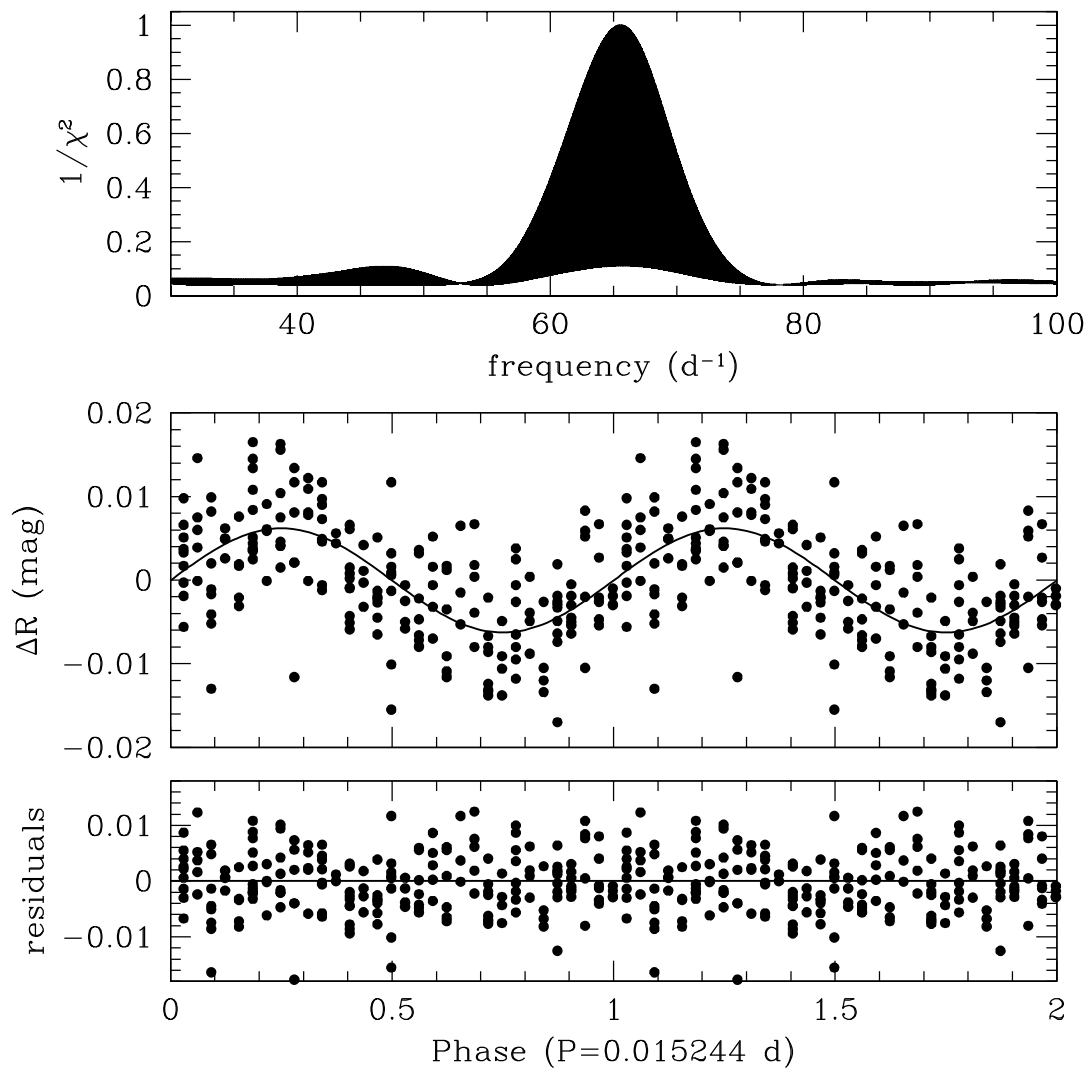


**Figure 5.7:** (Top panel) period analysis of the measured  $R$  photometric measurements. (Middle panel) photometric  $R$  magnitudes phased on the best rotation period and (bottom panel) residuals.

as in the zero field case. This approach has been used successfully for the Zeeman modelling of hot white dwarfs and has allowed the determination of the mass of the hot and ultra-massive magnetic white dwarfs 1RXS J0823.6-2525 ( $B \sim 2.8 - 3.5$  MG Ferrario et al., 1998) and PG 1658+441 ( $B \sim 3.5$  MG Ferrario et al., 1998; Schmidt et al., 1992). In the case of PG 1658+441, the spectroscopic mass was found to be in good agreement with that determined by the trigonometric parallax method (Dahn, 1999; Vennes & Kawka, 2008). No trigonometric parallax is as yet available for 1RXS J0823.6-2525. On the other hand, in cool white dwarfs such as NLTT 12758, the contribution due to Stark broadening is negligible and spectral line broadening is dominated by resonance. For  $H\alpha$  to  $H\gamma$ , we used parameters from the comprehensive self-broadening theory of Barklem et al. (2000), and for the upper Balmer lines we combined the impact parameters from Ali & Griem (1965, 1966) with the van der Waals parameters as described in Kawka & Vennes (2012b).

The modelling of the magnetised spectrum of NLTT 12758 has been conducted as follows. First, we have computed a zero-field grid of pure hydrogen white dwarf model atmospheres (see Kawka & Vennes, 2012a). We used the ML2 parameterization of the mixing length theory with  $\alpha = 0.6$ , where  $\alpha$  is the ratio of the mixing length to the pressure scale height. Convection is predicted to be suppressed in cool magnetic white dwarfs (Tremblay et al., 2015), however we will investigate the effect of suppressed convection on the spectral lines of stars such as NLTT 12758 in future work. This grid of models was then used as input for the magnetic atmosphere program of Wickramasinghe & Martin (1979), modified to allow for Doppler, resonance and Stark broadenings and magneto-optical effects which take into account the different refractive indices for radiation with different polarisation state (Martin & Wickramasinghe, 1981). The shifts and strengths in hydrogen lines, caused by the magnetic field, are included using the results of Zeeman calculations by Kemic (1974). Atmospheric models were then constructed at selected points on the visible hemisphere of the white dwarf taking into consideration the changes in field strength and direction. The resulting Stokes intensities were then appropriately summed to yield a synthetic spectrum.

The field geometry is strongly dependent on field strength and structure and models built on observations obtained at different phases, if the star rotates around its axis, are better constrained than those restricted to one single intensity spectrum corresponding to only one magnetic phase. The best constrained models are those based on observations at different rotational phases and for which *both* intensity and polarisation spectra are available as it is the case for NLTT 12758.

The modelling of a magnetic white dwarf usually starts with the assumption that the magnetic field configuration is that of a centred dipole. Then, if necessary, more

complex structures are investigated. These usually consist of offset dipoles or combinations of higher order multipoles. For the present set of observations of NLTT 12758 we found that a centred dipole model was inadequate to model the rotationally modulated Zeeman components by simply changing the viewing angle. This is because a centred dipole allows a field spread of at most of a factor 2, which is not sufficient to model the observations of NLTT 12758. It is possible to achieve a larger magnetic field spread by offsetting the dipole from the centre of the star. If the dipole is shifted by a fraction  $a_z$  of the stellar radius along the dipole axis, then the ratio of the field strengths  $B_{p1}$  and  $B_{p2}$  at the two opposite poles become

$$\frac{B_{p1}}{B_{p2}} = \left( \frac{1 - a_z}{1 + a_z} \right)^3 \quad (5.1)$$

We describe in detail how we have achieved the best-fit model for NLTT 12758 in the sections that follow.

### Spectroscopic analysis

We fitted the X-shooter spectra with two sets of model spectra. The first set of model spectra are for non-magnetic hydrogen-rich white dwarfs as described in Kawka & Vennes (2012a). The Balmer line profiles used in the synthetic spectra calculations are described in Kawka & Vennes (2012b). The second set of model spectra include a magnetic field (as described above).

The procedure fits simultaneously the effective temperature and surface gravity of both white dwarfs (4 parameters). We used the mass-radius relations of Benvenuto & Althaus (1999) to scale the flux for both stars and ensure that the relative flux contribution of each star is preserved imposing a common distance for both stars. A similar decomposition method was adopted in the analysis of the hot double degenerate EUVE J1439+750 (Vennes et al., 1999) and in the analysis of a sample of double degenerates by Rolland (2014) and Rolland & Bergeron (2015). The results are model dependent due to uncertainties in the treatment of line broadening in the presence of a magnetic field as previously noted by Külebi et al. (2009). However, the presence of a non-magnetic DA companion with a reliable radius measurement, as in the case of NLTT 12758, helps constrain the radius of the magnetic component. A direct constraint on the stellar radii would be achieved with a parallax measurement.

The Zeeman splitting observed in the X-shooter spectra ( $H\alpha$  and  $H\beta$ ) implies an averaged surface field of  $B_S = 1.70 \pm 0.04$  MG. We used this value as a starting point to calculate sets of magnetic field spectra with varying polar field strength and offset. We



fitted the spectra with the following magnetic field strengths and offsets: offset =  $-0.1$  at  $B_p = 2.8, 3.1, 3.4, 3.6$  MG; offset =  $0$  at  $B_p = 2.6, 3.0, 3.2, 3.4$  MG; offset =  $+0.1$  at  $B_p = 2.4, 2.9, 3.1, 3.3$  MG. We also fitted the X-shooter spectra at viewing angles of  $50^\circ$  and  $80^\circ$  for each offset and field strength value. Note that the total exposure time covers nearly two complete rotation cycles and the viewing angle represents a cycle average.

Figure 5.8 compares the X-shooter spectrum and the best-fitting models for the two stars. The magnetic white dwarf has a polar magnetic field  $B_p = 3.1$  MG offset by  $a_z = +0.1$  from the stellar centre. The magnetic white dwarf appears to be slightly cooler with  $T_{\text{eff,DAP}} = 7220 \pm 180$  K and a surface gravity of  $\log g = 8.16 \pm 0.08$ . The non-magnetic white dwarf is a little hotter and more massive with  $T_{\text{eff,DA}} = 7950 \pm 50$  K and  $\log g = 8.37 \pm 0.04$ . The best-fitting viewing angle to the dipole axis is on average  $\alpha = 80^\circ$ . Table 4 lists the stellar parameters. We computed the mass and cooling age of each component using the evolutionary models of Benvenuto & Althaus (1999). The spectroscopic mass ratio  $M_{\text{DA}}/M_{\text{DAP}} = 1.1 - 1.3$  is consistent with the orbital mass ratio, but also more accurate, and implies that the mass of the DA star may be slightly higher than the mass of the DAP star. We then estimated the absolute magnitude of each component and calculated the distance to the system.

Rolland (2014) and Rolland & Bergeron (2015) measured the stellar parameters of NLTT 12758 by fitting  $H\alpha$  together with the spectral energy distribution (SED) including only  $VJHK$ . They obtained  $T_{\text{eff,DAP}} = 6041$  K and  $T_{\text{eff,DA}} = 8851$  with a radius ratio of  $R_{\text{DA}}/R_{\text{DAP}} = 0.908$ . Although our radius ratio is in agreement with theirs, our effective temperatures differ from their effective temperatures.

Taking advantage of a broader wavelength coverage, we re-analysed the SED. First, we fitted the photometric data set ( $NUV, UVB, gri, JHK$  and  $W1, W2$ ) by fixing the surface gravity measurements to those obtained in the spectroscopic analysis. We allowed for both temperatures to vary and assumed null interstellar extinction. The resulting effective temperatures are nearly in agreement with the spectroscopic analysis showing that interstellar extinction in the line of sight toward NLTT 12758 is negligible when compared to the total extinction in the same line of sight,  $E(B - V) = 0.06$  (Schlegel et al., 1998). Figure 5.9 shows the model photometry fitted to the measured photometry and compares the confidence contours for the SED fit, as well as the confidence contours for the Balmer line fit (Fig. 5.8). The overlapping contours show that the two methods are consistent and imply that the two objects share similar stellar parameters. In the following discussion we adopt the results of the spectroscopic analysis.

Our results differ markedly from those of Rolland (2014) and Rolland & Bergeron (2015) who reported a temperature difference  $\Delta T = T_{\text{eff,DA}} - T_{\text{eff,DAP}} \approx 2800$  K

while we estimated much closer temperatures for the components ( $\Delta T \approx 700$  K). On the other hand we estimated a similar mass ratio. Our spectroscopic analysis includes the first four members of the Balmer line series ( $H\alpha$  to  $H\delta$ ), thereby lifting potential degeneracy in the  $T_{\text{eff}}/\log g$  solution, while Rolland (2014) and Rolland & Bergeron (2015) only include  $H\alpha$ . However, both solutions are model dependent and part of the discrepancy may also be attributed to different line-broadening prescriptions used in calculating magnetic synthetic spectra. The large temperature difference reported by Rolland (2014) and Rolland & Bergeron (2015) should also be noticeable in the SED, particularly in the near ultraviolet. Our own analysis based an extensive data set implies a temperature difference no larger than  $\approx 1100$  K ( $1\sigma$ ) while a larger temperature difference would be incompatible with the *GALEX NUV* measurement.

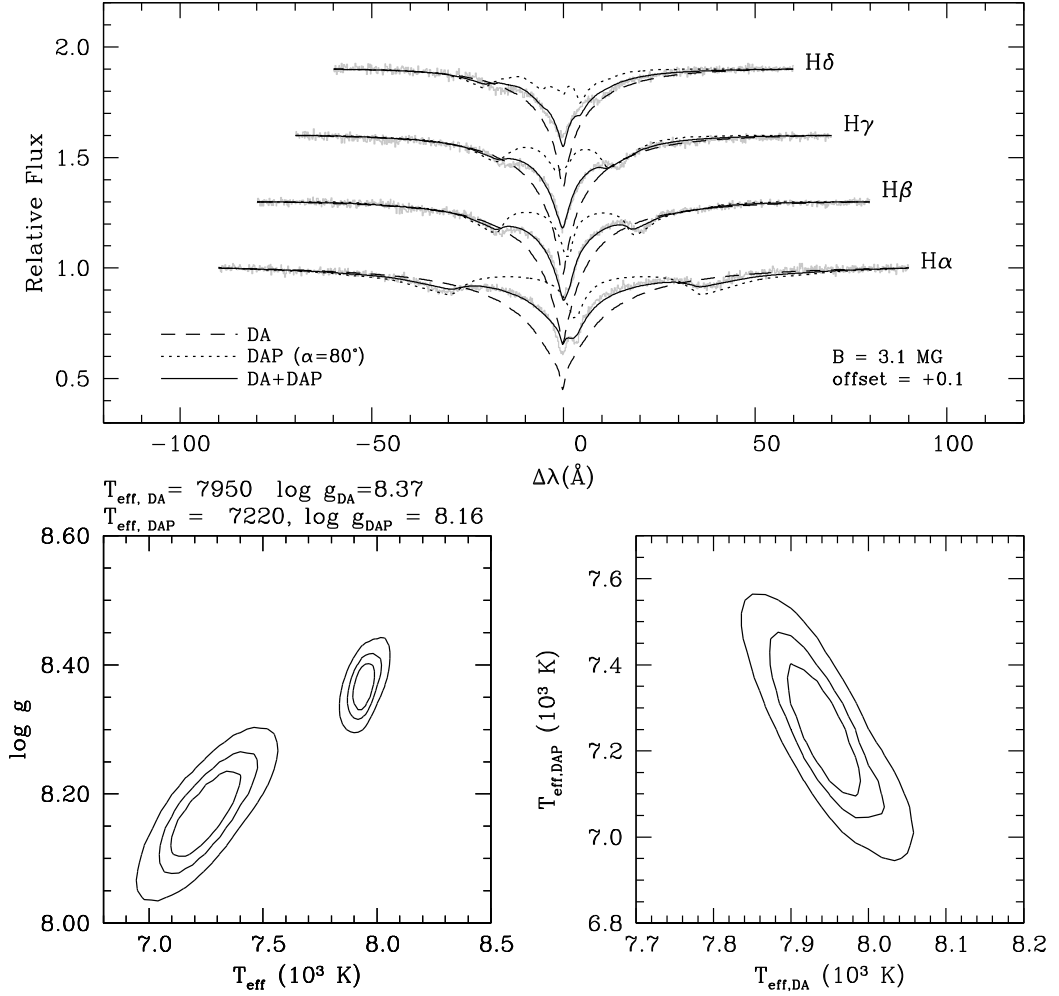


**Figure 5.8:** (Top panel) Observed Balmer line profiles of NLTT 12758 compared to the best-fitting models. The best-fit shows that the components of NLTT 12758 are a non-magnetic DA white dwarf (dashed lines) paired with a magnetic DA white dwarf (dotted lines). Confidence contours at 66, 90, and 99% are shown in the  $T_{\text{eff,DAP}}$  vs  $T_{\text{eff,DA}}$  plane (bottom right) and  $\log g$  vs  $T_{\text{eff}}$  for both stars (bottom left).

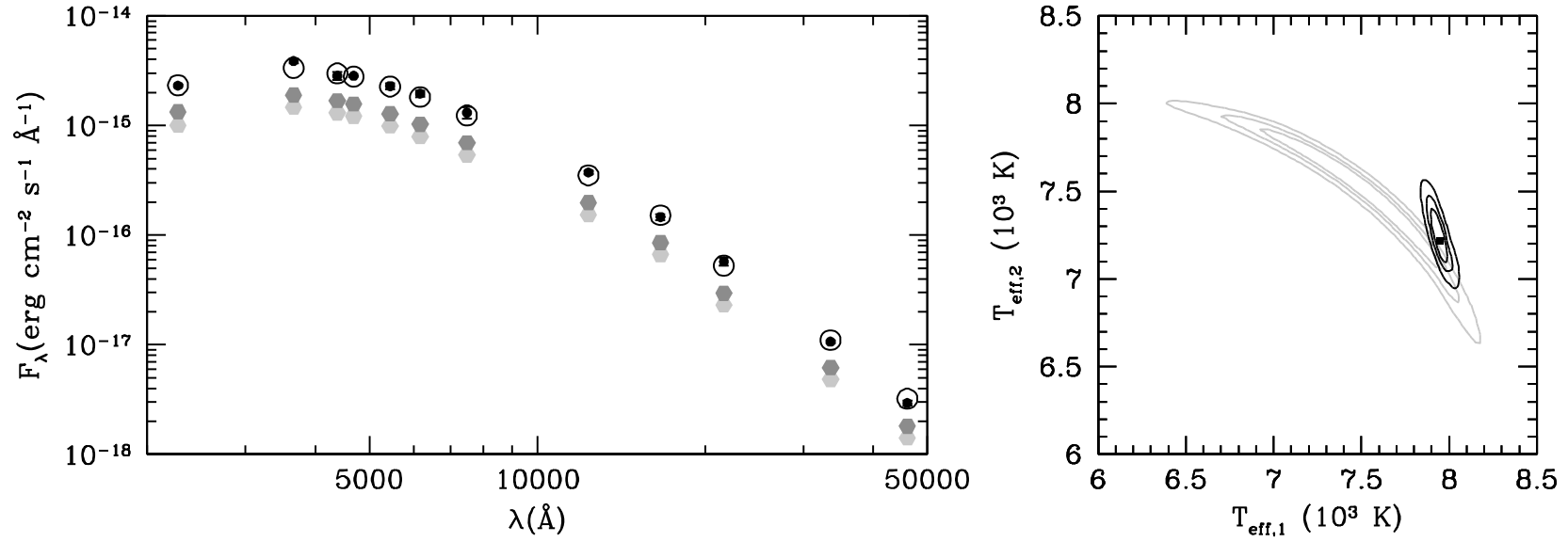


**Figure 5.9:** The left panel compares the best-fitting photometry (open circle) to the observed photometry (solid black circles). The contribution of individual stars are plotted in different grey shades as hexagonals. The right panel plots the confidence contours (66, 90, and 99%) of the spectroscopic fit (in black) and the contours of the SED fit (grey full lines). Note that  $\log g = 8.4$  for star 1 (DA) and  $\log g = 8.2$  for star 2 (DAP).

**Table 5.4:** Summary of NLTT 12758 parameters

Parameter	DA	DAP
$T_{\text{eff}}$ (K)	$7950 \pm 50$	$7220 \pm 180$
$\log g$ (c.g.s)	$8.37 \pm 0.04$	$8.16 \pm 0.08$
Mass ( $M_{\odot}$ )	$0.83 \pm 0.03$	$0.69 \pm 0.05$
Cooling age (Gyrs)	$2.2 \pm 0.2$	$1.9 \pm 0.4$
$M_V$ (mag)	$13.65 \pm 0.06$	$13.69 \pm 0.18$
Period (d)	$1.15401 \pm 0.00005$	
$K$ ( $\text{km s}^{-1}$ )	$81.9 \pm 17.3$	$89.7 \pm 3.8$
$\gamma$ ( $\text{km s}^{-1}$ )	$94.2 \pm 17.3$	$96.4 \pm 2.6$
$d$ (pc)	$32.6 \pm 3.5$	
$v_r$ ( $\text{km s}^{-1}$ )	$58.0 \pm 3.9$	

Using the evolutionary mass-radius relations of Benvenuto & Althaus (1999), we find that the cooling ages of the two white dwarfs in NLTT 12758 are comparable. However, Valyavin et al. (2014) have proposed that convection in cool white dwarfs is suppressed by magnetic fields, and therefore magnetic white dwarfs may appear younger than they are. The 3D radiation magnetohydrodynamic simulations of Tremblay et al. (2015) have confirmed that magnetic fields do suppress convection, however they do not affect the cooling of the white dwarf until temperatures have dropped below 6000 K. Since the magnetic white dwarf is hotter than this upper limit, it is likely that its age is not affected and that the two objects formed around the same time.

We derived an orbital inclination of  $i = 45^\circ$  for NLTT 12758 by combining the component masses with the orbital parameters and using:

$$\frac{M_{\text{DA}}^3 \sin^3 i}{(M_{\text{DA}} + M_{\text{DAP}})^2} = \frac{PK_{\text{DAP}}^3}{2\pi G} \quad (5.2)$$

where  $M_{\text{DA}}$  and  $M_{\text{DAP}}$  are the masses of the non-magnetic and magnetic white dwarfs respectively,  $P$  is the orbital period,  $K_{\text{DAP}}$  is the velocity semi-amplitude of the magnetic white dwarf and  $G$  is the gravitational constant. Setting the system inclination at  $i = 90^\circ$ , the maximum orbital period is  $P \approx 3.3$  d.

The calculated white dwarf gravitational redshifts ( $\gamma_{g,\text{DAP}} = 38.4 \pm 2.9$ ,  $\gamma_{g,\text{DA}} = 53.6 \pm 1.7$   $\text{km s}^{-1}$ ) may be subtracted from their respective systemic velocities to obtain an estimate of the radial velocity of the system. Using the more precise velocity of the DAP star we obtain  $v_r = 58.0 \pm 3.9$   $\text{km s}^{-1}$ . Combining the proper motion measurements (Kawka & Vennes, 2012a), the photometric distance estimate ( $d$ ) and the radial velocity ( $v_r$ ) of the system we determine the Galactic velocity components  $(U, V, W) = (-40 \pm 4, -48 \pm 5, -3 \pm 6)$   $\text{km s}^{-1}$  which suggest that the system is relatively young and belongs to the thin disc (Pauli et al., 2006).

#### 5.4.4 Evolution of NLTT 12758

In order to understand the evolution of NLTT 12758 we have used the rapid binary star evolution algorithm, `BSE`, of Hurley, Tout & Pols (2002). We have evolved a number of binaries from the Zero Age Main Sequence (ZAMS) to the age of the Galactic disc (9.5 Gyr, e.g. Oswalt et al., 1996; Liu & Chaboyer, 2000). This code is a derivation of the single star evolution code of Hurley, Pols & Tout (2000) where the authors use analytical formulae to approximate the full evolution of stars. The `BSE` takes into consideration stellar mass-loss, mass transfer, Roche lobe overflow, CE evolution, tidal interaction, supernova kicks and angular momentum loss caused by gravitational radiation and magnetic braking. In order to model the CE evolution, the `BSE` uses the  $\alpha_{\text{CE}}$  formalism, where  $\alpha_{\text{CE}}$  is a parameter with values in the range 0.1 – 0.9. In our calculations we have adopted  $\eta = 1.0$  for the Reimers’ mass-loss parameter, as outlined in chapter 2 (and Briggs et al., 2015) and a stellar metallicity,  $Z = 0.02$ .

We have then generated a synthetic population of binaries with ZAMS conditions of the mass of the primary star,  $M_1$ , between 3.5 and 4.5  $M_{\odot}$ , the mass of the secondary star,  $M_2$ , between 2.5 and 3.5  $M_{\odot}$  and the initial period  $P_0$  in the range 2000 – 3500 days, as these values were in the region of the expected initial conditions for the final properties of the components of NLTT 12758. We allowed 200 steps in each parameter in the `BSE` evolution of the population through to the age of the Galactic disk. In all cases we assumed an initially circular orbit for the progenitor binary, that is, an eccentricity of zero. The calculations were repeated for values of  $\alpha_{\text{CE}} = \{0.10, 0.20, 0.25, 0.30, 0.40, 0.50, 0.60, 0.70, 0.80, 0.90\}$ .

A number of stellar types are recognised by `BSE` within its logic throughout the stages of evolution. These types are set out in Table 1 of Briggs et al. (2015).

The evolved populations were searched for systems that resulted in a pair of Carbon/Oxygen white dwarfs (CO WDs), that is, type 11s in the `BSE` system. We have found that as  $\alpha_{\text{CE}}$  increases the number of CO WD double degenerate systems increases. However, not all of these systems correspond with the type of evolution path that would lead to the final parameters of NLTT 12758, i.e. cooling ages, period, masses.

A suitable near match to NLTT 12758 was achieved at  $\alpha_{\text{CE}} = 0.15$  with initial masses of 3.75  $M_{\odot}$  and 2.80  $M_{\odot}$  and with an initial period of 2656 days. As `BSE` consists of many approximations, the resulting solution is considered to be satisfactory and within the errors on the parameters of NLTT 12758 given in Table 5.4.

The evolution shown in Table 5.5 starts with two stars, S1 and S2, and follows each of them through their normal evolution until 256 Myr. Up until this time the

only interactions between the two stars are small mass losses due to winds and the consequent small changes in orbital separation and period. At 256 Myr the stars start to interact by common envelope evolution. First, the more massive star, S1, develops an extended envelope which overflows the Roche lobe. This draws the stars closer together by friction eroding the orbit. When Roche lobe overflow ceases and S1 reveals its core as a CO WD, the two stars are about  $588 R_{\odot}$  apart with a period of around 864 days. At this point, S2 is still a main sequence star. About 315 Myr later, S2 initiates its own common envelope evolution resulting in a second CO WD, an orbital separation of  $5.3 R_{\odot}$  and a period of only 1.161 days. One of the pair, S2, is now a magnetic WD resulting from the dynamo effect within the common envelope. S1 loses about  $2.8 M_{\odot}$  during the first common envelope phase while S2 loses about  $2 M_{\odot}$ . As the second common envelope evolution brings the two stars very close together by shrinking the orbit from about 500 to  $5 R_{\odot}$ , it is S2 that develops the magnetic field and the rapid rotation.

From this time the pair interact by gravitational radiation and magnetic braking with consequent orbital shrinkage until at 2791 Myr they reach the present day with a separation of  $5.278 R_{\odot}$  and an orbital period of 1.154 days. The cooling ages are 2535 Myr and 2220 Myr for the non-magnetic and magnetic white dwarfs respectively (for details of the method see Briggs et al., 2015, and chapter 2 of this work). Further evolution will see the orbit shrinking further until at some stage (over a time much longer than a Hubble time) Roche lobe overflow restarts and the two stars merge. The possible final fate of double degenerate white dwarf systems, such as NLTT 12758, is discussed in the section below.

**Table 5.5:** Evolution of a binary star system of approximately the size of NLTT 12758 starting from ZAMS through to the end of their interaction and the production of a double degenerate WD pair.  $M1$  and  $M2$  are the masses of the primary and secondary stars respectively (in solar masses),  $S1$  and  $S2$  are the stellar types varying throughout their evolution as shown in Table 1 in Briggs et al. (2015, and chapter 2).  $Sepn$  is the stellar separation in solar radii,  $Period$  is the orbital period in days and the *Event – Type* is the event happening to the system at the time given in column 2.

Step	<i>Time</i> (MYr)	$M1$ ( $M_{\odot}$ )	$M2$ ( $M_{\odot}$ )	$S1$	$S2$	<i>Period</i> (days)	<i>Sepn</i> ( $R_{\odot}$ )	<i>Event – Type</i>
1	0.000	3.750	2.800	1	1	2656.000	1510.578	ZAMS
2	210.988	3.750	2.800	2	1	2653.321	1509.562	$S1 \Rightarrow$ Hertzprung Gap
3	212.057	3.750	2.800	3	1	2653.713	1509.674	$S1 \Rightarrow$ RGB
4	212.955	3.747	2.800	4	1	2655.573	1510.204	$S1 \Rightarrow$ He core burning
5	253.754	3.676	2.800	5	1	2714.292	1526.805	$S1 \Rightarrow$ Early AGB
6	255.551	3.597	2.801	6	1	2668.247	1503.396	$S1 \Rightarrow$ Late AGB
7	255.989	2.787	2.827	6	1	2819.839	1493.233	Begin Roche lobe overflow
8	255.989	0.827	2.827	11	1	864.356	588.342	CEE, $S1 \Rightarrow$ CO WD
9	255.989	0.827	2.827	11	1	864.356	588.342	End Roche lobe overflow
10	443.089	0.827	2.827	11	1	864.356	588.342	$S2 \Rightarrow$ Blue straggler
11	449.391	0.827	2.827	11	2	864.356	588.342	$S2 \Rightarrow$ Hertzprung Gap
12	452.151	0.827	2.826	11	3	864.520	588.398	$S2 \Rightarrow$ RGB
13	455.303	0.827	2.824	11	4	865.691	588.810	$S2 \Rightarrow$ He core burning
14	567.390	0.827	2.774	11	5	889.679	596.911	$S2 \Rightarrow$ Early AGB
15	570.808	0.828	2.725	11	6	757.173	533.592	$S2 \Rightarrow$ Late AGB
16	571.109	0.828	2.662	11	6	689.277	498.253	Begin Roche lobe overflow
17	571.109	0.828	0.652	11	11	1.161	5.297	CEE, $S2 \Rightarrow$ CO WD
18	571.109	0.828	0.652	11	11	1.161	5.297	End Roche lobe overflow
19	2791.209	0.828	0.652	11	11	1.154	5.278	Present Day



## 5.5 Discussion

NLTT 12758 is a member of a growing class of double degenerate systems consisting of two white dwarfs, one magnetic and one not. Table 5.6 lists the currently known double degenerate systems containing at least one magnetic white dwarf. The table lists the names, orbital and rotational periods, the magnetic field strength, effective temperatures and masses of the components. It includes both close binaries and common proper motion (CPM) systems. Most of the systems for which effective temperatures and masses are determined appear to have formed, within uncertainties, at the same time. In the case of CPM systems, where it is assumed that the stars did not interact during their evolution, there are systems with inconsistencies in their ages if one assumes single star evolution for each star. Apart from the well documented case of EUVE J0317-855 (Ferrario et al., 1997b), another more recent example is given by PG 1258+593 and its common proper motion magnetic white dwarf companion SDSS J1300+5904. Girven et al. (2010) found that the masses of these white dwarfs are  $0.54 \pm 0.06 M_{\odot}$  for the non-magnetic and  $0.54 \pm 0.01 M_{\odot}$  for the magnetic component. Despite their very similar masses, SDSS J1300+5904 is a cool white dwarf ( $T_{\text{eff}} = 6300 \pm 300$  K) while PG 1258+593 is substantially hotter ( $T_{\text{eff}} = 14790 \pm 77$  K). Girven et al. (2010) find that the temperature discrepancy gives a difference in cooling age (and thus in formation age of the white dwarfs) of  $1.67 \pm 0.05$  Gyr. If one makes the plausible assumption that the progenitors of these CPM white dwarfs formed in the same protostellar cloud at roughly the same time, then the similar white dwarf masses and their large age discrepancy give rise to a paradox. A possible solution is that this system was initially a triple system where two stars interacted and merged to form the magnetic white dwarf SDSS J1300+5904 about 1.67 Gyr before the third non-interacting object evolved into the non-magnetic white dwarf PG 1258+593.

However, the situation appears to be rather different for the double degenerate system NLTT 12758, as reported in section 5.4.4. Since NLTT 12758 is a close binary system, it is highly unlikely that the field of the magnetic component was caused by the merging of two stars in an initially triple system. Instead, the magnetic field must have originated during CE evolution in a manner very similar to that occurring during the formation of a magnetic cataclysmic variable, as proposed by Briggs et al. (2018a, submitted to MNRAS). In this scenario, the closer the cores of the two stars are drawn during CE evolution, the greater the differential rotation and thus the larger the dynamo generated field will be. If CE evolution leads to the merging of the two stellar cores the resulting object would be an isolated highly magnetic white dwarf (see Wickramasinghe, Tout & Ferrario, 2014). If the two stars do not coalesce they are expected

to emerge from the CE as close binaries that are already interacting, and thus appear as magnetic cataclysmic variables, or are close to interaction. The low-accretion rate polars, where a magnetic white dwarf accretes matter from its companion through a stellar wind, have been suggested by Schwöpe et al. (2009) to be the progenitors of the polars, which are the highest field magnetic cataclysmic variables. In the polars a MWD accretes matter from an un-evolved low-mass (M-dwarf) companion via magnetically confined accretion flows. The orbital periods are typically between 70 minutes to a few hours and Zeeman and cyclotron spectroscopy from the UV to the IR bands have revealed the presence of fields between 7 to 230 MG (e.g. see Ferrario et al., 1992; Ferrario, Bailey & Wickramasinghe, 1993; Ferrario et al., 1996; Schmidt et al., 2001b) in the case of the polars, and 1 to 20 MG in the case of intermediate polars (Ferrario, Wickramasinghe & King, 1993). The difference between these systems and NLTT 12758 is that both progenitor stars of NLTT 12758 were too massive to evolve into a magnetic cataclysmic variable. However, the indications seem to be that the magnetic white dwarf component of NLTT 12758 acquired its field via a mechanism similar to that propounded to explain the origin of magnetic cataclysmic variables.

The properties of NLTT 12758 mean that the two white dwarfs will coalesce in a time much longer than a Hubble time ( $\sim 140$  Gyr; Ritter, 1986), however it is still interesting to speculate what the final fate of a system like this might be.

The first simulations of two merging CO WDs were conducted by Saio & Nomoto (1985) and showed that the fast mass accretion rate ( $\gtrsim 10^{-5} M_{\odot} \text{yr}^{-1}$ ) from the less massive to the more massive white dwarf ignites an off-centre carbon flash. The carbon nuclear burning then propagates toward the stellar centre turning the CO WD into an ONe WD quiescently. The outcome of such an event would not be a carbon deflagration but an accretion induced collapse (AIC) triggered by electron captures on  $^{24}\text{Mg}$  and  $^{20}\text{Ne}$ . The result would be a rapidly spinning neutron star that would appear as an isolated millisecond pulsar (MSP, e.g. Lorimer, 2008). The low space velocities of isolated MSPs suggest that there could not have been a substantial SNII kick imparted to the emerging neutron star, thus supporting the AIC hypothesis (Ferrario L., Wickramasinghe D. T., 2007b; Hurley et al., 2010). The calculations of Chen et al. (2013) lend further support to this idea since they show that it is unlikely that the isolated MSPs may be generated via the LMXB recycling scenario because this would require the total ablation of their donor star. Thus, merging events of systems similar to NLTT 12758, but with initial parameters that would allow faster evolutionary timescales, could provide a simple explanation for the existence of isolated MSPs.

On the other hand, the merging of the two stars in NLTT 12758 may give rise to a supernova event. Recent simulations conducted by Dan et al. (2014) and Dan et al.

(2015) showed that a merging system with a total mass  $M_{\text{tot}} \geq 2.1 M_{\odot}$  and comprised of two white dwarfs of similar mass may result in a Type Ia supernova; The total mass of NLTT 12758,  $M_{\text{tot}} = 1.52 M_{\odot}$ , would be below the predicted cutoff for this event to occur. However, other studies conducted by Pakmor et al. (2011) and Sato et al. (2016) found that systems with a mass ratio greater than  $\sim 0.8$  could indeed result into a SNIa explosion. Clearly, a consensus in this area of research still needs to be reached (e.g. Ferrario, 2013).

## 5.6 Conclusions

In this chapter we have reported our studies on the close, super-Chandrasekhar double degenerate system NLTT 12758 consisting of two CO WDs of similar masses and ages and with one of the two components highly magnetic. The magnetic white dwarf spins around its axis with a period of 23 minutes and they orbit around each other with a period of 1.15 days. Although the components of NLTT 12758 will not merge over a Hubble time, systems with very similar initial parameters will come into contact and merge thus undergoing either an accretion induced collapse to become a rapidly spinning neutron star (an isolated MSP) or a Type Ia supernova explosion. Given the theoretical uncertainties, the jury is still out on the fate of such systems.

## Acknowledgements

AK and SV acknowledge support from the Grant Agency of the Czech Republic (P209/12/0217 and 15-15943S) and the Ministry of Education of the Czech Republic (LG14013). This work was also supported by the project RVO:67985815 in the Czech Republic. SV acknowledges support from the Mathematical Sciences Institute of the Australian National University. EP acknowledges support by the Ministry of Education of the Czech Republic (grant LG15010). GPB gratefully acknowledges receipt of an Australian Postgraduate Award. We thank the referee, Pier-Emmanuel Tremblay, for a thorough report and helpful comments on line-broadening theory.

**Table 5.6:** Known double degenerates containing a magnetic white dwarf

Name	Alternate name	$P_{\text{orb}}$	$P_{\text{rot}}$	$B$ (MG)	$T_{\text{eff}}$ (K)		Mass ( $M_{\odot}$ )		Reference
					Magnetic	Companion	Magnetic	Companion	
0040+000	SDSS J004248.19+001955.3	...	...	14	11000		...	...	1
0121-429 <sup>a</sup>	LHS 1243	...	...	10.3	6105	5833	0.7 <sup>d</sup>	0.54 <sup>d</sup>	2,3,4
0239+109 <sup>a</sup>	G 4-34, LTT 10886	...	...	0.7	10060	7620	...	...	5,6
0325-857	EUVE J0317-855	~ 2095 yr	725 s	185-425	33000	16360	1.3	0.85	7,8,9,10
0410-114	NLTT 12758, G160-51	1.15 d	23 min	3.1	7220	7950	0.69	0.83	This work
0512+284 <sup>a</sup>	LSPM J0515+2839	...	...	2.15	5940	6167	0.81 <sup>d</sup>	0.61 <sup>d</sup>	3,4
0745+303	SDSS J074853.07+302543.5	CPM	...	11.4	21000	22702	0.81	0.88	11
0843+488 <sup>b</sup>	SDSS J084716.21+484220.4	...	...	...	19000		...	...	1
0924+135	SDSS J092646.88+132134.5	CPM	...	210	9500	10482	0.62	0.79	12
0945+246	LB 11146	~ 130 d	...	~ 670	16000	14500	0.90	0.91	13,14,15
1026+117 <sup>a</sup>	LHS 2273	...	...	17.8	5691	7350	0.75 <sup>d</sup>	0.64 <sup>d</sup>	3,4
1258+593	SDSS J130033.48+590407.0	CPM	...	6	6300	14790	0.54	0.54	16
1330+015 <sup>a</sup>	G 62-46	...	...	7.4	5712	7618	0.82 <sup>d</sup>	0.64 <sup>d</sup>	3,4
1440+753	EUVE J1439+750	...	...	10	42000	30000	0.9	1.1	17
1503-070 <sup>a</sup>	GD 175	...	...	2.9	6062	7051	0.95 <sup>d</sup>	0.73 <sup>d</sup>	3,4
1506+399	CBS 229	CPM	...	18.9	18000	16761	0.81	0.82	11
1506+523	SDSS J150746.80+520958.0	CPM	...	65.2	18000	17622	0.99	0.70	12
1514+282 <sup>a</sup>	SDSS J151625.07+280320.9	...	...	2.05	7168	7662	0.77 <sup>d</sup>	0.54 <sup>d</sup>	3,4
1713+393 <sup>a</sup>	NLTT 44447	...	...	2.1	6204	6556	0.94 <sup>d</sup>	0.54 <sup>d</sup>	3,4,18
1814+248 <sup>c</sup>	G 183-35	...	...	12.05/7.8	5998	5849	0.85 <sup>d</sup>	0.74 <sup>d</sup>	3,4,19
1818+126 <sup>a</sup>	G 141-2	...	...	3.75	5215	6451	0.64 <sup>d</sup>	0.54 <sup>d</sup>	3,4

<sup>a</sup> DAH+DC, <sup>b</sup> DAH+DB, <sup>c</sup> DAH+DAH

<sup>d</sup> Masses are calculated using the mass-radius relations of Benvenuto & Althaus (1999), the published parameters of the magnetic star and ratio of the stellar radii.

**Table 5.6** continued,

**References:** (1) Schmidt et al. (2003); (2) Subasavage et al. (2007); (3) Rolland (2014); (4) Rolland & Bergeron (2015); (5) Koester et al. (2009); (6) Gianninas et al. (2011); (7) Ferrario et al. (1997b); (8) Vennes et al. (2003); (9) Külebi et al. (2010); (10) Lawrie (2013); (11) Dobbie et al. (2013); (12) Dobbie et al. (2012); (13) Nelan (2007); (14) Glenn et al. (1994); (15) Liebert et al. (1993); (16) Girven et al. (2010); (17) Vennes et al. (1999); (18) Kawka & Vennes (2006); (19) Putney (1995)



# Chapter 6

## Conclusions

The realisation that there is a population of isolated WDs with extremely high magnetic fields led to attempts to explain their origin. The aim of this study was to model the evolution of a synthetic population of binary stars to test the hypothesis of Tout et al. (2008) regarding the origin of high magnetic fields in WDs. Two main mechanisms for the origin of these intense fields have been proposed. They are the fossil field model and the merging star model. The fossil field model (as first proposed by Woltjer, 1964; Landstreet, 1967) is based upon the fact that early type stars of classes Ap and Bp have maximum poloidal magnetic fields of similar strength to those observed in the magnetic WD. It was therefore supposed that the strong fields are maintained through the evolution of the star. However no model of stellar evolution has been able to explain how a strong fossil magnetic field can survive through the various stages of evolution from main sequence to WD. Nor has it been possible to show that there is a common cause for the observed maximum magnetic field strengths in the two classes of stars.

In the case of the WDs, a clue to the origin of their fields, in both isolated and binary systems, is given by the study of their binary properties (Liebert et al., 2005, 2015a). This led Tout et al. (2008) to propose that the origin of magnetic fields in WDs is related to their duplicity and stellar interaction during CEE (Paczynski, 1976). Additionally the dynamo model of Wickramasinghe, Tout & Ferrario (2014) provides physical reasons for similar maximum magnetic fluxes in the magnetic main sequence stars and the isolated MWDs if the fields are generated from differential rotation caused by merging.

The two stars that comprise a binary system are born from the protostellar cloud at about the same time. The more massive of the two, initially both main sequence stars, evolves faster and it is the first to evolve along the RGB. Here, its envelope expands greatly and engulfs the secondary star. The drag encountered by the secondary star, now within the envelope of the primary, causes the orbit of the two stars about the common centre of gravity to decay. As a consequence the two stars may merge at this stage. If they do not merge, more CE episodes can occur perhaps during the evolution

of the binary on the AGB and merging may occur at this point.

The proposal of Tout et al. (2008) posits that the high magnetic fields found in the sub population of isolated MWDs are caused by differential rotation of the envelope caused by the orbital revolution of the secondary within the CE. The first condition for the formation of high fields is that during CEE the core of the pre-WD star is degenerate. The second condition is no nuclear burning should occur from CEE until the time the star reveals its core as a WD. The requirement is necessary for the formation of high magnetic fields because any nuclear burning would create convection and destroy any strong ordered field created.

## 6.1 The Study Method in Review

In order to test the viability of this model, I have modified the BSE (Binary Star Evolution) code of Hurley, Tout & Pols (2002). This code builds on the SSE (Single Star Evolution) code of Hurley, Pols & Tout (2000) by adding the major phenomena of binary evolution comprising Roche lobe overflow, CE evolution, tidal interaction, collisions, gravitational radiation and magnetic braking. For the evolution through the CE phase BSE uses the energy formulation with the variable  $\alpha$  as the efficiency of envelope removal ( $0.0 \leq \alpha \leq 1.0$ ). In this study I have investigated how  $\alpha$  affects the binary evolution outcome.

I created a synthetic population of binaries by three parameters at the ZAMS, mass of the primary, mass of the secondary and the orbital period, each with two hundred members in a log scale. The mass of the secondary was constrained to be less than the mass of the primary. In all cases I assumed an initially circular orbit for the progenitor binary. The calculations were repeated for all  $\alpha \in \{0.10, 0.20, 0.25, 0.30, 0.40, 0.50, 0.60, 0.70, 0.80 \text{ and } 0.90\}$ . I took the metallicity to be solar,  $Z = 0.02$ , and  $\eta = 1.0$  for the Reimers' mass loss parameter as outlined in chapter 2.

This gave me a synthetic population of about seven million binaries covering all combinations of the above parameters. The evolution of each binary system was examined for satisfaction of the CE degeneracy and nuclear burning criteria detailed above. The qualifying systems gave the required CEE population of binaries numbering about one million. The matching binaries were then weighted according to the Salpeter (1955) initial mass function and integrated from the ZAMS to the age of the Galactic disk (9.5GYr, Kilic et al. (2017)). The properties of the pre and post CE binaries and/or remnant WDs could then be extracted and analysed.



## 6.2 The Isolated Magnetic WDs

In chapter 2 of this work the mass distributions of the theoretical high field magnetic WDs (HFMWDs) were reported. It was found that for models with  $0.1 \leq \alpha \leq 0.3$  the mean predicted mass of isolated HFMWDs is  $0.88 M_{\odot}$ . Observations indicate mean masses of  $0.85 M_{\odot}$  (Kepler et al., 2013) for HFMWDs and  $0.62 M_{\odot}$  (Kleinman et al., 2013) for all non-magnetic Galactic field WDs. A K–S test (Press et al., 1992) on the masses of the theoretical HFMWDs against the few reliably measured observed HFMWDs gave a probability of 0.71 that they were from the same distribution, while a K–S test of theoretical HFMWDs against observed non-magnetic WDs only gave a probability of  $3 \times 10^{-5}$  that the masses had the same distribution.

One of the main results from this work is that there are two possible paths to HFMWDs. In the CE path merging occurs during CEE. In the other path the merging occurs after both stars have evolved to the WD stage and merge as double degenerates (DD path). The CE path greatly outnumbers the DD path for all  $\alpha$ . The CE path yields mainly CO WDs with small numbers of He and ONe WDs while the DD path yields only CO WDs which populate the high end of the mass distribution. These calculations, when taken together with the observation that there are no examples of HFMWDs in detached binary systems, argue strongly in favour of the CE merging hypothesis for the formation of HFMWDs. Thus the progenitors of HFMWDs are the RGB or AGB degenerate cores of stars that merge with their lower-mass companions and then continue their evolution, as single stars no longer undergoing nuclear fusion, to the WD stage.

In chapter 3 I have assumed that the magnetic field strength induced in the core of the single coalesced star emerging from CEE is proportional to the orbital angular velocity of the binary at the point that the secondary is disrupted by tidal forces and merges with the primary as first proposed by Regós & Tout (1995); Tout & Regós (1995b); Tout et al. (2008); Wickramasinghe, Tout & Ferrario (2014). The maximum field strength that can be achieved by a compact core during a merging process is limited by the break-up angular velocity and this can only be reached if the merging stars are in a very compact binary, such as a merging DD system.

In this model two parameters must be empirically estimated. These are  $B_0$ , which is linked to the efficiency with which the poloidal field is regenerated by the decaying toroidal field (see Wickramasinghe, Tout & Ferrario, 2014) and the CE efficiency parameter  $\alpha$ . Having calculated the CDFs of the observed and theoretical field distributions, a K–S test was carried out between the observed and theoretical field distributions for a wide range of  $B_0$ . From the K–S probability,  $P$ , I determined that the observed field distribution is best fitted by models characterised by  $B_0 = 1.35 \times 10^{10}$  G

and  $\alpha = 0.2$  with  $P=0.61$ ,

It is also speculated that close stellar encounters can send a giant gaseous planet from the outer regions of a WD's planetary system into a highly eccentric orbit. The plunging of this super-Jupiter into the WD can generate a magnetic field and thus provide an answer as to why magnetism among cool WD, and particularly among cool DZ WDs, is higher than among hot WDs.

### 6.3 The Magnetic Cataclysmic Variables

Population synthesis studies of binary systems that survive the CE environment without merging can go on to form MCVs. By making use of synthetic population modelling similar to that for the isolated HFMDs it was shown that the same  $B_0$  can also explain the magnetic field distribution of magnetic binaries.

The population synthesis study of binary systems carried out for the HFMDs was modified to explain the origin of fields in the accreting WD in MCVs and the results are shown in chapter 4. The CE efficiency parameter  $\alpha$  was again varied to investigate its effects on the resulting synthetic population of MCVs. This showed that models with  $\alpha > 0.4$  are not able to reproduce the large range of WD masses, field strength, secondary types and masses that are observed in MCVs.

Quantitative support in favour of models with  $\alpha \leq 0.4$  was given by K-S tests conducted to compare the synthetic WD mass and magnetic field distributions with the observed populations. However, once again, it must be stressed that there are some shortcomings of this work and in particular those that arise from our comparison to observations.

Many of the parameters of the Galactic populations of MCVs and pre-polars (PREPs) that are needed for comparison studies (e.g., WD mass, magnetic field, secondary star mass and type, and orbital period) are often hard to determine owing to evolutionary effects and observational biases that are difficult to separate. For example, magnetic WDs in PREPs are the best objects with which to compare our theoretical results and in particular the mass distribution, because their mass has not been corrupted by accretion processes. However the members of this population are scarce. Owing to accretion and nova explosions nor can the much larger sample of MCVs be used for comparison purposes of the WD mass distribution, because masses vary over time. Instead the sample provided by the non magnetic pre CVs of Zorotovic et al. (2011) was used. This is not an ideal sample but it is the best currently at our disposal until a statistically significant number of PREPS has been discovered. A K-S test on the observed Pre CV masses against the theoretical population at the start of Roche lobe overflow (RLOF) gave a probability of a match of the two populations of  $P=0.95$  at  $\alpha=0.10$  while the K-S test

of the observed population of MCVs from Ferrario et al. (2015a) against the theoretical population only gave an  $P = 0.02$  at  $\alpha = 0.1$  indicating that WD masses do vary over time.

The situation is somewhat alleviated when we consider the magnetic field distribution because fields are not expected to change over time (Ferrario et al., 2015a). However, the observed magnetic field distribution of MCVs may not be reliable because it may be afflicted by observational biases. For example, at field strengths below a few  $10^7$  G, most systems (the intermediate polars) have an accretion disc from which continuum emission and broad emission lines swamp the Zeeman and cyclotron spectral features that are essential to determine their field strengths arising from the WD surface (Ferrario et al., 1992). Very high field polars are also likely to be under represented in the observations because mass accretion from the companion is hampered by the presence of strong fields (Ferrario et al., 1989; Liu & Chaboyer, 2000) making these systems very dim wind accretors. Despite these restrictions, the characteristics of the MCVs are generally consistent with those of a population of binary systems that are born already in contact (exchanging mass) or close to contact, as suggested by Tout et al. (2008) and is generally in agreement with the speculation of Schwöpe et al. (2009) that the binaries known as PREPs, where a HFMWD accretes matter from the wind of a low mass companion, are the progenitors of the MCVs.

## 6.4 Evolution of a Double Degenerate System: NLTT 12578

The binary system NLTT 12758 is a close super Chandrasekhar double degenerate system consisting of two CO WDs of similar masses ( $0.83 M_{\odot}$  and  $0.69 M_{\odot}$ ). One of the two components is highly magnetic and spins around its axis with a period of 23 min. The orbital period was determined to be 1.15 d (See chapter 5).

In order to understand the evolution of NLTT 12758 I created a number of binaries and evolved them from the ZAMS to the age of the Galactic disc. The mass of the primary star was chosen to vary between  $3.5 M_{\odot}$  and  $4.5 M_{\odot}$  and the mass of the secondary star between  $2.5 M_{\odot}$  and  $3.5 M_{\odot}$  and the initial period in the range 2000 to 3500 d. These values were chosen because they were in the region of the expected initial conditions that would lead to the final properties of the components of NLTT 12758.

The evolved populations were searched for systems that resulted in a pair of CO WDs at the correct stage of evolution. It was found that, as  $\alpha$  increases, the number of CO WD double degenerate systems increases. However, not all of these systems correspond with the type of evolution path that would lead to the final parameters of NLTT 12758, its cooling age, period and mass. A suitable near match to NLTT 12758

was achieved at  $\alpha = 0.15$  with initial masses of  $3.75 M_{\odot}$  and  $2.80 M_{\odot}$  and with an initial period of 2656 d.

The future evolution of NLTT 12758 will see the orbit shrinking further until at some stage Roche lobe overflow will restart and the two stars will coalesce in approximately 140 Gyr. At this time they will undergo either an accretion induced collapse to become a rapidly spinning neutron star (an isolated millisecond pulsar) or undergo a Type Ia supernova explosion.

## 6.5 A Final Word

The CE merging theory for the formation of high fields in magnetic WD as proposed by Tout et al. (2008) has successfully predicted the mass distribution of the observed HFMWDs and shown that it is significantly different from that of Galactic field WDs. My modelling has also successfully computed the magnetic field distribution of HFMWDs. In addition it has accurately predicted the post CE characteristics of those systems that become MCVs.

For the double degenerate WD system NLTT 12758, I was able to successfully construct the history of the evolution of the system and explained the genesis of the magnetic field in one of the components of the binary.

I can therefore conclude that the CEE theory of the genesis of high magnetic fields in isolated WDs, in cataclysmic variables and in double degenerate systems is the most likely so far to explain all observations of these systems.

## Bibliography

- Achilleos N., Wickramasinghe D. T., 1989, *ApJ*, 346, 444
- Alecian E. et al., 2015, in *IAU Symp. 307*, Meynet G., Georgy C., Groh J., Stee P., eds., Vol. 307, Geneva, Switzerland, pp. 330
- Ali A. W., Griem H. R., 1965, *Phys. Rev. A*, 140, 1044
- Ali A. W., Griem H. R., 1965, *Phys. Rev. A*, 144, 366
- Angel J. R. P., Illing R. M. E., Landstreet J. D., 1972, *ApJ*, 175, L85
- Angel J. R. P. 1977, *ApJ*, 216, 1
- Angel J. R. P. 1978, *ARA&A*, 16, 487
- Angel J. R. P., Borra E. F., Landstreet J. D., 1981, *ApJS*, 45, 457
- Angel J. R. P., Liebert J., Stockman H. S., 1985, *ApJ*, 292, 260
- Anselowitz T., Wasatonic R., Matthews K., Sion E. M., McCook G. P., 1999, *PASP*, 111, 702
- Arnett D., *Supernovae and Nucleosynthesis*, 1996, Princeton University Press
- Araujo-Betancor S., Gänsicke B.T, Long K.S., Beuermann K., de Martino D., Sion E.M., Szkody P., 2005, *ApJ*, 622, 589
- Aznar Cuadrado R., Jordan S., Napiwotzki R., Schmid H. M., Solanki S. K., Mathys G., 2004, *A&A*, 423, 1081
- Barklem P. S., Piskunov N., O'Mara B. J., 2000, *A&A*, 363, 1091
- Barstow M.A., Jordan S., O'Donoghue D., Burleigh M. R., Napiwotzki R., Harrop-Allin M.K., 1995, *MNRAS*, 277, 971
- Benvenuto O. G., Althaus L. G., 1999, *MNRAS*, 303, 30

- Bergeron P., Ruiz M. T., Leggett S. K., 1992, *ApJ*, 400, 315
- Bergeron P., Ruiz M. T., Leggett S. K., 1993, *ApJ*, 407, 733
- Bergeron P., Ruiz M. T., Leggett S. K., 1997, *ApJS*, 108, 339
- Bergeron P., Leggett S. K., Ruiz M. T., 2001, *ApJS*, 133, 413
- Bisnovatyi-Kogan G. S., Sunyaev R. A., 1971, *Astron. Zh.*, 48, 881
- Braithwaite J., 2009, *MNRAS*, 397, 763
- Briggs G. P., Ferrario L., Tout C. A., Wickramasinghe D. T., Hurley J. R., 2015, *MNRAS*, 447, 1713
- Briggs G. P., Ferrario L., Tout C. A., Wickramasinghe D. T., 2018a, *MNRAS*, in publication
- Briggs G. P., Ferrario L., Tout C. A., Wickramasinghe D. T., 2018b, *MNRAS*, submitted for publication
- Brinkworth C. S., Burleigh M. R., Wynn G. A., Marsh T. R., 2004, *MNRAS*, 348, L33
- Brinkworth C. S., Marsh T. R., Morales-Rueda L., Maxted P. F. L., Burleigh M. R., Good S. A., 2005, *MNRAS*, 357, 333
- Brinkworth C. S., Burleigh M. R., Lawrie K., Marsh T. R., Knigge C., 2013, *ApJ*, 773, 47
- Cardelli J. A., Clayton G. C., Mathis J. S., 1989, *ApJ*, 345, 245
- Charbonnel C., Meynet G., Ma A., Schaller G., Schaerer D., 1993, *A and AS*, 101, 415
- Chen H-L, Chen X., Tauris T. M., Han Z., 2013, *ApJ*, 775, 27
- Colpi M., Geppert U., Page D., 2000, *ApJL*, 529, L29
- Cutri R. M., et al., 2012, *VizieR Online Data Catalog*, 2311
- Dahn C. C., 1999, 11th European Workshop on White Dwarfs, *ASP Conference Series*, 169, 24
- Dan M., Rosswog S., Brüggen M., Podsiadlowski P., 2014, *MNRAS*, 438, 14

- Dan M., Guillochon J., Brüggen M., Ramirez-Ruiz E., Rosswog S., 2015, MNRAS, 454, 4411
- de Kool M., 1990, ApJ, 358, 189
- de Kool M., 1992, A&A, 261, 188
- Dobbie P. D., Baxter R., Külebi B., Parker Q. A., Koester D., Jordan S., Lodieu N., Euchner F., 2012, MNRAS, 421, 202
- Dobbie P. D. et al., 2013, MNRAS, 428, L16
- Dufour P., Bergeron P., Fontaine G., 2005, ApJ, 627, 404
- Dufour P., Bergeron P., Schmidt G. D., Liebert James., Harris H. C., Knapp G. R., Anderson S. F., Schneider D. P., 2006, ApJ, 651, 1112
- Eggen O. J., 1968, ApJ, 153, 195
- Eggleton, P.P., 1971, MNRAS, 151, 351
- Fabrika S., Valyavin G. 1999, in ASP Conf. Ser. 169, 11th European Workshop on White Dwarfs, ed. J. E. Solheim & E. G. Meistas (San Francisco: ASP), 214
- Farihi J., Dufour P., Napiwotzki R., Koester D., 2011, MNRAS, 413, 2559
- Ferrario, L., Wickramasinghe D.T., Tuohy I.R., 1989, ApJ, 341, 327
- Ferrario L., Wickramasinghe D. T., Bailey J. A., Hough J. H., Tuohy I. R. 1992, MNRAS, 256, 252
- Ferrario L., Wickramasinghe D. T., King A. R. 1993, MNRAS, 260, 149
- Ferrario L., Bailey J., Wickramasinghe D. T., 1993, MNRAS, 262, 285
- Ferrario L., Wickramasinghe D. T., 1993, MNRAS, 265, 605
- Ferrario L., Bailey J., Wickramasinghe D. T., 1996, MNRAS 282, 218
- Ferrario L., Wickramasinghe D. T., Liebert J., Schmidt G. D., Biegging J. H., 1997a, MNRAS, 289, 105
- Ferrario L., Vennes S., Wickramasinghe D. T., Bailey J. A., Christian D. J., 1997b, MNRAS, 292, 205

Ferrario L., Vennes S., Wickramasinghe D. T., 1998, MNRAS, 299, L1

Ferrario L., Li J. Saxton C., Wu K. 1999, PASA, 16, 234

Ferrario L., Wehrse R., 1999, MNRAS, 310, 189-202

Ferrario L., Wickramasinghe D. T., 1999, MNRAS, 309, 517-527

Ferrario L., 2004, RevMexAA, 20, 111

Ferrario L., Wickramasinghe D. T., 2005, MNRAS, 356, 615

Ferrario L., Wickramasinghe D. T., 2007a, ASP Conference Series, 372, 163

Ferrario L., Wickramasinghe D. T., 2007b, MNRAS, 375, 1009

Ferrario L., Wickramasinghe D.T., 2008, MNRAS:Letters, 389, L66

Ferrario L., Pringle J. E., Tout C. A., Wickramasinghe D. T. 2009, MNRAS, 400, L71

Ferrario L., 2012, MNRAS, 426, 2500

Ferrario L., 2013, “Binary Paths to Type Ia Supernovae Explosions”, Proc. IAU Symposium No 281, Cambridge University Press, Cambridge (UK), Eds: R. Di Stefano, M. Orio, M. Moe, Vol. 281, p. 341

Ferrario L., Melatos A., Zrake J., 2015a, Space Science Review, 191, 77

Ferrario L., de Martino D., Gänsicke, B. T., 2015b, Space Science Review, 191, 111

Fouqué P. et al., 2000, A&A, 141, 313

Gänsicke B.T., Dillon M., Southworth J., et al., 2009, MNRAS, 397, 2170

García-Berro E. et al., 2012, ApJ, 749, 25

Gianninas A., Bergeron P., Ruiz M. T., 2011, ApJ, 743, 138

Giovannini O., Kepler S. O., Kanaan A., Wood M. A., Claver C. F., Koester, D., 1998, Baltic Astron., 7, 131

Girven J., Gänsicke B. T., Külebi B., Steeghs D., Jordan S., Marsh T. R., Koester D., 2010, MNRAS, 404, 159

Glenn J., Liebert J., Schmidt, G. D., 1994, PASP, 106, 722



Green R. F., Liebert J., 1981, *PASP*, 93, 105

Greenstein J. L., Henry R. J. W., O'Connell R. F., 1985, *ApJ*, 289, L25

Greenstein J. L., 1986, *ApJ*, 304, 334

Han Z., Podsiadlowski P., Eggleton P. P., *MNRAS*, 270,121

Han Z., Podsiadlowski, P., Maxted P. F. L., Marsh T. R., Ivanova N., *MNRAS*, 336, 449

Hansen B.M.S., Liebert J., 2003, *Annu. Rev. Astron. Astrophys.*, 41, 465

Hjellming M. S., Webbink R. F., 1987, *ApJ*, 318, 794

Henden A. A., Templeton M., Terrell D., et al. 2016, *VizieR Online Data Catalog*, 2336

Hoard D. W., Schmidt Gary D., Szkody Paula, Ferrario Lilia, Fraser Oliver, Wolfe Michael A., Gänsicke B. T., 2004, *AJ*, 128, 1894

Hollands M. A., Gänsicke B. T., Koester D., 2015, *MNRAS*, 450, 681

Hollands M. A., Koester D., Alekseev V., Herbert E. L., Gänsicke B. T., 2017, *MNRAS*, 467, 4970

Hong J., 2012, *MNRAS*, 427, 1633

Hurley J. R., Pols O.R., Tout C. A., 2000, *MNRAS*, 315, 543

Hurley J.R., Shara M.M., 2002, *ApJ*, 570, 184

Hurley J. R., Tout C. A., Pols O. R., 2002, *MNRAS*, 329, 897

Hurley J. R., 2008, *Lecture Notes in Physics*, 730, 283, *N-Body Stellar Evolution*

Hurley J. R., Tout C. A., Wickramasinghe D. T., Ferrario L. Kiel P. D. 2010, *MNRAS*, 402, 1437

Iben I. Jr., 1965, *ApJ*, 142, 1447

Iben I. Jr., Livio M., 1993, *PASP*, 105, 1373

Iben I. Jr., *Stellar Evolution Physics, Volumes 1 & 2*, 2013, Cambridge, UK: Cambridge University Press

- Isern J., Garcia-Berro E., Hernanz M., Salaris M., 2002, *Contributions to Science*, 2, 237
- Jordan S., 1992, *A&A*, 265, 570
- Jordan S., Schmelcher P., Becken W., Schweizer W., 1998, *A&A*, 336, L33
- Jordan S. 2007, “15th European Workshop on White Dwarfs”, *ASP Conf. Series*, Vol. 372, Ed: Ralf Napiwotzki and Matthew R. Burleigh. San Francisco: ASP, 2007, p.139
- Jura M., 2003, *ApJ*, 584, L91
- Kahabka P., van den Heuvel E. P. J. 1997, *ARA&A*, 35, 69
- Kawka A., Vennes S. 2004, in *IAU Symp. 224, The A-Star Puzzle*, ed. J. Zverko, et al. (Cambridge U. Press), 879
- Kawka A., Vennes S., 2006, *ApJ*, 643, 402
- Kawka A., Vennes S., Schmidt G. D., Wickramasinghe D. T., Koch R., 2007, *ApJ*, 654, 499
- Kawka A., Vennes S., 2012a, *MNRAS*, 425, 1394
- Kawka A., Vennes S., 2012b, *A&A*, 538, A13
- Kawka A., Vennes S., 2014, *MNRAS*, 439, L90
- Kawka A., Briggs G. P., Vennes S., Ferrario L., Paunzen E., Wickramasinghe D.T., 2017, *MNRAS*, 466, 1127
- Kemic S. B., 1974, *JILA REP. No.* 113
- Kepler S. O., et al., 2007, *MNRAS*, 375, 1315
- Kepler S. O. et al., 2013, *MNRAS*, 429, 2934
- Kilic M., Munn J.A., Harris H.C., von Hippel T., Liebert J., Williams K.A., Jeffery E., DeGennaro S., 2017, *ApJ*, 837, 2
- Kippenhahn R., Weigert A., Hofmeister E., 1967, *Meth. Comp. Phys.*, 7, 129
- Kippenhahn T., Weigert A., *Stellar Structure and Evolution*, 1990, *A&A library*, Springer, Heidelberg

Kleinman S. J. et al., 2013, ApJS, 204, 5

Koester D., Voss B., Napiwotzki R., Christlieb N., Homeier D., Lisker T., Reimers D., Heber U., 2009, A&A, 505, 441

Kowalski P. M., Saumon D., 2006, ApJ, 651, L137

Külebi B., Jordan S., Euchner F., Gänsicke B. T., Hirsch H. 2009, A&A, 506, 1341

Külebi B., Jordan S., Nelan E., Bastian U., Altmann M., 2010, A&A, 524, A36

Lamb F. K., Sutherland P. G., 1974, IAUS, 53, 265

Landstreet J. D., 1967, Phys Rev 153, 1372L

Landstreet J. D., Bagnulo S., Valyavin G. G., Fossati L., Jordan S., Monin D., Wade G. A., 2012, A&A, 545, A30

Landstreet J. D., Bagnulo S., Martin A., Valyavin, G., 2016, A&A, 591, 80

Lawrie K. A., 2013, PhD Thesis, University of Leicester

Liebert J., Sion E. M., 1979, ApJ, 20, 53L

Liebert J., Schmidt G. D., Sion E. M., Starrfield S. G., Green R. F., Boroson T. A., 1985, PASP, 97, 158

Liebert J., 1988, PASP, 100, 1302

Liebert J., Bergeron P., Schmidt G. D., Saffer R. A., 1993, ApJ, 418, 426

Liebert J., Bergeron P., Holberg J.B., 2003, AJ, 125, 348

Liebert J., Bergeron P., Holberg J. B., 2005, ApJS, 156, 47

Liebert J. et al., 2005, AJ, 129, 2376

Liebert, J., 2009, 16th European White Dwarfs Workshop, J.Phys, Conf. Series, 172

Liebert J., Smith P., Ferrario L., Wickramasinghe D.T., 2015, ASP Conference series Vol.493, p493

Liebert J., Ferrario L., Wickramasinghe D. T., Smith P. S. 2015a, ApJ, 804, 93

Li J. K., Wu K. W., Wickramasinghe D. T., 1994, MNRAS, 268, L61

- Li J., Ferrario L., Wickramasinghe D. T., 1998, ApJ, 503, L151
- Liu W. M., Chaboyer B., 2000, ApJ, 544, 818
- Livio M., Soker N., 1988, ApJ, 329, 764
- Lorimer D. R. 2008, Living Rev. Relativity 11, 8
- Martin B., Wickramasinghe D. T. 1981, MNRAS, 196, 23
- Main J., Schwacke M., Wunner G., 1998, Phys. Rev. A, 57, 1149-1
- Martin B., Wickramasinghe D. T. 1982, MNRAS, 200, 993
- Maxted P. F. L., Ferrario L., Marsh T. R., Wickramasinghe D. T., 2000, MNRAS, 315, L41
- Meggitt S. M. A. & Wickramasinghe D. T., 1982, MNRAS, 198, 71
- Meng X., Chen X., Han Z. 2008, A&A, 487,625
- Mestel L., Landstreet J. D., 2005, in Wielebinski R., Beck R., eds, Cosmic Magnetic Fields. Springer-Verlag, Berlin, p. 183
- Moran C., Marsh T. R., Dhillon V. S., 1998, MNRAS, 299, 218
- Morrissey P., et al., 2007, ApJS, 173, 682
- Mowlavi, N., Schaerer, D., Meynet, G., Bernasconi, P.A., Charbonnel, C., Maeder, A., 1998, A & AS, 128, 471
- Muno M.P., Baganoff F.K., Bautz M.W., Feigelson E.D., Garmire G.P., Morris M.R., Park S., Ricker G.R., Townsley L.K., 2004, ApJ, 613, 326
- Nauenberg M., 1972, ApJ 175, 417
- Nebot Gómez-Morán A., Gänsicke B. T., Schreiber M. R., et al., 2011, A&A, 536, 43
- Nelan E. P., 2007, AJ, 134, 1934
- Nordhaus J., Wellons S., Spiegel D. S., Metzger B. D., Blackman E. G., 2011, PNAS, 108, 3135
- Ostriker, J. 1976, in Structure and Evolution of Close Binary Systems, Proceedings of the Symposium, Cambridge, England, July 28-August 1, 1975. Eds. P. Eggleton, S. Mitton, and J. Whelan. Reidel Publishing Co. (IAU Symposium No. 73), 1976. p206

- Oswalt T. D., Smith J. A., Wood M. A., Hintzen P., 1996, *Nature*, 382, 692
- Pakmor R., Hachinger S., Röpké F. K., Hillebrandt W., 2011, *A&A*, 528, A117
- Paczyński B., 1976, in *Structure and Evolution of Close Binary Systems*, Proceedings of the Symposium, Cambridge, England, July 28-August 1, 1975. Eds. P. Eggleton, S. Mitton, and J. Whelan. Reidel Publishing Co. (IAU Symposium No. 73), 1976., p.75
- Parsons S.G., Marsh T.R., Gänsicke B.T., Schreiber M.R., Bours M.C.P., Dhillon V.S., Littlefair S.P., 2013, *MNRAS* 436, 241
- Patterson J., 1998, *PASP*, 110, 1132
- Pauli E.-M., Napiwotzki R., Heber U., Altmann M., Odenkirchen M., 2006, *A&A*, 447, 173
- Paunzen E., Vanmunster T., 2016, *AN*, 337, 239
- Pols O.R., Tout C.A., Eggleton P.P., Han Z., 1995, *MNRAS*, 274, 964
- Pols O.R., Schröder K.P., Hurley J.R., Tout C.A., Eggleton P.P., 1998, *MNRAS*, 298, 525
- Potter A.T., Tout C.A., 2010, *MNRAS*, 402, 1072
- Potter A. T., Chitre S. M., Tout C. A., 2012, *MNRAS*, 424, 2358
- Power J., Wade G. A., Aurière M., Silvester J., Hanes D., 2008, *Contrib. Astron. Obs. Skalnaté Pleso*, 38, 443
- Pragal M., Bues I., 1989, *Astron. Ges. Abstr. Ser.*, 2, 45
- Press W. H., Teukolsky S. A., Vetterling W. T., Flannery B. P., 1992, *Numerical Recipes in Fortran 77, The Art of Scientific Computing.*, Cambridge Univ. Press, Cambridge
- Pretorius M.L., Knigge C., Schwöpe A. D., 2013, *MNRAS*, 432, 570P
- Putney A., Jordan S., 1995, *ApJ*, 449, 863
- Putney A., 1995, *ApJL*, 451, L67
- Rappaport S., Verbunt F., Joss P.C., 1983, *ApJ*, 275, 713

Regős E., Tout C.A., 1995a, MNRAS, 273, 146

Regős E., Tout C.A., 1995, ASP Conference Series, 85, 458

Reimers D., Hagen H.-J., Hopp U., 1999, A&A, 343, 157

Reis R.C., Wheatley P.J., Gänsicke B.T., Osborne J.P., 2013, MNRAS, 430, 1994

Ricker, P.M., Taam, R.E., 2012, ApJ, 746(1), 74

Ritter H., 1986, A&A, 169, 139

Ritter H., Kolb U., 2003, A&A, 404, 301

Rolland B. 2014, M.Sc. Thesis, Université de Montréal

Rolland B., Bergeron P., 2015, ASP Conference Ser., 493, 53

Saio H. & Nomoto K., 1985, A&A, 150, L21

Salpeter E. E., 1955, ApJ, 121, 161

Sato Y., Nakasato N., Tanikawa A., Nomoto K., Maeda K., Hachisu I., 2016, ApJ, 821, 67

Schaller, G., Schaerer, D., Meynet, G., Maeder, A., 1992, A and AS, 96, 269

Schenker K., King A. R., Kolb U., Wynn G. A., Zhang Z. 2002, MNRAS, 337, 1105

Schlegel D. J., Finkbeiner D. P., Davis M. 1998, ApJ, 500, 525

Schwarzschild, Martin, Structure and Evolution of the Stars, Princeton Univ. Press, Princeton, NJ, 1958, Dover, 1965

Schmidt G. D., Latter W. B., Foltz C. B., 1990, ApJ, 350, 758

Schmidt G. D., Bergeron P., Liebert J., Saffer R. A., 1992, ApJ, 394, 603

Schmidt G. D., Stockman H. S., Smith P. S., 1992, ApJ, 398, L57

Schmidt G. D., Smith P. S., 1994, ApJ, 423, L63

Schmidt G. D., Smith P. S., 1995, ApJ, 448, 305

Schmidt G. D., Allen R. G., Smith P. S., Liebert J., 1996, ApJ, 463, 320

- Schmidt G. D., Vennes S., Wickramasinghe D. T., Ferrario L., 2001, MNRAS, 328, 203
- Schmidt G. D., Ferrario L., Wickramasinghe D. T., Smith P. S., 2001, ApJ, 553, 823
- Schmidt G. D., et al., 2003, ApJ, 595, 1101
- Schreiber M. R., Zorotovic M., Wijnen T. P. G., 2016, MNRAS, 455, L16
- Schwarzenberg-Czerny A., 1996, ApJ, 460, L107
- Schwope A.D., Brunner H., Hambaryan V., Schwarz R., 2002, in “The Physics of Cataclysmic Variables and Related Objects”, ASP Conf. Series, Eds: Gänsicke B.T., Beuermann K., Reinsch K., 261, 102
- Schwope A.D., Nebot Gomez-Moran A., Schreiber M.R., Gänsicke B.T. 2009, A&A, 500, 867
- Silvestri N.M., Lemargie M.P., Hawley et al., 2007, AJ., 13, 741
- Sion E. M., Fritz M., McMullin J. P., Lallo M. D., 1988, AJ, 96, 251
- Sion E. M., Holberg J. B., Oswalt T. D., McCook G. P., Wasatonic R., 2009, AJ, 138, 1681S
- Skrutskie M. F., 2006, AJ, 131, 1163
- Stellingwerf R. F., 1978, ApJ, 224, 953
- Spruit H.C., Ritter H., A&A, 124, 267
- Stetson P. B., 1987, PASP, 99, 191
- Subasavage J. P., Henry T. J., Bergeron P., Dufour P., Hambly N. C., Beaulieu T. D., 2007, AJ, 134, 252
- Tauris T. M., Dewi J. D. M., 2001, A&A, 369, 170
- Regós E., Tout C. A., 1995a, MNRAS, 273, 146
- Tout C. A., Regós E., 1995b, ASP Conference Series, 85, 1995
- Tout C. A., Pols O. R., Eggleton P. P., Han Z., 1996, MNRAS, 281, 257
- Tout C. A., Aarseth S. J., Pols O. R., Eggleton P. P., 1997, MNRAS, 291, 732

- Tout C. A., Wickramasinghe D. T., Ferrario L., 2004, MNRAS, 355, L13
- Tout C.A., European Astronomical Society Publications Series, 2006, 19, 31 .
- Tout C. A., Wickramasinghe D. T., Liebert J., Ferrario L., Pringle J. E., 2008, MNRAS, 387, 897
- Tout C.A., Wickramasinghe D.T., Lau H. H.-B., Pringle J.E., Ferrario L., 2011, MNRAS, 410, 2458
- Tremblay P.-E., Bergeron P., Gianninas A., 2011, ApJ, 730, 128
- Tremblay P.-E., Fontaine G., Freytag B., Steiner O., Ludwig H.-G., Steffen, M., Wedemeyer S., Brassard P. 2015, ApJ, 812, 19
- Valyavin G., Bagnulo S., Monin D., Fabrika S., Lee B. C., Galazutdinov G., Wade G. A., Burlakova T., 2005, A&A, 439, 1099
- Valyavin G., Wade G. A., Bagnulo S., Szeifert T., Landstreet J. D., Han I., Burenkov A., 2008, ApJ, 683, 466
- Valyavin G., et al. 2014, Nature, 515, 88
- van den Heuvel E. P. J., 1976, in Eggleton P., Mitton S., Whelan J., eds, Proc. IAU Symp. 73, Structure and Evolution of Close Binary Systems. Reidel, Dordrecht, p.35
- Vanlandingham K. M. et al., 2005, AJ, 130, 734
- Vennes S., Ferrario L., Wickramasinghe D. T., 1999, MNRAS, 302, L49
- Vennes S., Schmidt G. D., Ferrario L., Christian D. J., Wickramasinghe D. T., Kawka A., 2003, ApJ, 593, 1040
- Vennes S., Kawka A., 2008, MNRAS, 389, 1367
- Verbunt F., 1984, MNRAS, 209, 227
- Vernet J., et al., 2011, A&A, 536, 105
- Wade G. A., et al., 2016, MNRAS, 456, 2
- Warner B., 1995, "Cataclysmic variable stars", Cambridge University Press
- Webbink R.F., Wickramasinghe, D.T., 2002, MNRAS, 335, 1



Weiss A., Schattl H., 2008, *Atrophys Space Sci*, 316, 99

Wickramasinghe D. T., Martin B. 1979, *MNRAS*, 188, 165

Wickramasinghe D. T., Ferrario L., 1988, *ApJ*, 327, 222

Wickramasinghe D. T., Ferrario L., 2000, *PASP*, 112, 873

Wickramasinghe D.T., Schmidt G., Ferrario L., Vennes S., 2002, *MNRAS*, 33.2, 29

Wickramasinghe D. T., Ferrario L., 2005, *MNRAS*, 356, 615

Wickramasinghe D. T., Tout C. A., Ferrario L., 2014, *MNRAS*, 437, 675

Wijnen T. P. G., Zorotovic M., Schreiber M. R., 2015, *A&A*, 577, A143

Wisotzki L., Reimers D., Wamsteker W., 1991, *A&A*, 247, L17

Woltjer L., 1964, *ApJ*, 140, 1309

York D. G., et al. 2000, *AJ*, 120, 1579

Zhang C.M., Wickramasinghe D.T., Ferrario L., 2009, *MNRAS*, 397, 2208

Zangrilli L., Tout C. A., Bianchini A., 1997, *MNRAS*, 289, 59

Zorotovic M., Schreiber M. R., Gänsicke B. T., Nebot Gómez-Morán A., 2010, *A&A*, 520, 86

Zorotovic M., Schreiber M. R., Gänsicke B. T., 2011, *A&A*, 536, 42

Zorotovic M., Schreiber M. R., 2017, *MNRAS*, 466, L63

Zuckerman B., Koester D., Reid I. N., Hünsch M., 2003, *ApJ*, 596, 477